

**DEVELOPMENT OF TRUE TRIAXIAL LOAD FRAME
USING CANTILEVER SYSTEM**

Roengchai Thosuwat

**A Thesis Submitted in Partial Fulfillment of the Requirements for the
Degree of Master of Engineering in Geotechnology
Suranaree University of Technology
Academic Year 2009**

การพัฒนาโครงกดทดสอบในสามแกนจริงโดยใช้ระบบคานทอดแรง

นายเริงชัย ถอสวรรณ์

วิทยานิพนธ์นี้เป็นส่วนหนึ่งของการศึกษาตามหลักสูตรปริญญาวิศวกรรมศาสตรมหาบัณฑิต

สาขาวิชาเทคโนโลยีธรณี

มหาวิทยาลัยเทคโนโลยีสุรนารี

ปีการศึกษา 2552

**DEVELOPMENT OF TRUE TRIAXIAL LOAD FRAME
USING CANTILEVER SYSTEM**

Suranaree University of Technology has approved this thesis submitted in partial fulfillment of the requirements for a Master's Degree.

Thesis Examining Committee

(Asst. Prof. Thara Lekuthai)

Chairperson

(Assoc. Prof. Dr. Kittitep Fuenkajorn)

Member (Thesis Advisor)

(Dr. Prachya Tepnarong)

Member

(Prof. Dr. Pairote Sattayatham)

Acting Vice Rector for Academic Affairs

(Assoc. Prof. Dr. Vorapot Khompis)

Dean of Institute of Engineering

เริงชัย ถอสุวรรณ : การพัฒนาโครงกวดทดสอบในสามแกนจริงโดยใช้ระบบคานทคแรง
(DEVELOPMENT OF TRUE TRIAXIAL LOAD FRAME USING CANTILEVER
SYSTEM) อาจารย์ที่ปรึกษา : รองศาสตราจารย์ ดร.กิตติเทพ เพ็องขจร, 92 หน้า

วัตถุประสงค์ของงานวิจัยนี้คือเพื่อการพัฒนาเครื่องกวดทดสอบในสามแกนจริงโดยใช้ระบบคานทคแรงและเพื่อทดสอบศักยภาพของเครื่องมือ โดยเปรียบเทียบกับผลการทดสอบที่ได้จากการทดสอบในสามแกนแบบดั้งเดิม ข้อกำหนดหลักของการออกแบบเครื่องกวดทดสอบในสามแกนจริงประกอบไปด้วย (1) ให้แรงดันด้านข้างที่คงที่สูงถึง 100 กิโลนิวตัน และให้แรงในแนวแกนได้สูงถึง 1,000 กิโลนิวตัน (2) กำหนดให้ขนาดของตัวอย่างหินที่ใช้ในการทดสอบมีขนาด $5 \times 5 \times 10$ ลูกบาศก์เซนติเมตร (ซึ่งมีปริมาตรทัดเทียมกับตัวอย่างหินที่ใช้ในการทดสอบในสามแกนแบบดั้งเดิม) และ (3) สามารถตรวจวัดการเปลี่ยนแปลงรูปร่างของหินได้ทั้งสามทิศทางในขณะที่ทำการทดสอบ ข้อจำกัดคือเครื่องมือที่พัฒนาขึ้นใหม่นี้จะต้องมีราคาไม่แพงและง่ายต่อการใช้ เพื่อตอบสนองต่อจุดประสงค์หลักของการออกแบบ ระบบคานทคแรงจึงถูกนำมาใช้ในการออกแบบเพื่อทำการส่งถ่ายแรงโน้มถ่วงให้เป็นแรงดันด้านข้างที่คงที่บนตัวอย่างหิน ด้วยวิธีนี้จะทำให้แน่ใจว่าแรงที่กระทำอยู่ยังคงที่อย่างแท้จริงในขณะที่ทำการทดสอบ ศักยภาพของเครื่องมือกวดทดสอบจะถูกประเมินโดยการทดสอบการกวดในสามแกนกับตัวอย่างหินทรายอย่างน้อย 10 ตัวอย่าง ซึ่งการทดสอบจะกระทำโดยการผันแปรค่าความเค้นหลักกลางและค่าความเค้นหลักต่ำสุด ผลการทดสอบที่ได้จะถูกนำไปเปรียบเทียบกับผลที่ได้จากการทดสอบการกวดในสามแกนแบบดั้งเดิมซึ่งทำตามมาตรฐานของ ASTM

ผลการทดสอบระบุว่าเครื่องกวดในสามแกนจริงที่พัฒนาขึ้นสามารถใช้งานได้เป็นอย่างดีสำหรับการประเมินผลกระทบที่เกิดขึ้นของความเค้นหลักกลางต่อลักษณะการเปลี่ยนแปลงรูปร่างของหินทราย การวัดการเปลี่ยนแปลงรูปร่างของตัวอย่างโดยการตรวจวัดการเคลื่อนตัวของคานทคแรงมีความถูกต้องมากพอและมีความอ่อนไหวต่อการตรวจวัดพฤติกรรมที่เหมือนกันในทิศทางที่ตัดขวางกันของหินทราย หินทรายเหล่านี้แสดงให้เห็นถึงคุณสมบัติในทิศทางที่ตัดขวางกันเมื่อค่าสัมประสิทธิ์ความยืดหยุ่นในทิศทางที่ขนานกับระนาบชั้นหินซึ่งมีค่ามากกว่าค่าในทิศทางที่ตั้งฉากกับระนาบชั้นหิน อัตราส่วนของปีวส์ของในทิศทางที่ขนานกับระนาบชั้นหินมีค่าน้อยกว่าในทิศทางที่ตั้งฉากกับระนาบชั้นหิน ความแตกต่างของผลการทดสอบจากการกวดในสามแกนแบบดั้งเดิมและการทดสอบการกวดในสามแกนจริงอาจเป็นเพราะรูปร่างของตัวอย่างหินมีความแตกต่างกัน และมีความไม่เหมือนกันในทุกทิศทางของหินทราย

เครื่องมือใหม่นี้สามารถใช้เป็นเครื่องมือสำหรับการสอนนักศึกษาระดับบัณฑิตและบัณฑิตศึกษา
ได้ และมีประโยชน์สำหรับการทำวิจัยในระดับสูงทางการทดสอบกลศาสตร์หิน

สาขาวิชา เทคโนโลยีธรณี

ปีการศึกษา 2552

ลายมือชื่อนักศึกษา _____

ลายมือชื่ออาจารย์ที่ปรึกษา _____

ROENGCHAI THOSUWAN : DEVELOPMENT OF TRUE TRIAXIAL
LOAD FRAME USING CANTILEVER SYSTEM. THESIS ADVISOR :
ASSOC. PROF. KITTITEP FUENKAJORN, Ph.D., PE., 92 PP.

SANDSTONE/TRUE TRIAXIAL/POLYAXIAL/CANTILEVER BEAM/
STRESS ANISOTROPY

The objectives of this research are to invent a polyaxial load frame using cantilever beam system and to assess its performance by comparing the test results with those obtained from the conventional method. Key design requirements of the polyaxial load frame include (1) maintaining constant lateral loads in mutually perpendicular directions up to 100 kN with the maximum axial load up to 1,000 kN, (2) accommodating the rock sample size up to $5 \times 5 \times 10 \text{ cm}^3$ (with volume equivalent to those used in the conventional method), and (3) being capable of monitoring the rock deformation in three directions during loading. A constraint is that the new device must be inexpensive and easy to operate. To satisfy these requirements, a cantilever beam system is proposed as a design solution by transferring the gravitational force to constant lateral loads on the rock samples. This ensures that the applied loads will remain truly constant during testing. Performance of the load frame are assessed by conducting polyaxial compression tests on sandstone specimens. A minimum of 10 samples are tested under a variety of σ_2 and σ_3 values. The results are compared with those obtained from the conventional (ASTM) test method.

The test results indicate that the invented polyaxial load frame perform well for the assessment of the effects of σ_2 on the deformation characteristics of the sandstones. Measuring the specimen deformations by monitoring the movement of

the cantilever beams is sufficiently accurate and sensitive to detect the transversely isotropic behavior of the sandstones. These sandstones show transversely isotropic properties where the elastic modulus in the direction parallel to the bedding planes is greater than that normal to the bedding. The Poisson's ratio on the plane parallel to the bedding is lower than those on the plane normal to the bedding. The discrepancies of the results of the conventional triaxial tests and true triaxial tests are probably because of the difference in specimen shapes and the transversely isotropic of the sandstones. The new device can be used as a teaching tool for undergraduate and graduate students, and are useful for future high-level researches in rock mechanics testing.

School of Geotechnology

Academic Year 2009

Student's Signature_____

Advisor's Signature_____

ACKNOWLEDGMENTS

I wish to acknowledge the funding support of Suranaree University of Technology (SUT).

I would like to express my sincere thanks to Assoc. Prof. Dr. Kittitep Fuenkajorn, thesis advisor, who gave a critical review and constant encouragement throughout the course of this research. Further appreciation is extended to Asst. Prof. Thara Lekuthai : Chairman, School of Geotechnology and Dr. Prachya Tepnarong, School of Geotechnology, Suranaree university of Technology who are member of my examination committee. Grateful thanks are given to all staffs of Geomechanics Research Unit, Institute of Engineering who supported my work.

Finally, I most gratefully acknowledge my parents and friends for all their supported throughout the period of this research.

Roengchai Thosuwan

TABLE OF CONTENTS

	Page
ABSTRRACT (THAI)	I
ABSTRACT (ENGLISH)	III
ACKNOWLEDGEMENTS	V
TABLE OF CONTENTS	VI
LIST OF TABLES	IX
LIST OF FIGURES	X
LIST OF SYMBOLS AND ABBREVIATIONS.....	XIV
CHAPTER	
I INTRODUCTION	1
1.1 Background of problems and significance of the study	1
1.2 Research objectives	1
1.3 Research methodology	2
1.3.1 Literature review	3
1.3.2 Sample collection and preparation	4
1.3.3 Development of true triaxial load frame.....	4
1.3.4 Calibration of true triaxial load frame.....	4
1.3.5 Laboratory experiments.....	4
1.3.6 Comparisons	5
1.3.7 Conclusions and thesis writing.....	5

TABLE OF CONTENTS (Continued)

	Page
1.4 Scope and limitations of the study	5
1.5 Thesis contents	5
II LITERATURE REVIEW	7
2.1 Introduction	7
2.2 Deformation and strength of rocks	7
2.3 True triaxial load frame	9
2.4 Effect of intermediate principal stresses.....	13
III POLY AXIAL LOAD FRAME	16
3.1 Introduction	16
3.2 Design requirements and components.....	16
3.3 Calculations of factor of safety.....	19
3.3.1 Calculation of factor of safety of cantilever beam	19
3.3.2 Factor of safety of lower beam.....	30
3.3.3 Factor of safety of rectangular column.....	30
3.3.4 Factor of safety of hinge.....	31
3.3.5 Factor of safety of U-link and steel rod.....	31
3.3.6 Factor of safety at screw of rectangular column.....	32
IV LABORATORY TESTING.....	33
4.1 Introduction	33
4.2 Sample preparation	33
4.3 Characterization tests	35

TABLE OF CONTENTS (Continued)

	Page
4.3.1 Uniaxial compression tests	35
4.3.2 Conventional triaxial compression tests	35
4.4 True triaxial compression tests	39
4.4.1 Test method	44
4.4.2 Test results	45
4.5 Comparisons	46
V DISCUSSIONS, CONCLUSIONS AND	
RECOMMENDATIONS FOR FUTURE STUDIES	64
5.1 Discussions and conclusions	64
5.2 Recommendations for future studies	65
REFERENCES	66
APPENDIX A LIST OF PUBLICATIONS	69
BIOGRAPHY	92

LIST OF TABLES

Table		Page
3.1	Mechanical properties of structural steel A36.....	29
4.1	Mineral compositions of tested sandstones	34
4.2	Elastic properties from conventional triaxial compression tests	43
4.3	Elastic properties from true triaxial compression test	47
4.4	Elastic properties from characterization tests and true triaxial compression tests.....	63

LIST OF FIGURES

Figure	Page
1.1 Research Methodology	3
2.1 Schematic diagram of the University of Wisconsin true triaxial testing system.....	10
2.2 Pressure cell for application of radial stresses to core	11
2.3 Sandia true-triaxial testing system with “floating” pressure vessel shell	12
3.1 Polyaxial load frame developed for rock testing under true triaxial stresses	17
3.2 Cantilever beam weighed at outer end applies lateral stress to the rock specimen	18
3.3 Cantilever beam of true triaxial load frame	20
3.4 Lower beam for carrying dead weight for the true triaxial load frame	20
3.5 Half spherical bolt use for transmit compressive load from cantilever beam to lateral load platen	21
3.6 Circular steel column linking between lower steel plate and steel stand	22
3.7 Rectangular steel column used for hosting the cantilever beam.....	23

LIST OF FIGURES (Continued)

Figure	Page
3.8	Steel rod and U-links used for connecting between cantilever beam and lower steel bar 24
3.9	Lower steel plate 25
3.10	Lateral loading platen for $5 \times 5 \times 10 \text{ cm}^3$ specimen 26
3.11	Upper steel plate 27
3.12	Steel stand supporting the frame 28
3.13	Calibration curves obtained from electronic load cell of beam N-S and beam E-W. A and B indicate the forces at which only lower steel bar is hanging on the beams 29
4.1	Sandstone specimens prepared for the conventional triaxial compressive strength test and true triaxial compressive strength test. Left is PW, middle is PP and right is PK 34
4.2	Stress-strain curves of Phra Wihan sandstone from uniaxial compressive strength test 36
4.3	Stress-strain curves of Phu Kradung sandstone from uniaxial compressive strength test 37
4.4	Stress-strain curves of Phu Phan sandstone from uniaxial compressive strength test 38
4.5	Laboratory set-up for the conventional triaxial compressive strength test 39

LIST OF FIGURES (Continued)

Figure	Page
4.6	Stress-strain curves of Phu Kradung sandstone at condition $\sigma_2 = \sigma_3 = 1$ MPa..... 40
4.7	Stress-strain curves of Phu Phan sandstone at condition $\sigma_2 = \sigma_3 = 1$ MPa 41
4.8	Stress-strain curves of Phra Wihan sandstone at condition $\sigma_2 = \sigma_3 = 2$ MPa..... 42
4.9	Directions of loading with respect to the bedding planes (left). Elastic parameters for transversely isotropic conditions (right) 45
4.10	Stress-strain curves of Phra Wihan sandstone at condition $\sigma_2 = 10.1$ MPa and $\sigma_3 = 1.2$ MPa..... 48
4.11	Stress-strain curves of Phra Wihan sandstone at condition $\sigma_2 = 6.6$ MPa and $\sigma_3 = 1.2$ MPa..... 49
4.12	Stress-strain curves of Phra Wihan sandstone at condition $\sigma_2 = 6.6$ MPa and $\sigma_3 = 6.6$ MPa..... 50
4.13	Stress-strain curves of Phra Wihan sandstone at condition $\sigma_2 = 10.1$ MPa and $\sigma_3 = 6.6$ MPa..... 51
4.14	Stress-strain curves of Phra Wihan sandstone at condition $\sigma_2 = 6.6$ MPa and $\sigma_3 = 3$ MPa..... 52
4.15	Stress-strain curves of Phu Phan sandstone at condition $\sigma_2 = 6.6$ MPa and $\sigma_3 = 3.0$ MPa..... 53

LIST OF FIGURES (Continued)

Figure	Page
4.16 Stress-strain curves of Phu Phan sandstone at condition $\sigma_2 = 13.8$ MPa and $\sigma_3 = 6.6$ MPa.....	54
4.17 Stress-strain curves of Phu Phan sandstone at condition $\sigma_2 = 10.1$ MPa and $\sigma_3 = 0$ MPa.....	55
4.18 Stress-strain curves of Phu Phan sandstone at condition $\sigma_2 = 13.8$ MPa and $\sigma_3 = 0$ MPa.....	56
4.19 Stress-strain curves of Phu Phan sandstone at condition $\sigma_2 = 10.1$ MPa and $\sigma_3 = 3$ MPa.....	57
4.20 Stress-strain curves of Phu Kradung sandstone at condition $\sigma_2 = 6.6$ MPa and $\sigma_3 = 6.6$ MPa.....	58
4.21 Stress-strain curves of Phu Kradung sandstone at condition $\sigma_2 = 13.8$ MPa and $\sigma_3 = 6.6$ MPa.....	59
4.22 Stress-strain curves of Phu Kradung sandstone at condition $\sigma_2 = 10.1$ MPa and $\sigma_3 = 3$ MPa.....	60
4.23 Stress-strain curves of Phu Kradung sandstone at condition $\sigma_2 = 3$ MPa and $\sigma_3 = 1.2$ MPa.....	61
4.24 Stress-strain curves of Phu Kradung sandstone at condition $\sigma_2 = 10.1$ MPa and $\sigma_3 = 0$ MPa.....	62

LIST OF SYMBOLS AND ABBREVIATIONS

A_t	=	Tensile stress area
c	=	Perpendicular distance from the neutral axis to a point farthest away
d	=	Outside (major) diameter
d_p	=	Pitch diameter
d_r	=	Minor (root) diameter
E	=	Modulus of elasticity of steel
E_j	=	Elastic modulus of joint
E_n	=	Elastic modulus in the direction normal to bedding plane
E_p	=	Elastic modulus in the direction parallel to bedding plane
F	=	Axial tensile load
I	=	Moment of inertia of the cross-section area
L	=	Length
M	=	Internal moment
m	=	Peak empirical strength parameters
N	=	Number of threads per inch
P	=	Vertical load
P_{cr}	=	Critical load capacity of column
q_{cmass}	=	Average uniaxial compressive strength of block of rock
R	=	Plastic zone radius
r	=	Cavity radius

LIST OF SYMBOLS AND ABBREVIATIONS (Continued)

s	=	Peak empirical strength parameters
V_O	=	Excess oil volume
V_R	=	Volume of rock specimen
V_S	=	Volume of oil displaced by loading platen
ε_1	=	Strains in maximum principal stress direction
ε_2	=	Strains in intermediate principal stress direction
ε_3	=	Strains in minimum principal stress direction
ε_V	=	Volumetric strain
θ_{\max}	=	Maximum slope of hinge
v_{\max}	=	Maximum deflection or vertical displacement of hinge
v_n	=	Poisson's ratio in the direction normal to bedding plane
v_p	=	Poisson's ratio in the direction parallel to bedding plane
σ_1, σ_θ	=	Maximum principal stress
σ_2, p_o	=	Intermediate principal stress
σ_3, σ_γ	=	Minimum principal stress
σ_c	=	Uniaxial compressive strength of the intact rock
σ_{\max}	=	Maximum normal stress in the member
σ_t	=	Tensile stress

CHAPTER I

INTRODUCTION

1.1 Background of problems and significance of the study

Rock deformation and strength are one of the important parameters for the design and stability analysis of geological structures, e.g., foundations of dam, building and bridge, and host rocks for tunnels and underground mines. The effects of the confining pressures at great depth on those properties are commonly simulated in the laboratory by performing triaxial compression testing of cylindrical rock core specimens. A significant limitation of this conventional test method is that the intermediate and minimum principal stresses have to be equal during the test while the rock in actual in-situ condition is normally subjected to anisotropic stress state where the maximum, intermediate and minimum principal stresses are not equal ($\sigma_1 \neq \sigma_2 \neq \sigma_3$). Testing under such anisotropic stress conditions require special loading devices, such as true triaxial cell or polyaxial load frame. These devices are not only expensive but difficult to use. They require complex computer-controlled system to ensure that the applied σ_2 and σ_3 magnitudes are maintained strictly constant during sample deformation.

1.2 Research objectives

The objectives of this research are to develop a polyaxial load frame using cantilever beam system and to assess its performance by comparing the test results with those obtained from the conventional method. The key design requirements of

the polyaxial load frame include (1) maintaining constant lateral loads in mutually perpendicular directions up to 100 kN with the maximum axial load up to 1,000 kN, (2) accommodating the rock sample size up to $5 \times 5 \times 10 \text{ cm}^3$ (with volume equivalent to those used in the conventional method), and (3) being capable of monitoring the rock deformation in three directions during loading. A key constraint is that the new device must be inexpensive and easy to operate.

To satisfy those requirements, a cantilever beam system is proposed as a design solution by transferring the gravitational force to constant lateral loads on the rock samples. This ensures that the applied loads will remain truly constant during testing. Performance of the load frame will be assessed by conducting polyaxial compression tests on sandstone specimens. A minimum of 10 samples will be tested under a variety of σ_2 and σ_3 values. The results will be compared with those obtained from the conventional (ASTM) test method. The comparison will be made in terms of the elastic modulus and Poisson's ratio measured from the rock samples. Similarity and discrepancy of the results will be examined and discussed.

1.3 Research methodology

As shown in Figure 1.1, the research methodology comprises 7 steps including literature review, sample collection and preparation, design and invent true triaxial load frame, calibrate true triaxial load frame, laboratory experiments, comparison and discussions and conclusions.

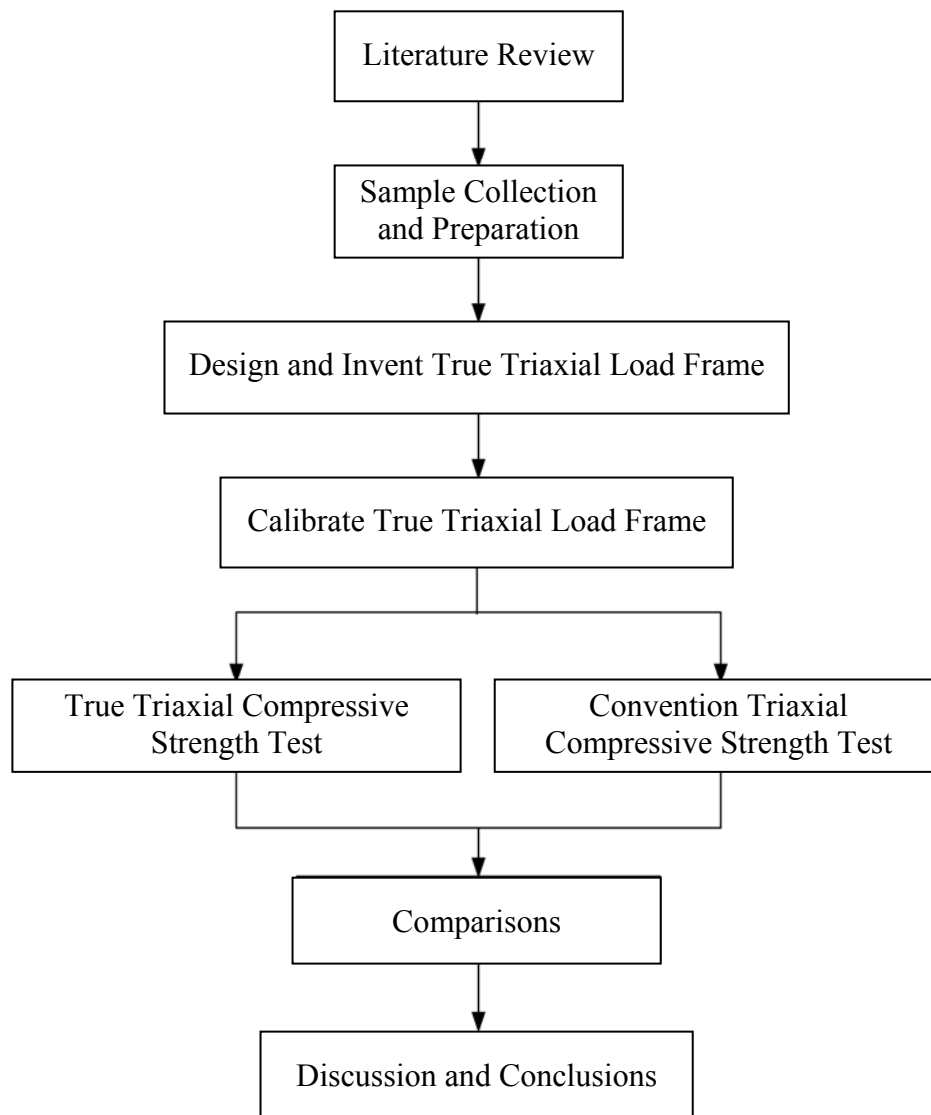


Figure 1.1 Research Methodology

1.3.1 Literature review

Literature review is carried out to study the rock deformation and strength in true triaxial stress state, review another type of true triaxial or polyaxial load frame and criterion of anisotropic rock. The sources of information are from text books, journals, technical reports and conference papers. A summary of the literature review is given in the thesis.

1.3.2 Sample collection and preparation

Sandstone samples will be collected from the site. A minimum of 3 sandstone types will be collected. Sample preparation will be carried out in the laboratory at the Suranaree University of Technology. Samples prepared for the conventional triaxial compressive strength test are 5 cm in diameter and 10 cm long. Samples for the true triaxial compressive strength test are $5 \times 5 \times 10 \text{ cm}^3$ rectangular blocks. A minimum of 10 samples will be prepared for each test and each rock types.

1.3.3 Development of true triaxial load frame

A true triaxial load frame using cantilever system is proposed. Detailed design and design components are developed.

1.3.4 Calibration of true triaxial load frame

After construction, the lateral and axial loads of true triaxial load frame are calibrated using electronic load cell. The calibration curves are developed for use in the determination of the lateral and axial stresses during testing.

1.3.5 Laboratory experiments

The laboratory experiments are divided into two groups; i.e. conventional triaxial compressive strength test and true triaxial compressive strength test.

This test method follows ASTM D7012-04. The test results are used to compare and analyze with those of the true triaxial compressive strength test. A series of true triaxial compressive strength tests are performed using the confinements (σ_2 and σ_3) comparable to those of the conventional methods. Three types of sandstone are used as rock samples.

1.3.6 Comparisons

Results from laboratory measurements in terms of stress and strain are used to calculate elastic modulus and Poisson's ratio of the rocks. Both factors will be used in the comparison between conventional (ASTM) test methods and true triaxial compression test method. Similarity and discrepancy will be discussed.

1.3.7 Conclusions and thesis writing

All research activities, methods and results are documented and compiled in the thesis.

1.4 Scope and limitations of the study

The scope and limitations of the research include as follows.

1. Laboratory experiments are conducted on specimens from three types of sandstone from the Phu Kra-dueng, Pra Wihan, and Phu Phan formations.
2. Rock samples have a nominal dimension of 5x5x10 cm³ (with volume equivalent to those used in the conventional method).
3. Testing are made under σ_2 and σ_3 up to 17 MPa with σ_1 up to 400 MPa.
4. All tested rocks are prepared in the laboratory.
5. Monitoring of rock deformation in three directions during loading.
6. All tests are conducted under ambient temperature.
7. A minimum of 10 samples are tested for each sandstone.

1.5 Thesis contents

Chapter I introduces the thesis by briefly describing the background of problems and significance of the study. The research objectives, methodology, scope

and limitations are identified. **Chapter II** summarizes results of the literature review. **Chapter III** describes the design, invent and calibration procedure for true triaxial load frame. **Chapter IV** presents the results obtained from the laboratory testing and comparison the results between two tests method. The experiments are divided into two tests, including (1) True triaxial compressive strength tests, and (2) Conventional triaxial compressive strength tests. **Chapter V** concludes the research results, and provides recommendations for future research studies. **Appendix A** provides detailed of technical publications.

CHAPTER II

LITERATURE REVIEW

2.1 Introduction

Relevant topics and previous research results are reviewed to improve an understanding of rock deformation and strength in true triaxial stress states. These include review the existing true triaxial cells or polyaxial load frames.

2.2 Deformation and strength of rocks

Kwasniewski et al. (2003) use prismatic samples of medium-grained sandstone from Śląsk Colliery for testing under uniaxial compression, conventional triaxial compression and true triaxial compression conditions. Results of the studies show that confining pressure strongly inhibited dilatant behavior of rock samples tested under conventional triaxial compression conditions; the increasing confinement resulted in the growing compaction of the rock material. The effect of dilatancy was also highly suppressed by the intermediate principal stress. While important dilatant, negative volumetric strain corresponded to the peak differential stress at low intermediate principal stress conditions, at high intermediate stresses the rock material was damaged to much lesser extent. As a result, faulting of rock samples in the post-peak region was much more violent and was accompanied by a strong acoustic effect.

Tiwari and Rao (2004) describe physical modeling of a rock mass under a true triaxial stress state by using block models having three smooth joint sets. The testing uses true-triaxial system (TTS) developed by Rao and Tiwari (2002). The test results show that the strength of rock mass (σ_1) and deformation modulus (E_j) increase significantly which is confirmed by fracture shear planes developed on σ_2 face of specimen. Most of the specimens failed in shearing with sliding in some cases. The effect of interlocking (s) and rotation of principal stresses σ_2 and σ_3 on strength and deformation response was also investigated for few specimens with $q = 60^\circ$.

Chang and Haimson (2005) conducted rock strength experiments in two ultra-fine-grained brittle rocks. True triaxial compression experiments of the specimens orientation show a consistent angle to banding, in which the magnitudes of the least (σ_3) and the intermediate principal stresses (σ_2) are different but kept constant during testing while the maximum principal stress is increased until failure. Strains measured in all three principal directions during loading were used to obtain plots of σ_1 versus volumetric strain. Authors infer that strength independence of σ_2 in the Long Valley rocks derives directly from their non-dilatant deformation.

Tiwari and Rao (2006) provide results of triaxial and true triaxial testing conducted on physical models of a rock mass to describe its post failure behaviour. The testing was performed using a True Triaxial System (TTS) developed by the authors. The results show estimate post peak modulus in triaxial and true triaxial stress conditions.

2.3 True triaxial load frame

Haimson and Chang (1999) have designed, fabricated, and successfully calibrated and tested a new true triaxial (polyaxial) cell (Figure 2.1) capable of applying very high loads to $19 \times 19 \times 38 \text{ mm}^3$ rock specimens. Its main feature is very high loading capability in all three orthogonal directions, enabling the testing to failure of hard crystalline rocks subjected to large least and intermediate principal stresses. An apparatus has measurements of strain in all three principal directions. The true triaxial tests also demonstrate that for the same least horizontal stress the main fracture dip angle in Westerly granite increases as a function of the intermediate principal stress, suggesting a strengthening effect. Limited thin section and SEM study shows that microcrack propagation, crack localization, and main fracture characteristics are basically similar to those observed in common triaxial tests.

Smart et al. (1999) develop triaxial test cells to apply the axial stress to a cylindrical sample using steel platens, with the confining stress developed via an annulus of hydraulic fluid retained by a liner in a pressure cell. An array of 24 trapped tubes replaces the single annulus which usually generates the uniform radial stress. Pressure cell (Figure 2.2) does not allow differentiation between the two principal stresses around the core and inhibits the realism with which the rocks can be tested, for example in determining the effect of the intermediate principal stress on the strength of the sample.

Wawersik et al. (1997) develop true-triaxial apparatus (Figure 2.3) that makes use of conventional triaxial pressure vessels in combination with specially configured, high-pressure hydraulic jacks inside these vessels. The new true-triaxial apparatus uses conventional triaxial pressure vessels in combination with specially configured,

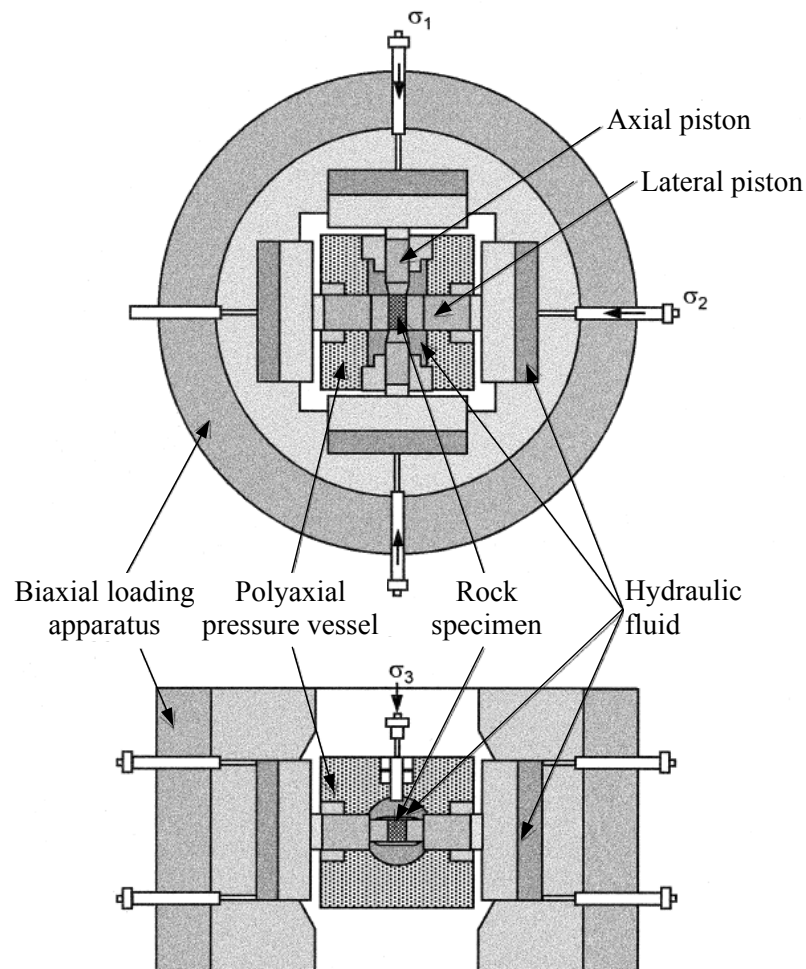


Figure 2.1 Schematic diagram of the University of Wisconsin true triaxial testing system. (Haimson and Chang, 1999)

high-pressure hydraulic jacks inside these vessels. The development combines advantages not found in existing facilities, including a compact design, pore-pressure and flow-through capabilities, the ability to attain high principal stresses and principal stress differences, direct access to parts of the sample, and provisions to relatively large deformations without developing serious stress field inhomogeneities.

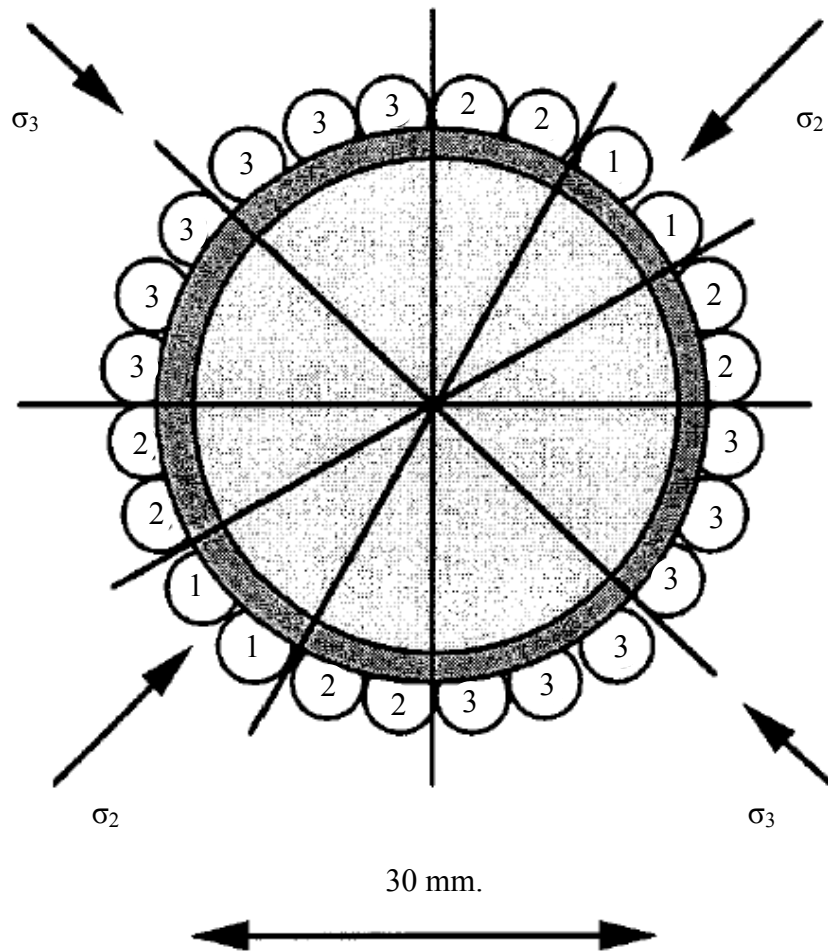


Figure 2.2 Pressure cell for application of radial stresses to core.(Smart et al., 1999)

Alexeev et al. (2004) present two generations of true triaxial loading (TTAL) apparatus. First generation was intended primarily for true stress state imitation in rock or mineral specimens. Advanced second-generation is designed to provide precise measurements in any stress and simulation of rock outburst at sudden relief of one sample face. Both TTAL apparatuses can apply pressure up to 250 MPa, corresponding to earth depth about 10,000 m, independently along each of three axes. Experimental results are given on effect of absorbed water on ultimate state in coal as well as adsorbed methane influence on simulated coal outbursts.

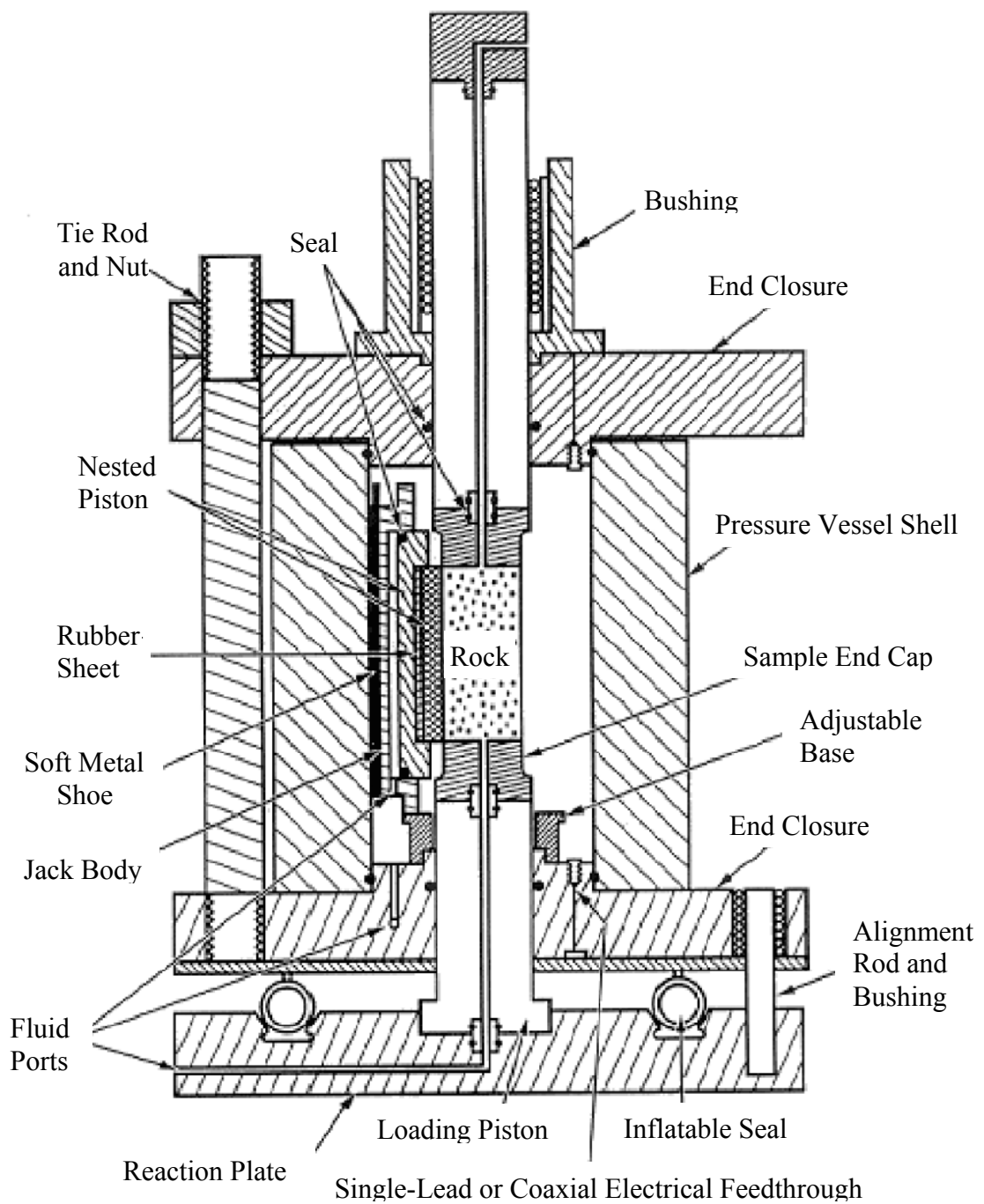


Figure 2.3 Sandia true-triaxial testing system with “floating” pressure vessel shell.

(Wawersik et al., 1997)

2.4 Effect of intermediate principal stresses

Oku et al. (2007) conducted true triaxial compression tests to examine the effect of the intermediate principal stress (σ_2) on brittle failure and deformability of the siltstone overlying the Chelungpu fault, Taiwan. Strength data are well fitted by a Mogi-modified Nadai criterion relating the octahedral shear stress at failure to the mean normal stress on the induced shear fracture or faults. The modulus of elasticity and the onset of dilatancy exhibit a similar behaviour to that of σ_1 , as they increase with σ_2 when subjected to a constant σ_3 .

Haimson (2006) studies the effect of the intermediate principal stress (σ_2) on brittle fracture of rocks, and on their strength criteria. Testing equipment emulating Mogi's but considerably more compact was developed at the University of Wisconsin and used for true triaxial testing of some very strong crystalline rocks. Test results revealed three distinct compressive failure mechanisms, depending on loading mode and rock type: shear faulting resulting from extensile microcrack localization, multiple splitting along the σ_1 axis, and nondilatant shear failure. The true triaxial strength criterion for the KTB amphibolite derived from such tests was used in conjunction with logged breakout dimensions to estimate the maximum horizontal in situ stress in the KTB ultra deep scientific hole.

Singh et al. (1998) use the Mohr-Coulomb criterion needs for highly anisotropic rock material and jointed rock masses. Taking σ_2 into account, a new strength criterion is suggested because both σ_2 and σ_3 would contribute to the normal stress on the existing plane of weakness. This criterion explains the enhancement of strength (σ_2 - σ_3) in the underground openings because σ_2 along the tunnel axis is not relaxed significantly. Another cause of strength enhancement is less reduction in the

mass modulus in tunnels due to constrained dilatancy. Empirical correlations obtained from data from block shear tests and uniaxial jacking tests have been suggested to estimate new strength parameters. A correlation for the tensile strength of the rock mass is presented. Finally, Hoek and Brown theory is extended to account for a σ_2 common strength criterion for both supported underground openings and rock slopes is suggested. It can be re-written as

$$\sigma_1 - \sigma_3 = q_{\text{cmass}} + A \left[\frac{\sigma_2 + \sigma_3}{2} \right] \quad (2.1)$$

where q_{cmass} is average uniaxial compressive strength of block of rock mass for various orientations of principal stresses, $\sigma_1, \sigma_2, \sigma_3$ = final effective principal stresses which are equal to in-situ stress plus induced stress minus seepage pressure, A is average constant for various orientations of principal stresses. The average constant are

$$A = \frac{2\sin\theta_p}{1 - \sin\theta_p} \quad (2.2)$$

Yang et al. (2007) provide the linear Mohr-Coulomb and nonlinear Hoek-Brown failure criteria, which neglect the effects of intermediate principal stress, widely used in soil and rock engineering. However, much experimental data shows that the failure envelope relates to the intermediate principal stress. Employing the failure criterion and the generalized plastic potential function, the stability of rock cavity driven in an isotropic and homogeneous medium was investigated under the condition of plane strain considering the effects of intermediate principal stress. The closed-form solutions for stresses and displacement around a rock cavity were given

in the elastic and plastic zones. Based on the closed-form solutions, the intermediate principal stress has an important effect on cavity stability. Those closed-form solutions are as follows.

$$\sigma_r = p_0 - (R/r)^2 \left\{ \frac{1}{16} [m^2 \sigma_c^2 + 64(m\sigma_c p_0 + s\sigma_c^2)]^{0.5} + \frac{1}{16} m\sigma_c \right\} \quad (2.3)$$

$$\sigma_\theta = p_0 + (R/r)^2 \left\{ \frac{1}{16} [m^2 \sigma_c^2 + 64(m\sigma_c p_0 + s\sigma_c^2)]^{0.5} + \frac{1}{16} m\sigma_c \right\} \quad (2.4)$$

where p_0 = intermediate principal stress, m and s are peak empirical strength parameters, σ_c is uniaxial compressive strength of the intact rock, R is the plastic zone radius, r is the cavity radius, σ_θ is a maximum principal stress, σ_r is a minimum principal stress.

CHAPTER III

POLYAXIAL LOAD FRAME

3.1 Introduction

A polyaxial load frame has been built for use to test rock specimens under true triaxial stress states. The frame performance is assessed by conducting polyaxial compression tests to study the deformation and failure characteristics of sandstone specimens. This chapter describes the design requirements and components of the polyaxial load frame and calculation of elastic modulus and poisson's ratio of the rock specimens.

3.2 Design requirements and components

The functional requirements for the polyaxial load frame are: (1) capable of maintaining constant lateral stresses (σ_2 and σ_3) during the test, (2) capable of testing specimen with volume equal to or larger than those used in the conventional triaxial testing, and (3) allowing monitoring of specimen deformation along the principal axes. Figure 3.1 shows the polyaxial load frame developed in this research.

To meet the load requirement above, two pairs of cantilever beams are used to apply the lateral stresses in mutually perpendicular directions to the rock specimen. The outer end of each opposite beam is pulled down by dead weight placed in the middle of a steel bar linking the two opposite beams underneath (Figure 3.2). The inner end is hinged by a pin mounted on vertical bars on each side of the frame.

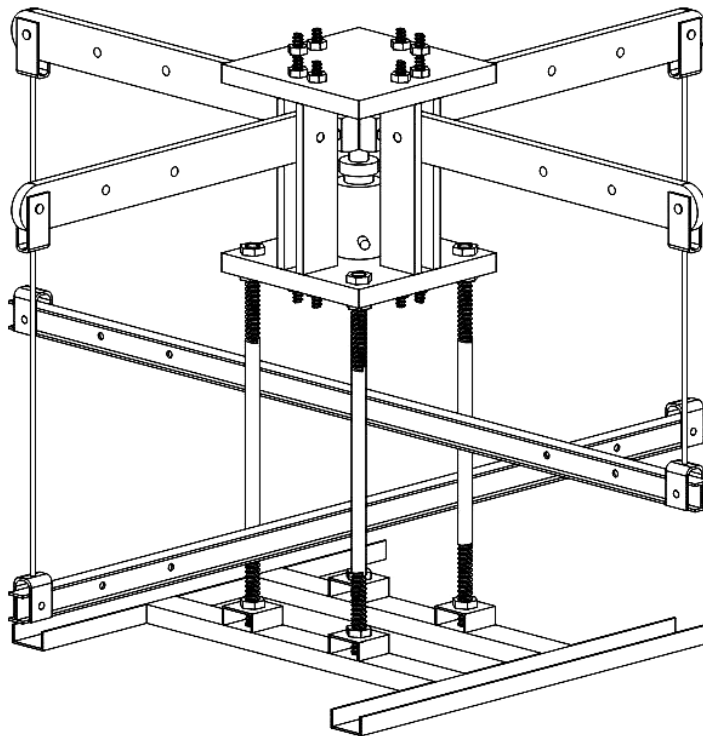
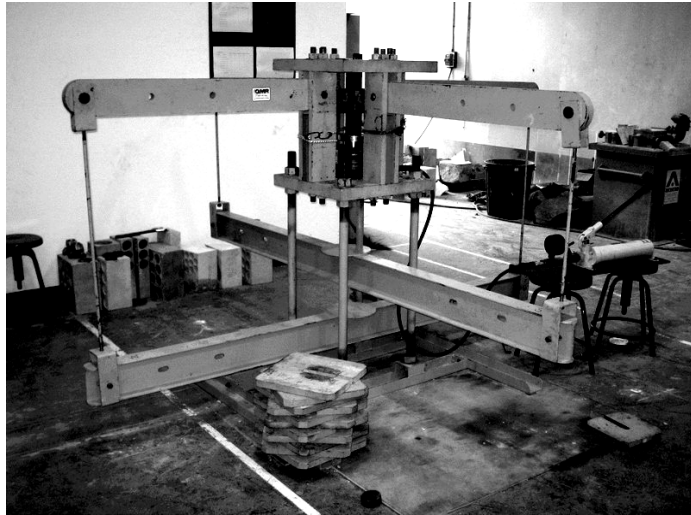


Figure 3.1 Polyaxial load frame developed for rock testing under true Triaxial stresses.

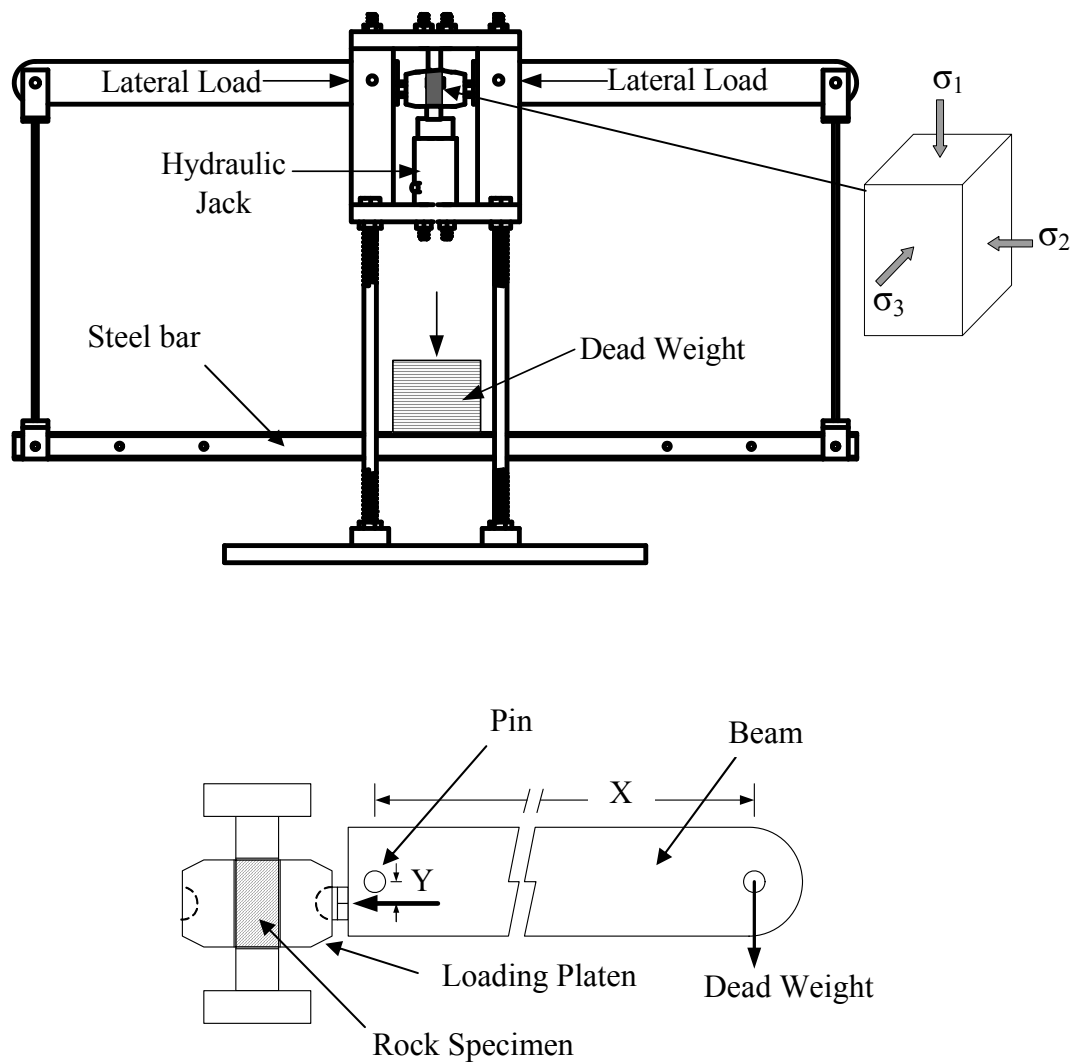


Figure 3.2 Cantilever beam weighed at outer end applies lateral stress to the rock specimen.

During testing all beams are arranged perfectly horizontally, and hence a lateral compressive load results on the specimen placed at the center of the frame. Due to the different distances from the pin to the outer weighting point and from the pin to the inner loading point, a load magnification of 17 to 1 is obtained from load calibration with an electronic load cell. This loading ratio is also used to determine the lateral deformation of the specimen by monitoring the vertical movement of the two steel bars below. The maximum lateral load is designed for 100 kN. The axial load is applied by a 1000-kN hydraulic load cell. The load frame can accommodate specimen sizes from $2.5 \times 2.5 \times 2.5 \text{ cm}^3$ to $10 \times 10 \times 20 \text{ cm}^3$. The different specimen sizes and shapes can be tested by adjusting the distances between the opposite loading platens. Note that virtually all true triaxial and polyaxial cells previously developed elsewhere can test rock samples with the maximum size not larger than $5 \times 5 \times 10 \text{ cm}^3$. Figures 3.3 through Figure 3.12 show the dimensions of each component of the true triaxial load frame. Figure 3.13 shows lateral load calibration curves from electronic load cell of the beam N-S and beam E-W when applied dead weight.

3.3 Calculations of factor of safety

Polyaxial load frame uses structural steel A36. The mechanical properties of the material are shown in Table 3.1.

3.3.1 Calculation of factor of safety of cantilever beam

The factor of safety of cantilever beam in bending is calculated by using (Hibbeler, 2003).

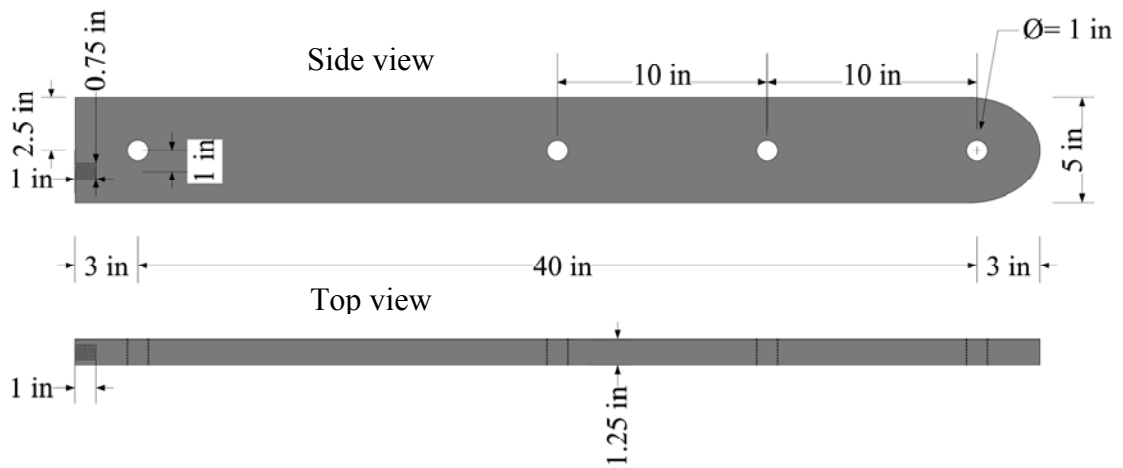


Figure 3.3 Cantilever beam of true triaxial load frame.

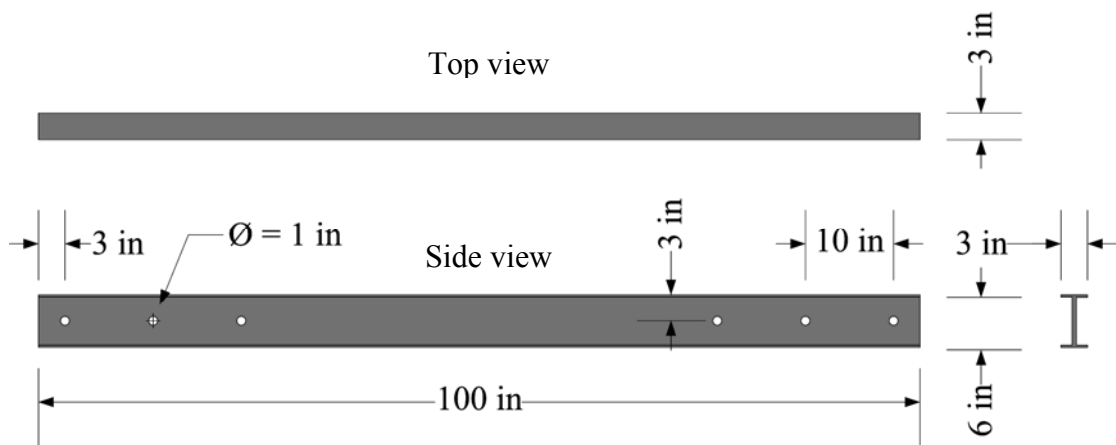


Figure 3.4 Lower beam for carrying dead weight for the true triaxial load frame.

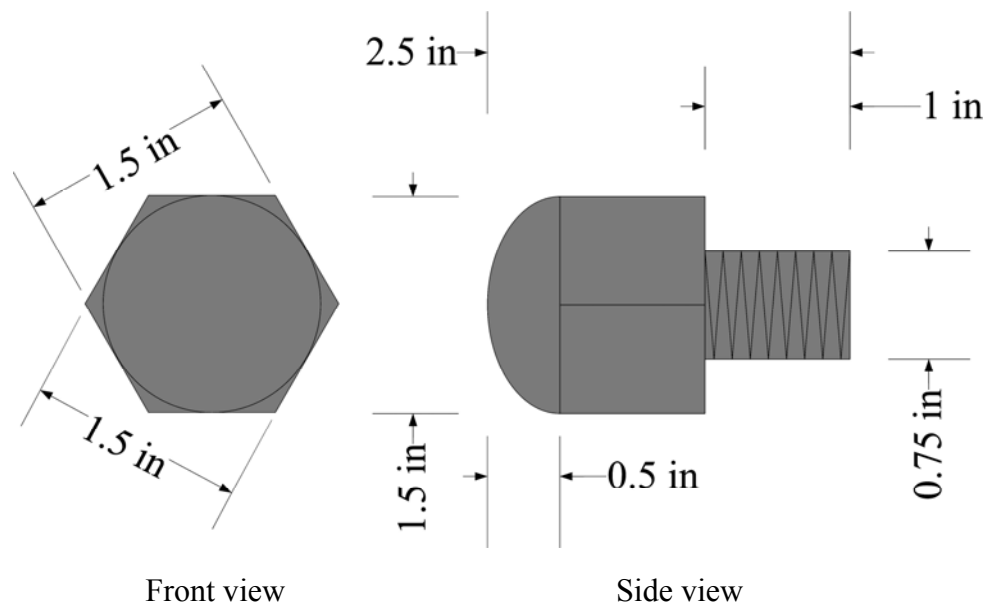


Figure 3.5 Half spherical bolt use for transmit compressive load from cantilever beam to lateral load platen.

$$\sigma_{\max} = \frac{Mc}{I} \quad (3.1)$$

where σ_{\max} is the maximum normal stress in the member, M is the internal moment, I is the moment of inertia of the cross-section area and c is the perpendicular distance from the neutral axis to a point farthest away from the neutral axis, where σ_{\max} acts.

The maximum internal moment in cantilever beam is 3,000 N.m, the moment of inertia is $4.3 \times 10^{-6} \text{ m}^4$, perpendicular distance is 0.0635 m and yielding strength of steel is 250 MPa. The factor of safety is 5.8.

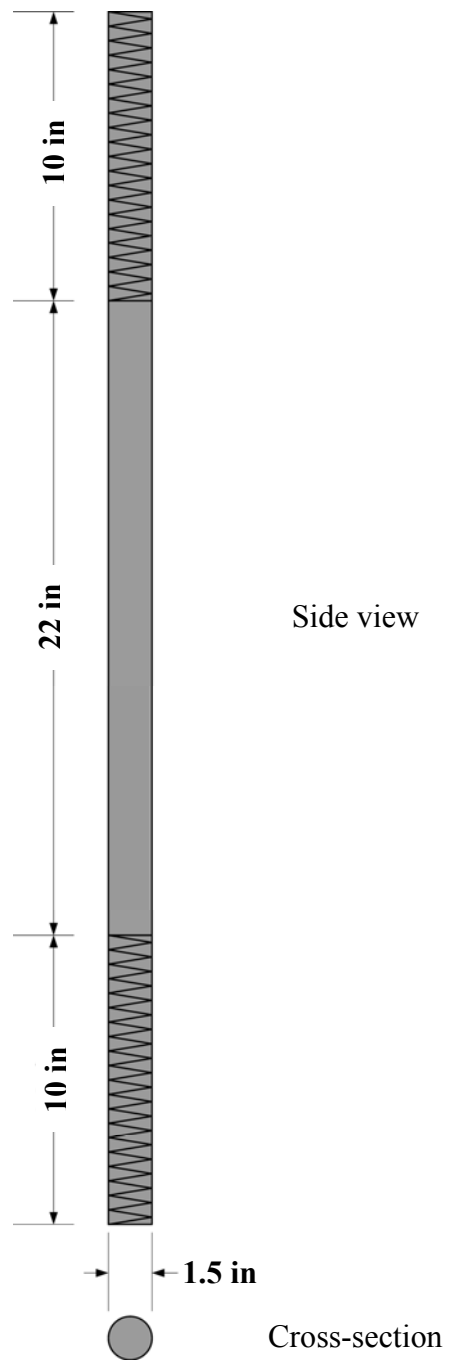


Figure 3.6 Circular steel column linking between lower steel plate and steel stand.

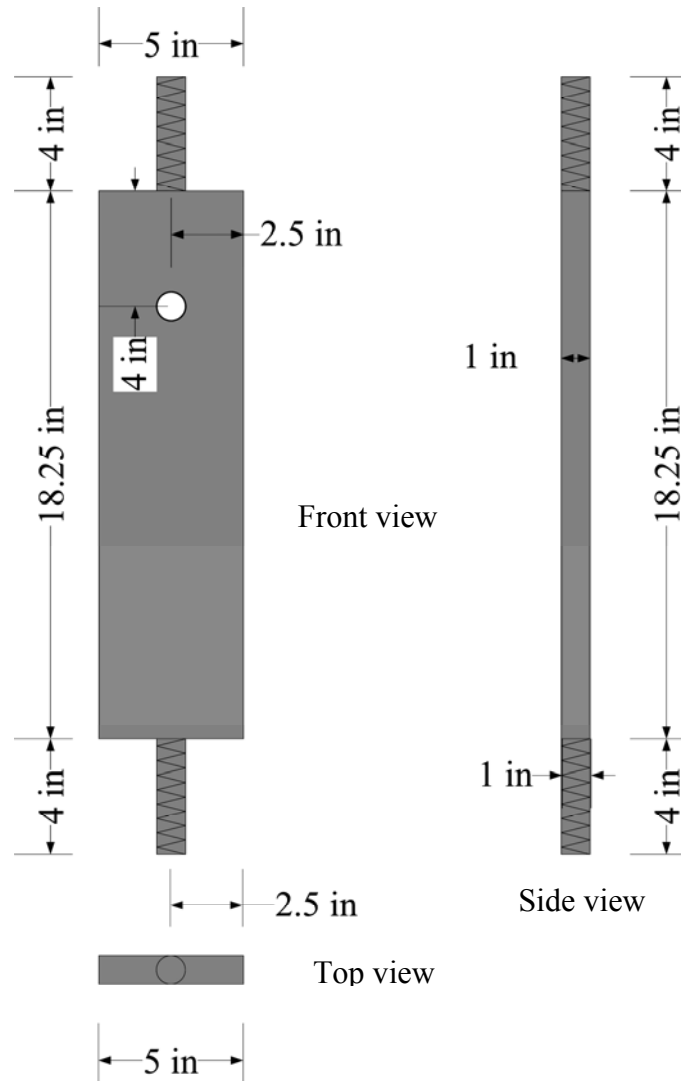


Figure 3.7 Rectangular steel column used for hosting the cantilever beam.

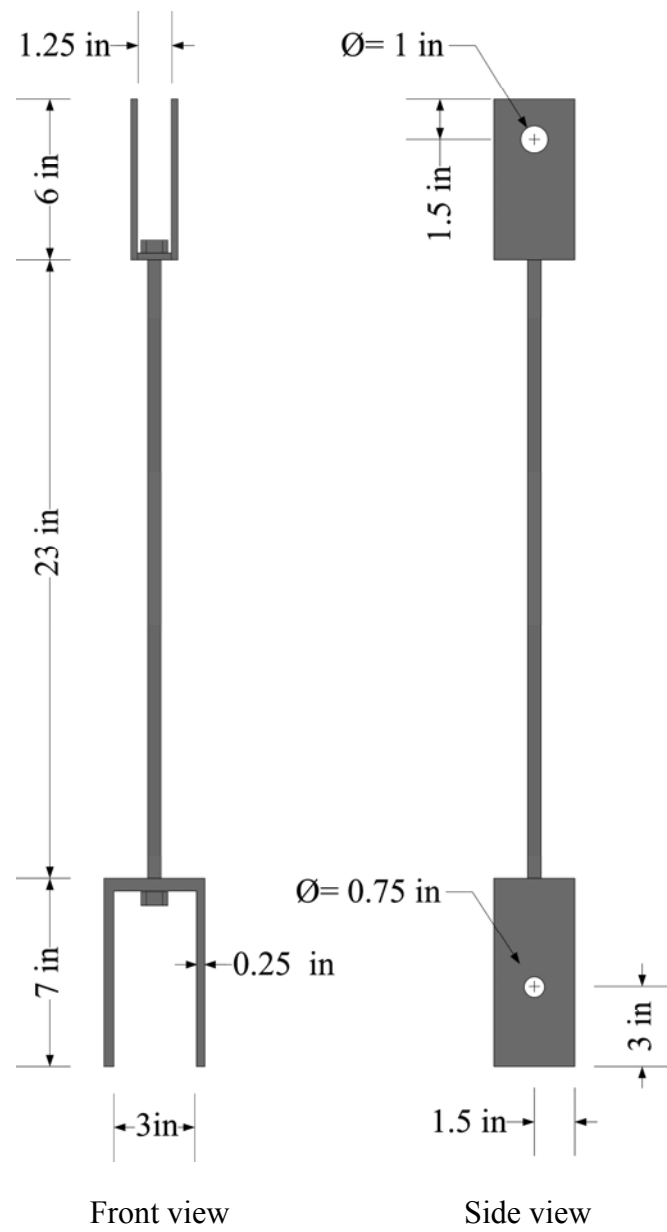


Figure 3.8 Steel rod and U-links used for connecting between cantilever beam and lower steel bar

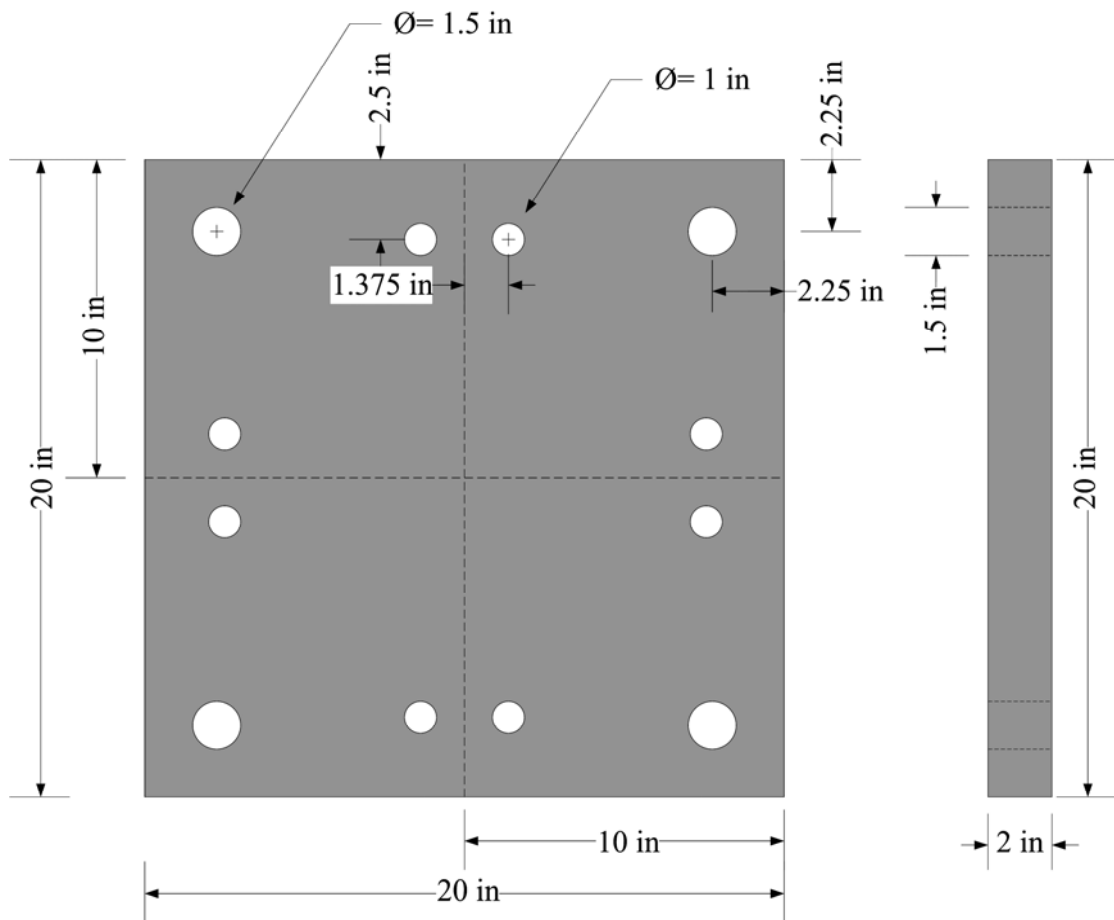


Figure 3.9 Lower steel plate.

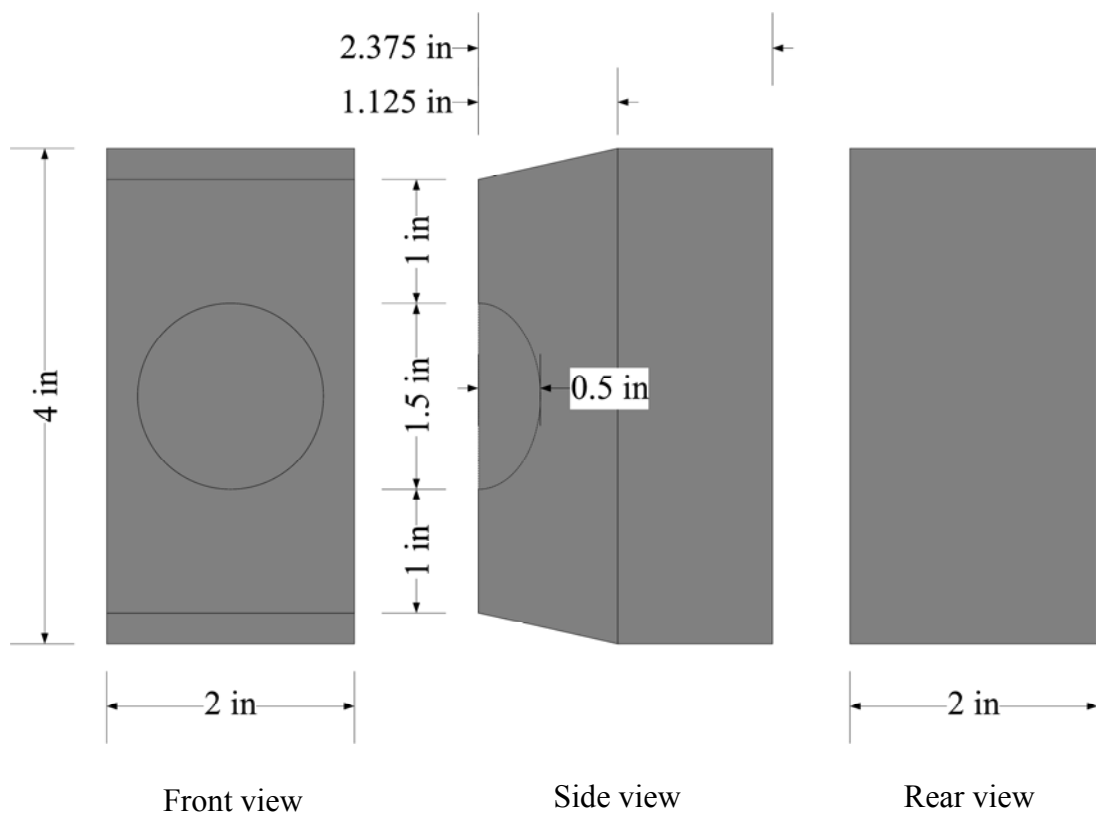


Figure 3.10 Lateral loading platen for $5 \times 5 \times 10 \text{ cm}^3$ specimen.

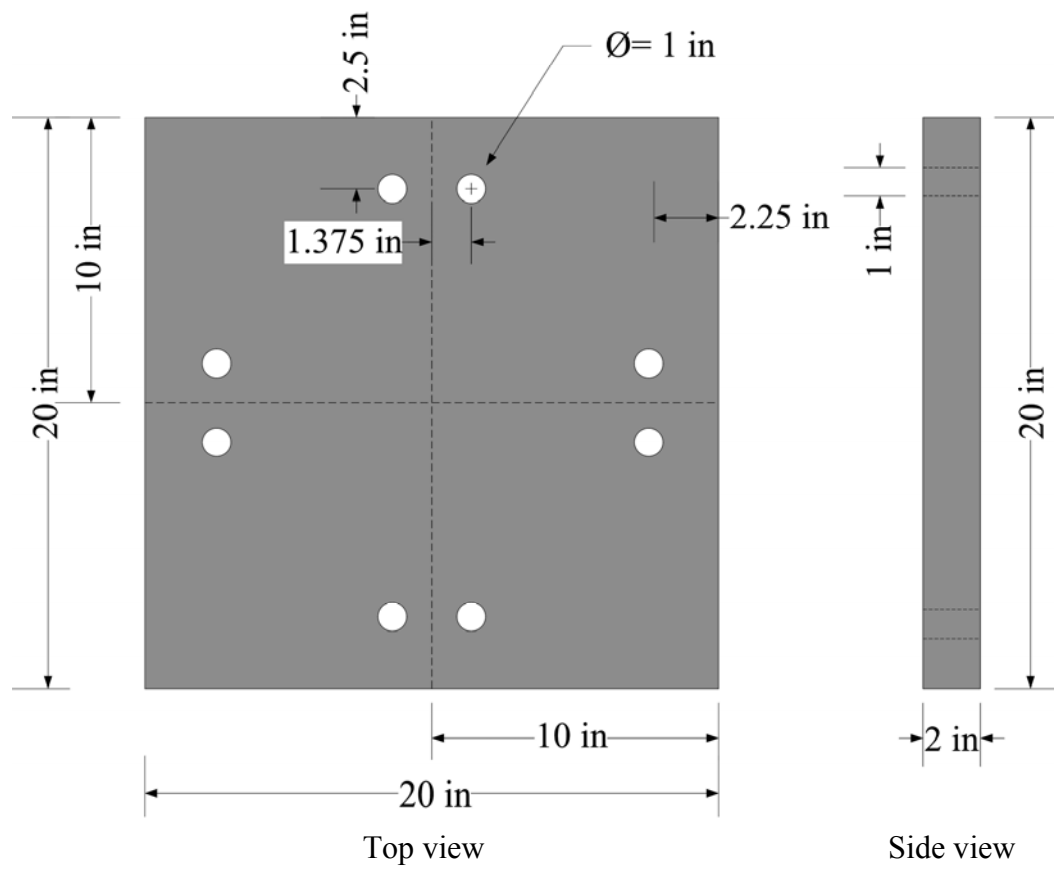


Figure 3.11 Upper steel plate

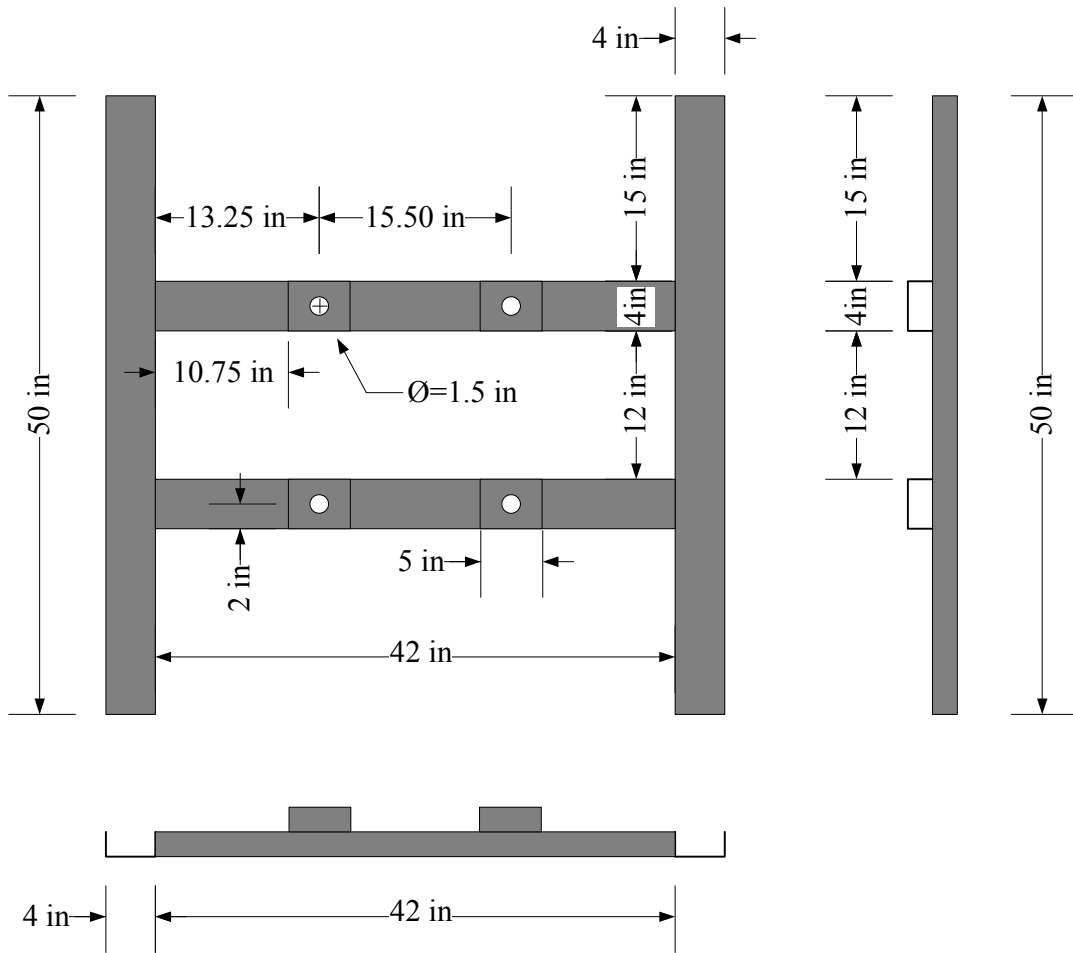


Figure 3.12 Steel stand supporting the frame.

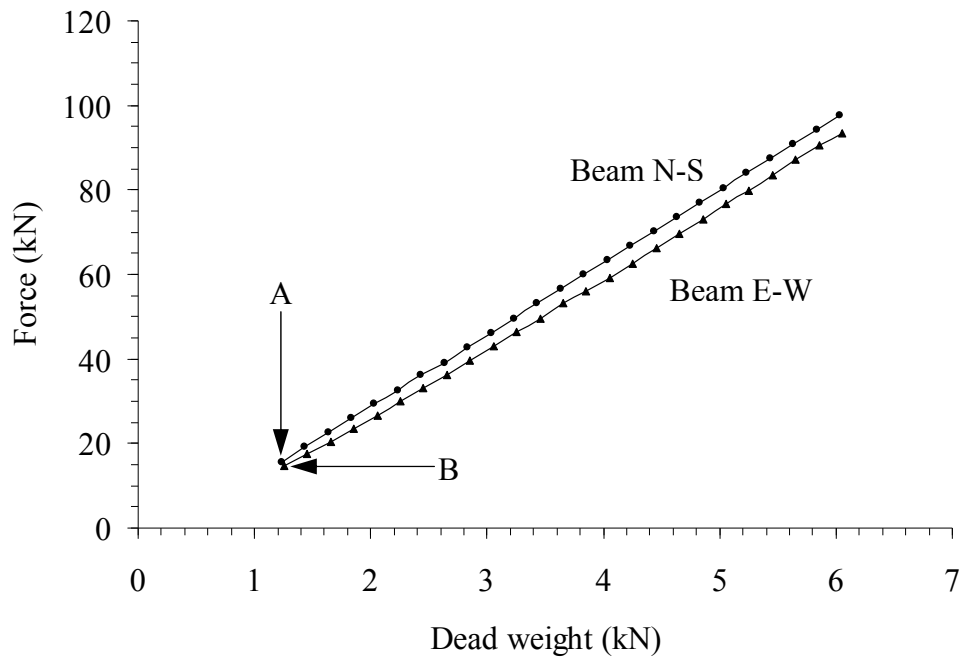


Figure 3.13 Calibration curves obtained from electronic load cell of beam N-S and beam E-W. A and B indicate the forces at which only lower steel bar is hanging on the beams.

Table 3.1 Mechanical properties of structural steel A36. (Hibbeler, 2003)

Density (Mg/m ³)	Poisson's Ratio (ν)	Modulus of Elasticity (GPa)	Modulus of Rigidity (GPa)	Yield Strength (MPa)		Ultimate Strength (MPa)	
				Tens	Com	Tens	Com
7.85	0.32	200	75	250	250	400	400

3.3.2 Factor of safety of lower beam

The factor of safety of lower beam in bending is calculated by using equation (3.1). The maximum internal moment in cantilever beam is 6,750 N.m, the moment of inertia is $6.8 \times 10^{-6} \text{ m}^4$, perpendicular distance is 0.076 m and yielding strength of steel is 250 MPa. The factor of safety from the calculation is 3.3.

3.3.3 Factor of safety of rectangular column

The factor of safety of rectangular column in compression stress condition is calculated by: (Hibbeler, 2003)

$$P_{cr} = \frac{\pi^2 EI}{L^2} \quad (3.2)$$

where P_{cr} is critical load capacity of column, E is modulus of elasticity of steel, I is the moment of inertia of the cross-section area and L is length of column.

The maximum axial load uses is 1,500 N per column. The modulus of elasticity of beam is 200 GPa, the moment of inertia is $1.7 \times 10^{-7} \text{ m}^4$ yielding strength of steel is 250 MPa and length of column is 0.463 m. The critical axial load on the column just before it begins to buckle is 1,562 kN. The factor of safety for rectangular column is calculated as 1,041.

3.3.4 Factor of safety of hinge

Hinge is a steel pin for connecting between cantilever beam and rectangular column. Factor of safety calculation for bending is uses (3.1). The slope and deflection of hinge is calculated using are equation (Hibbeler, 2003).

$$\theta_{\max} = \frac{-PL^2}{16EI} \quad (3.3)$$

$$v_{\max} = \frac{-PL^3}{48EI} \quad (3.4)$$

where θ_{\max} is maximum slope of hinge, v_{\max} is maximum deflection or vertical displacement of hinge, P is vertical load on the hinge, L is length of hinge, E is modulus of elasticity of steel and I is the moment of inertia.

The maximum load on hinge is designed as 5,410 N. The modulus of elasticity of beam is 200 GPa, the moment of inertia is $2 \times 10^{-8} \text{ m}^4$, yielding strength of steel is 250 MPa and length of hinge is 0.11 m. Factor of safety for hinge is 1.3, maximum slope of hinge is 0.001 degrees and maximum deflection or vertical displacement of hinge is 0.000038 m.

3.3.5 Factor of safety of U-link and steel rod

Factor of safety of U-link is calculated at the screws connecting between U-link and steel rod. Tensile stress and screw areas for U-link and steel rod are calculated by using equations (Norton, 2006).

$$\sigma_t = \frac{F}{A_t} \quad (3.5)$$

$$A_t = \frac{\pi}{4} \left(\frac{d_p + d_r}{2} \right)^2 \quad (3.6)$$

$$d_p = \frac{d - 0.649519}{N} \quad (3.7)$$

$$d_r = \frac{d - 1.299038}{N} \quad (3.8)$$

where σ_t is tensile stress, F is axial tensile load, A_t is tensile stress area, d_p is pitch diameter, d_r is minor (root) diameter, d is outside (major) diameter and N is number of threads per inch.

Maximum axial tensile stress is designed as 2,900 N, yielding strength of steel is 250 MPa, screws for U-link and steel rod uses coarse screw thread that has outer diameter 0.5 in, minor diameter is 0.4001 in with 13 threads per inch, and the tensile stress area is 0.1419 in². Factor of safety at the screws for U-link and steel rod is 7.8.

3.3.6 Factor of safety at screw of rectangular column

Factor of safety of rectangular column is calculated at the screws connecting between upper and lower steel plate. Tensile stress and screw areas at screw are calculated by using equations (3.5) through (3.8).

Maximum axial tensile stress is designed as 1,500 N per column, yielding strength of steel is 250 MPa, screws for rectangular column uses fine screw thread that has outer diameter 1 in, minor diameter is 0.8917 in with 12 threads per inch, and the tensile stress area is 0.6631 in². Factor of safety at the screws for rectangular column is 71.4.

CHAPTER IV

LABORATORY TESTING

4.1 Introduction

The objectives of the laboratory testing are to assess the performance of the developed polyaxial load frame and to compare the test results with the convention triaxial compression results.

4.2 Sample preparation

The tested rocks are sandstones from four sources: Phu Phan, Phra Wihan and Phu Kradung (hereafter designated as PP, PW and PK) formations. They belong to the Khorat group and widely expose in the north and northeast of Thailand. X-ray diffraction analyses have been performed to determine their mineral compositions. Table 4.1 summarizes the results. These fine-grained quartz sandstones are selected for this study primarily because they have highly uniform texture, grain size and density. The conventional triaxial compressive strength test uses cylindrical specimens with a nominal diameter of 50 mm with a thickness-to-diameter ratio of 2.0 to comply with ASTM D7012-04. The specimens for true triaxial compressive strength testing are rectangular blocks with a nominal dimension of $5 \times 5 \times 10 \text{ cm}^3$ (Figure 4.1).

Table 4.1 Mineral compositions of tested sandstones.

Rock Name	Density (g/cc)	Color	Compositions				
			Quartz (%)	Albite (%)	Kaolinite (%)	Feldspar (%)	Mica (%)
PW sandstone	2.35	white	99.47	-	0.53	-	-
PP sandstone	2.45	yellow	98.40	-	-	-	1.60
PK sandstone	2.63	green	48.80	46.10	5.10	-	-

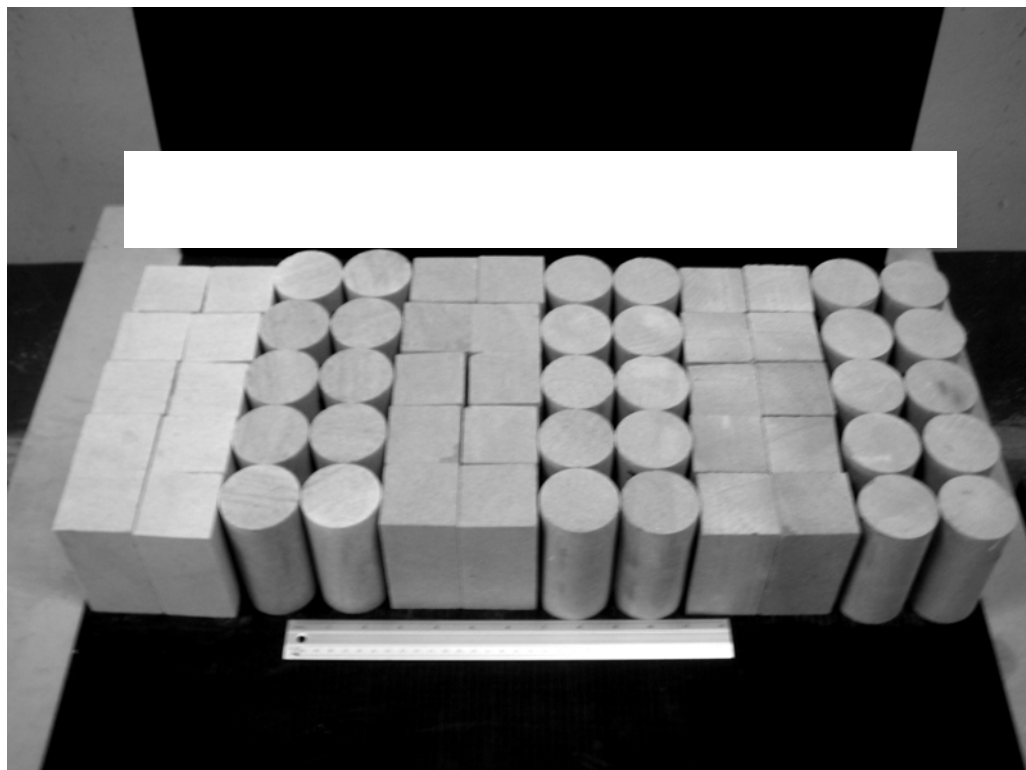


Figure 4.1 Sandstone specimens prepared for the conventional triaxial compressive strength test and true triaxial compressive strength test. Left is PW, middle is PP and right is PK.

4.3 Characterization tests

The characterization tests performed here include the uniaxial compression tests and triaxial compression tests. The objective of these tests is to develop a data basis to compare with the true triaxial compression test results.

4.3.1 Uniaxial compression tests

The primary objective of uniaxial compression test is to determine the unconfined compressive strength of the sandstone specimens. The test procedure followed the ASTM standard (ASTM D7012-04) and the suggest method by ISRM (Brown, 1981). Uniform axial load was applied to the sandstone cylinder at a constant rate of 0.1 MPa/second until failure. The axial displacements are monitored by dial gauges with a precision of 0.001 mm. Figures 4.2 through Figure 4.4 plot the stress-strain curves for three types of sandstone. The average elastic modulus (E) of PK, PP and PW sandstones are 8.6 ± 0.5 , 11.9 ± 1.2 and 11.5 ± 1.2 GPa. The strengths of PK, PP and PW sandstones are 73.3 ± 3.2 , 73.6 ± 4.5 and 63.7 ± 5.5 MPa.

4.3.2 Conventional triaxial compression tests

The triaxial compressive strength test method follows the ASTM D7012-04. The constant confining pressures vary from 1, 2, 3 and 6 MPa. After the constant confining pressure is applied while the axial stress is increased until failure occurs. A high precision pipette is used to collect the excess oil released from the triaxial cell by the specimen dilation (Figure 4.5). It will be used to calculate the volumetric strain (ε_V) of the specimen during loading:

$$\varepsilon_V = (V_O - V_S) / V_R \quad (4.1)$$

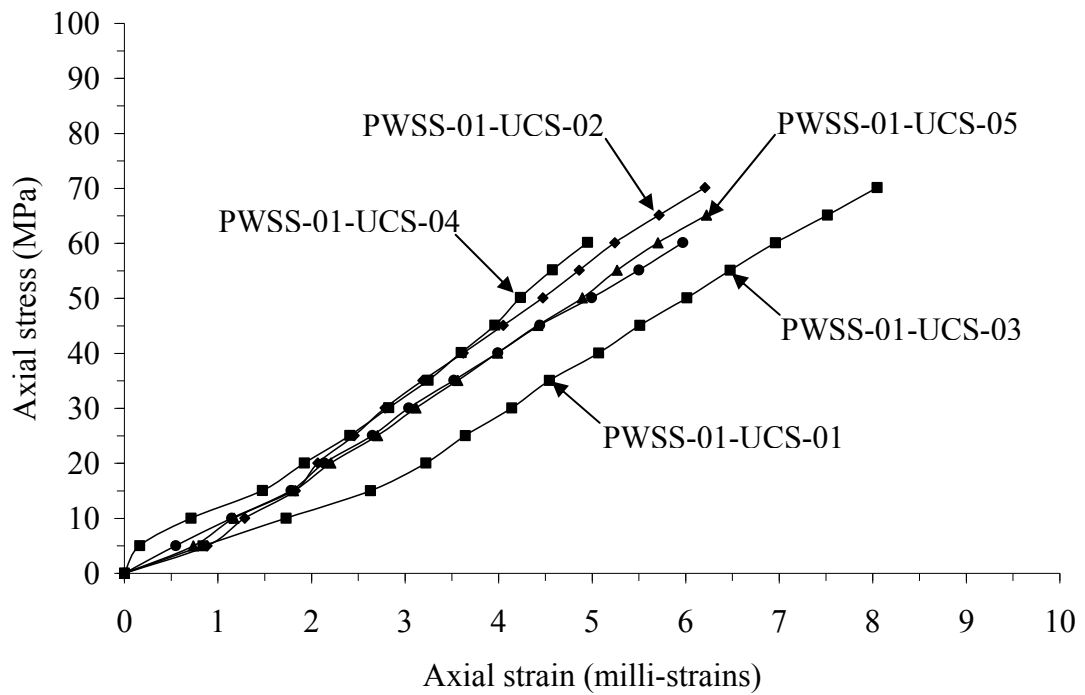


Figure 4.2 Stress-strain curves of Phra Wihan sandstone from uniaxial compressive strength test.

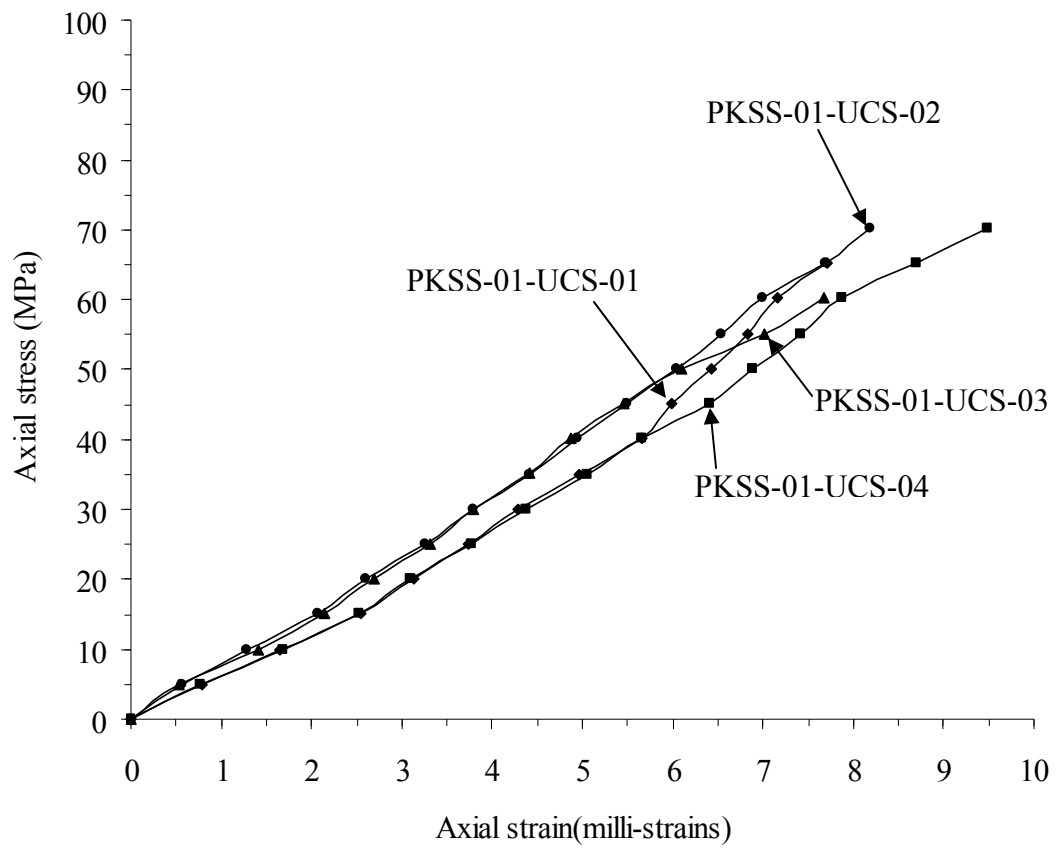


Figure 4.3 Stress-strain curves of Phu Kradung sandstone from uniaxial compressive strength test.

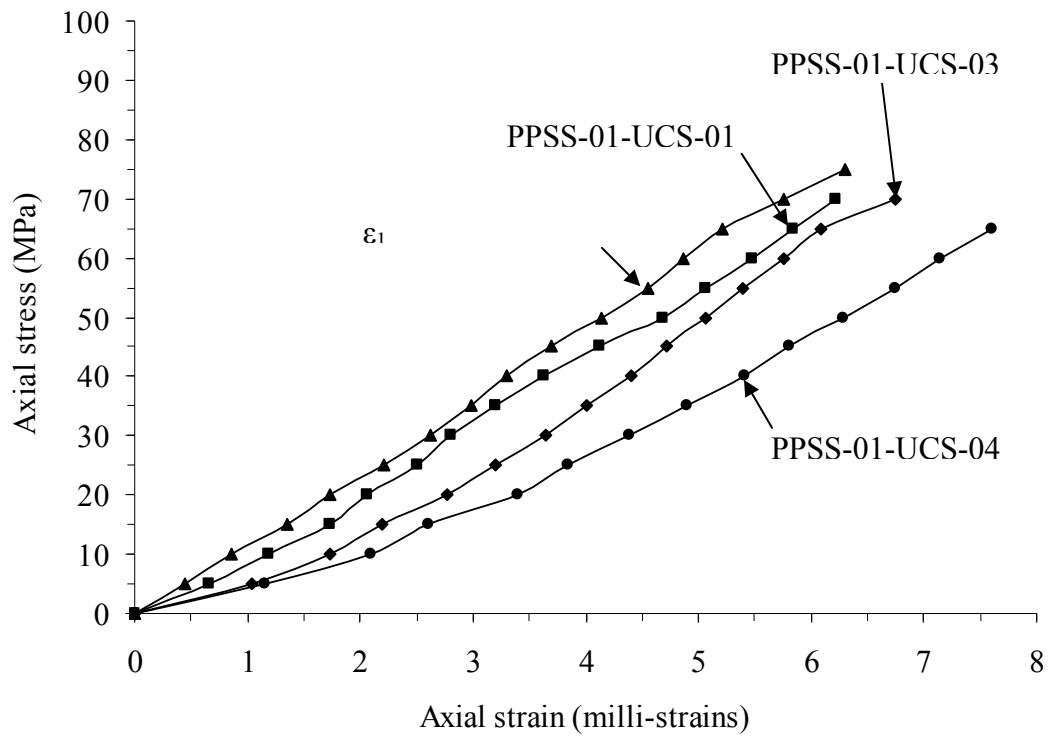


Figure 4.4 Stress-strain curves of Phu Phan sandstone from uniaxial compressive strength test.

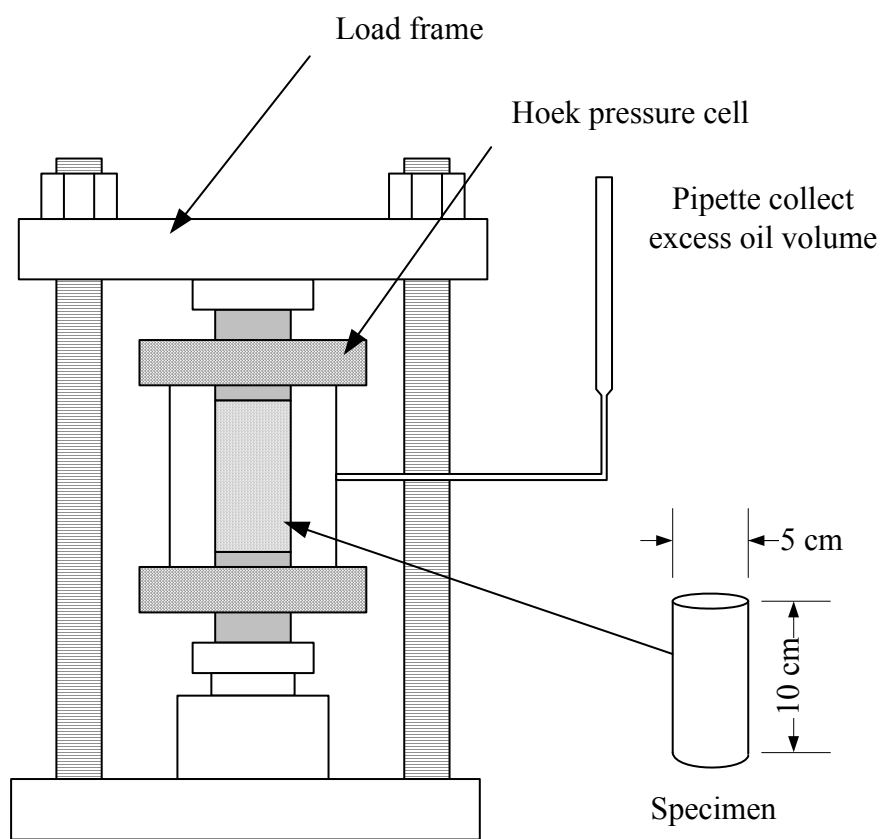


Figure 4.5 Laboratory set-up for the conventional triaxial compressive strength test.

where V_O is the excess oil volume, V_S is the volume of oil displaced by loading platen, and V_R is the volume of rock specimen.

The test results of three types sandstone are plotted in Figures 4.6 through Figure 4.8. Table 4.2 summarizes the test parameters and the results of the triaxial tests.

4.4 True triaxial compression tests

The true triaxial compression tests are performed to determine the deformation behavior of the PK, PP and PW sandstones under true triaxial stresses. The intermediate (σ_2) and minimum (σ_3) principal stresses are maintained constant

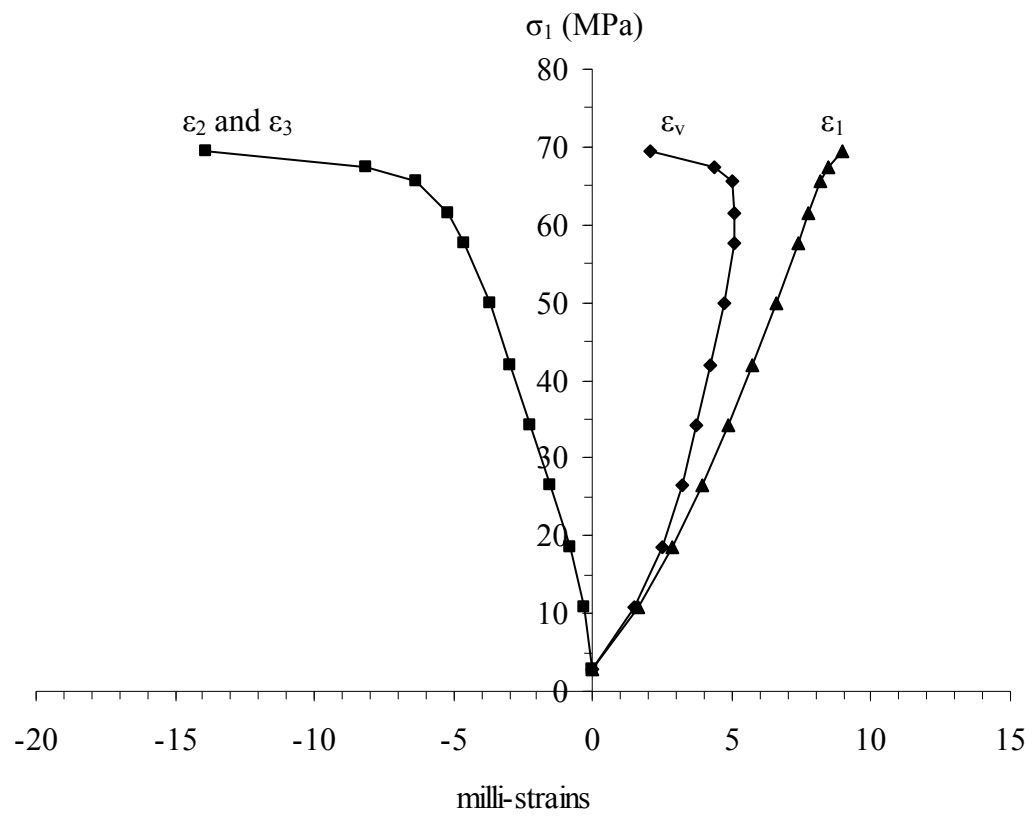


Figure 4.6 Stress-strain curves of Phu Kradung sandstone at condition $\sigma_2 = \sigma_3 = 1$ MPa.

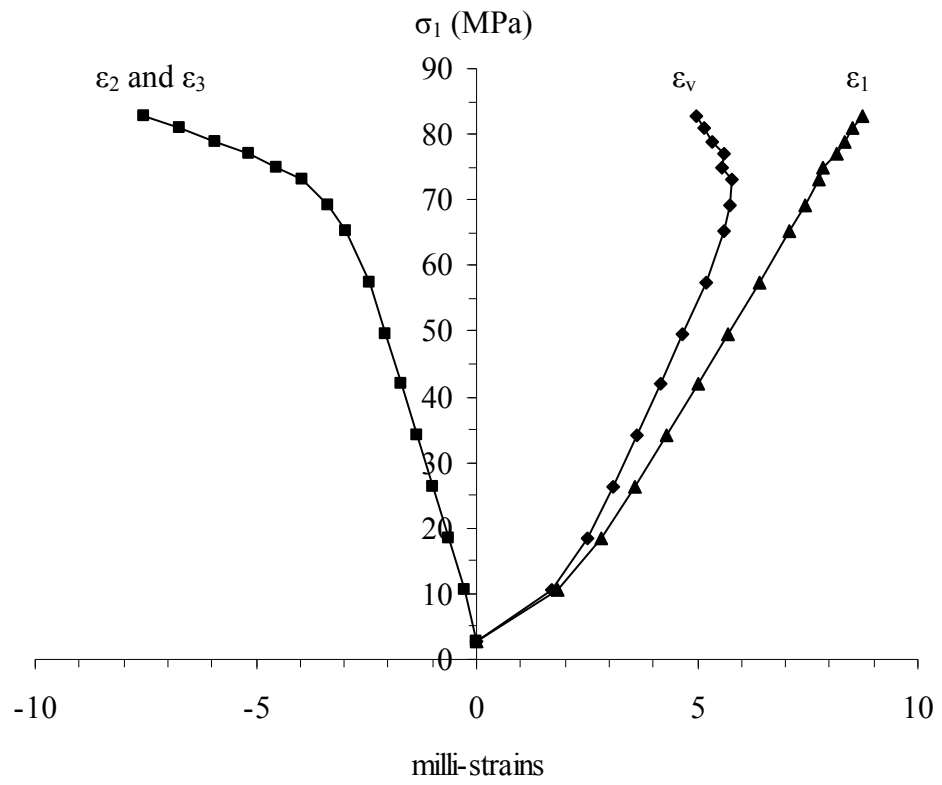


Figure 4.7 Stress-strain curves of Phu Phan sandstone at condition $\sigma_2 = \sigma_3 = 1$ MPa.

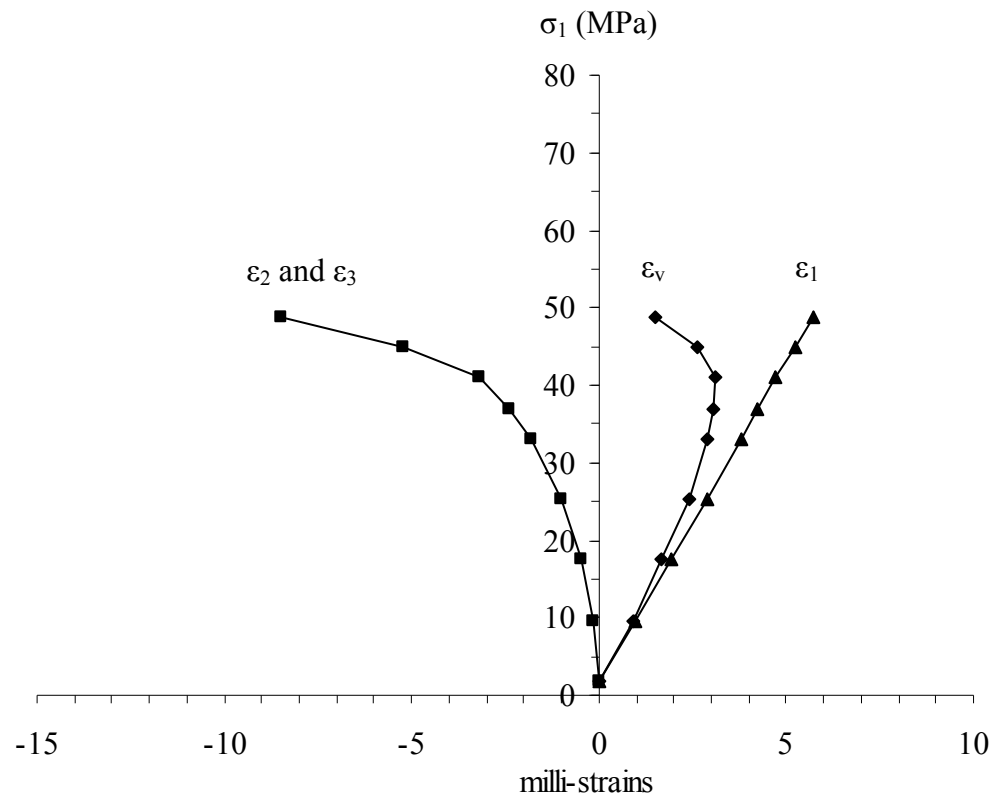


Figure 4.8 Stress-strain curves of Phra Wihan sandstone at condition $\sigma_2 = \sigma_3 = 2$ MPa.

Table 4.2 Elastic properties from conventional triaxial compression tests.

Rock types	Sample No.	Confining Pressure (MPa)	E (GPa)	ν
Phra Wihan Sandstone	PWSS-TR-01	1	9.3	0.23
	PWSS-TR-02	2	9.1	0.25
	PWSS-TR-03	3	8.5	0.33
	PWSS-TR-04	6	11.9	0.29
Average \pm SD			9.7 \pm 1.5	0.28 \pm 0.04
Phu Kradung Sandstone	PKSS-TR-01	1	8.1	0.27
	PKSS-TR-02	2	8.9	0.24
	PKSS-TR-03	3	9.1	0.23
Average \pm SD			8.7 \pm 0.5	0.25 \pm 0.02
Phu Phan Sandstone	PPSS-TR-01	1	9.6	0.25
	PPSS-TR-02	2	9.3	0.13
	PPSS-TR-03	3	10.1	0.18
Average \pm SD			9.6 \pm 0.4	0.19 \pm 0.06

while σ_1 is increased until failure. Here the constant σ_2 is varied from 0 to 17 MPa, and σ_3 from 0 to 6 MPa. Neoprene sheets are used to minimize the friction at all interfaces between the loading platen and the rock surface. Figure 4.9 shows the applied principal stress directions with respect to the bedding planes for all specimens. The measured sample deformations are used to determine the strains along the principal axes during loading. The failure stresses are recorded and mode of failure examined.

4.4.1 Test method

Prepared rock specimen has a nominal dimension of $5 \times 5 \times 10 \text{ cm}^3$. Use neoprene sheet on six side of rock specimen. Install hydraulic pump with hydraulic cylinder and check level of oil in pump. The rock specimen with neoprene is placed on the loading platen. The lateral loading platens contact the sides of specimen. Raise the cantilever beam in North and South direction. Put the rock specimen with neoprene and lateral loading platen into loading machine. Lateral loading platen must be straight with half spherical bolt. Slowly reduce the level of cantilever beam until half spherical bolt and lateral loading platen are in contact. Raise the cantilever beam in West and East direction. Place the lateral loading platen on remains side of specimen. Slowly reduce level of cantilever beam. Place the loading platens on top and bottom of specimen. Increase oil pressure from hydraulic pump until specimen, loading platen and upper steel plate are in contact. If confining pressure is more than 6.4 kN, install the lower beam in N-S direction with U-links for carry dead weight by using steel axle. Beam in W-E direction is installed similar with beam in N-S direction. Put a steel plate (Dead weight) on the middle of each beam to increase lateral load. Axial load and lateral

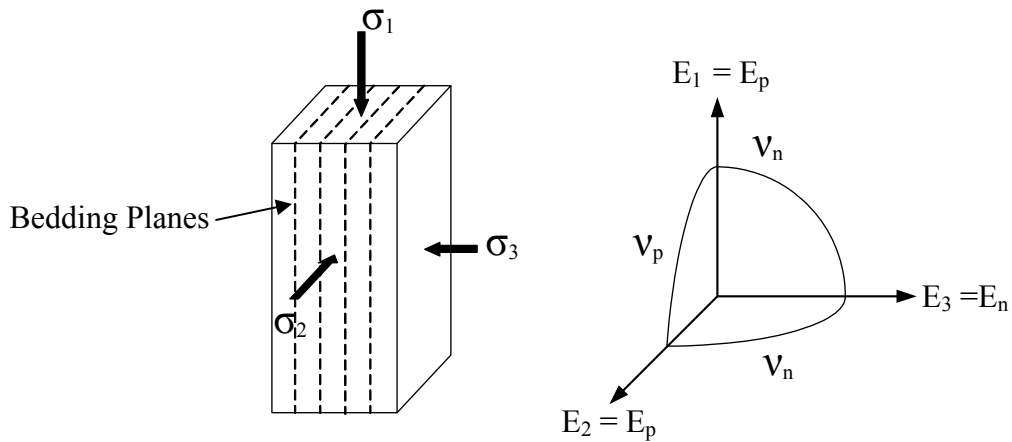


Figure 4.9 Directions of loading with respect to the bedding planes (left). Elastic parameters for transversely isotropic conditions (right).

load must be increased simultaneously up to pre-test pressure so that rock specimen will be in hydrostatic condition. Install dial gages in monitoring directions.

4.4.2 Test results

The elastic modulus and Poisson's ratio are calculated for the directions normal and parallel to the bedding planes. Under the stress orientation used here where σ_1 and σ_2 are parallel to the bedding planes, the three-dimensional principal stress-strain relations given by Jaeger and Cook (1979) can be simplified to obtain a set of governing equations for a transversely isotropic material as:

$$\varepsilon_1 = \frac{\sigma_1}{E_p} - \frac{\sigma_2 v_p}{E_p} - \frac{\sigma_3 v_n}{E_n} \quad (4.2)$$

$$\varepsilon_2 = -\frac{\sigma_1 v_p}{E_p} + \frac{\sigma_2}{E_p} - \frac{\sigma_3 v_n}{E_n} \quad (4.3)$$

$$\varepsilon_3 = -\frac{\sigma_1 \nu_n}{E_p} - \frac{\sigma_2 \nu_n}{E_p} + \frac{\sigma_3}{E_n} \quad (4.4)$$

where: σ_1 , σ_2 and σ_3 are principal stresses, ε_1 , ε_2 and ε_3 are principal strains, E_n and E_p are elastic moduli normal and parallel to the bedding planes, and ν_n and ν_p are Poisson's ratio's on the planes normal and parallel to the bedding.

The calculations of the Poisson's ratios and tangent elastic moduli are made at 50% of the maximum principal stress. The sandstone exhibit a small transversely isotropic behavior. Table 4.3 summarizes the elastic parameters with respect to the bedding plane orientation of true triaxial compression tests. Figures 4.10 through Figure 4.24 plot the stress-strain curves from the start of loading to failure for PW, PP and PK sandstone specimens in true triaxial stress state.

4.5 Comparisons

The elastic modulus in the direction normal to the bedding planes is slightly lower than that parallel to the bedding planes. The Poisson's ratio on the plane parallel to the beds is more than that across the beds. Table 4.4 summarizes the elastic parameters for PW, PP and PK sandstone specimens in characterization tests and true triaxial compression test.

Table 4.3 Elastic properties from true triaxial compression test.

Rock type	Sample No.	E_p (GPa)	ν_p	E_n (GPa)	ν_n
Phra Wihan Sandstone	PWSS-PX-01	11.2	0.38	9.1	0.28
	PWSS-PX-02	10.7	0.37	9.2	0.30
	PWSS-PX-03	12.0	0.36	9.5	0.22
	PWSS-PX-04	10.4	0.33	8.9	0.16
	PWSS-PX-05	11.7	0.29	10.2	0.20
Average \pm SD		11.2 \pm 0.7	0.35 \pm 0.04	9.3 \pm 0.51	0.23 \pm 0.05
Phu Kradung Sandstone	PKSS-PX-01	11.0	0.37	9.6	0.24
	PKSS-PX-02	10.4	0.20	8.8	0.18
	PKSS-PX-03	11.5	0.24	9.1	0.23
	PKSS-PX-04	11.2	0.36	10.6	0.25
	PKSS-PX-05	10.6	0.27	9.0	0.20
Average \pm SD		10.9 \pm 0.4	0.29 \pm 0.07	9.4 \pm 0.7	0.22 \pm 0.03
Phu Phan Sandstone	PPSS-PX-01	10.7	0.46	9.6	0.25
	PPSS-PX-02	10.5	0.20	9.3	0.13
	PPSS-PX-03	11.3	0.32	10.1	0.18
	PPSS-PX-04	11.5	0.19	8.6	0.11
	PPSS-PX-05	10.8	0.21	10.0	0.20
Average \pm SD		11.0 \pm 0.4	0.28 \pm 0.12	9.5 \pm 0.6	0.17 \pm 0.05

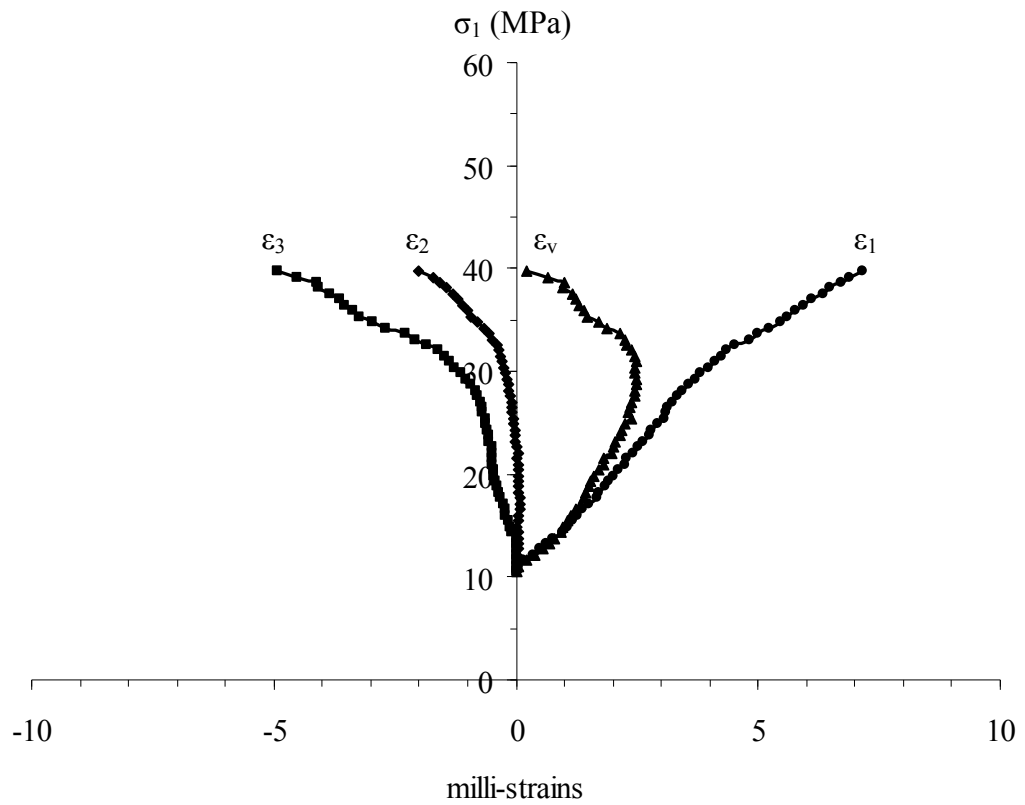


Figure 4.10 Stress-strain curves of Phra Wihan sandstone at condition $\sigma_2 = 10.1$ MPa and $\sigma_3 = 1.2$ MPa.

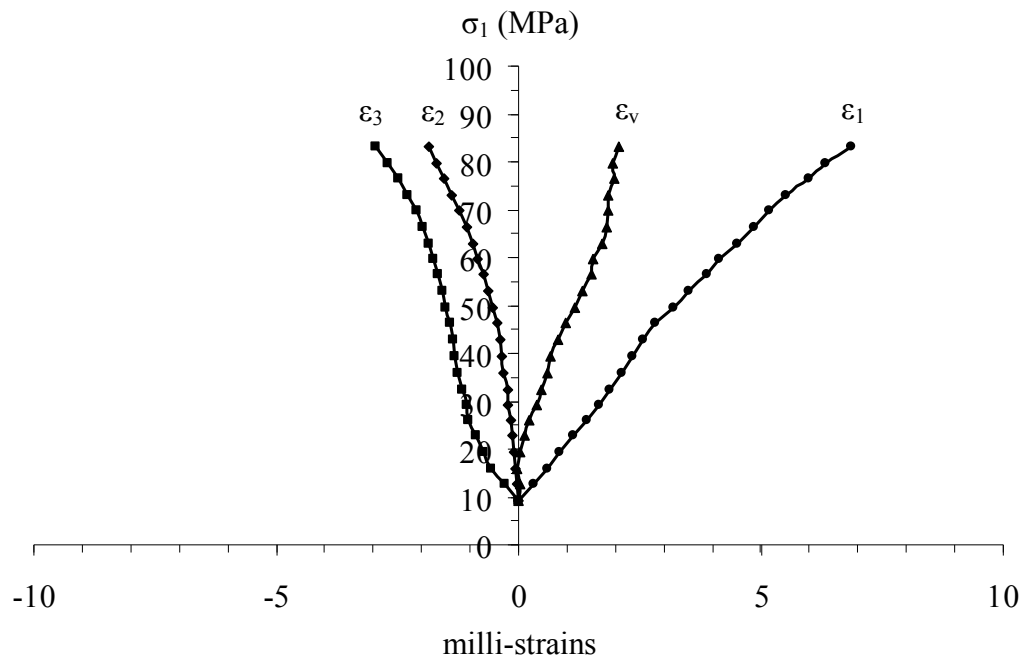


Figure 4.11 Stress-strain curves of Phra Wihan sandstone at condition $\sigma_2 = 6.6$ MPa and $\sigma_3 = 1.2$ MPa.

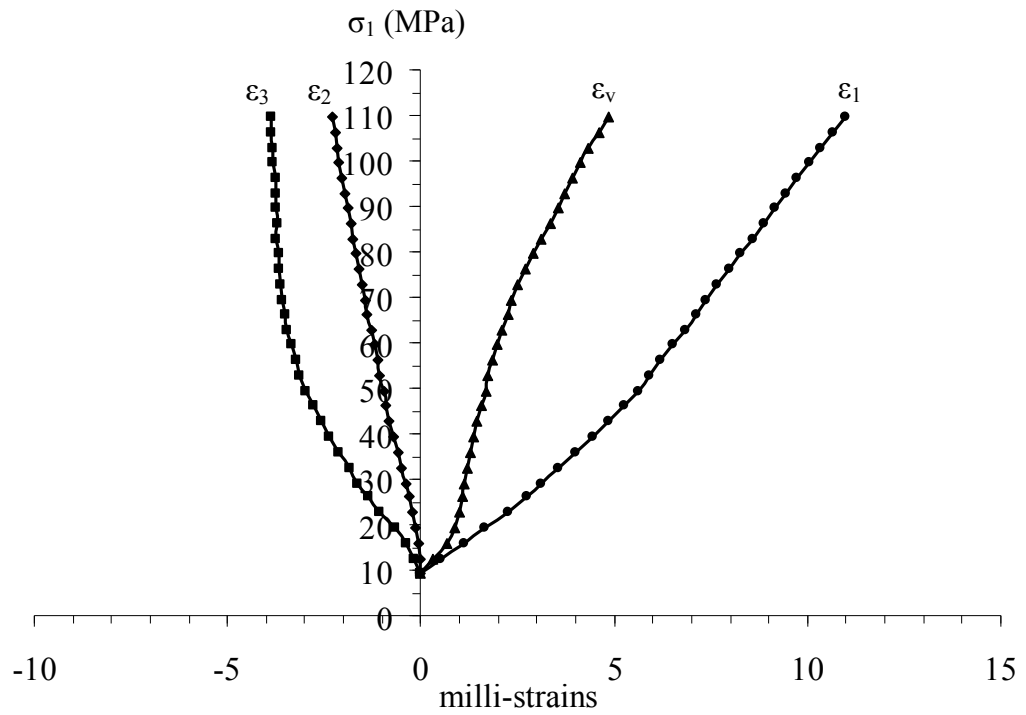


Figure 4.12 Stress-strain curves of Phra Wihan sandstone at condition $\sigma_2 = 6.6$ MPa and $\sigma_3 = 6.6$ MPa.

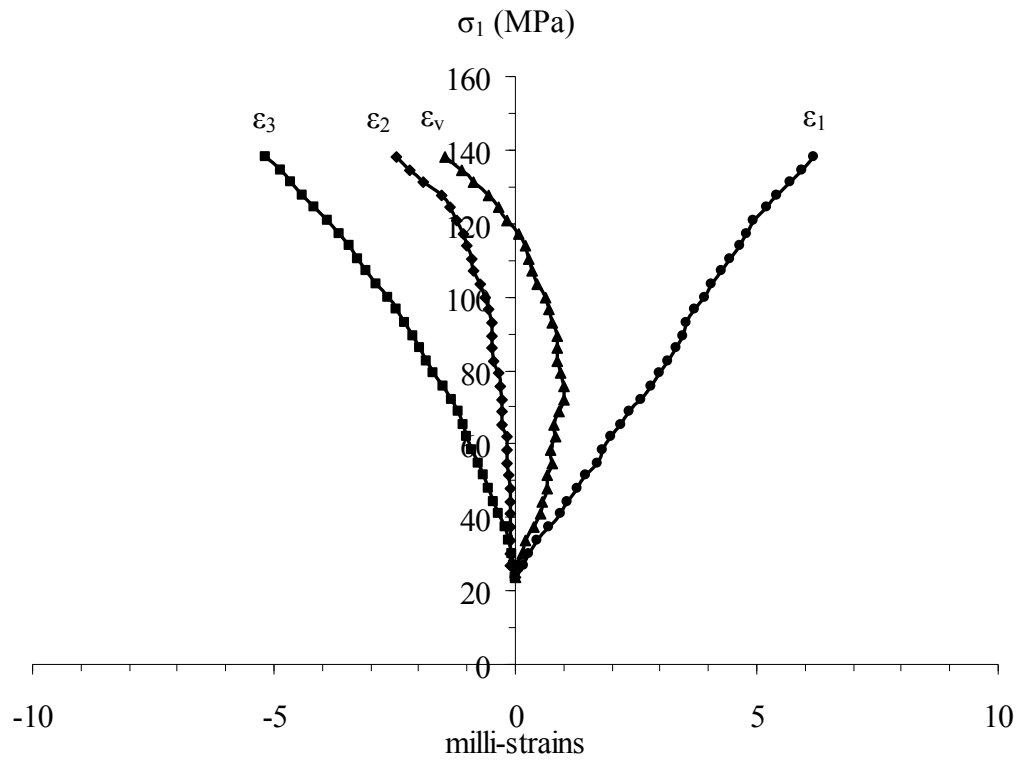


Figure 4.13 Stress-strain curves of Phra Wihan sandstone at condition $\sigma_2 = 10.1$ MPa and $\sigma_3 = 6.6$ MPa.

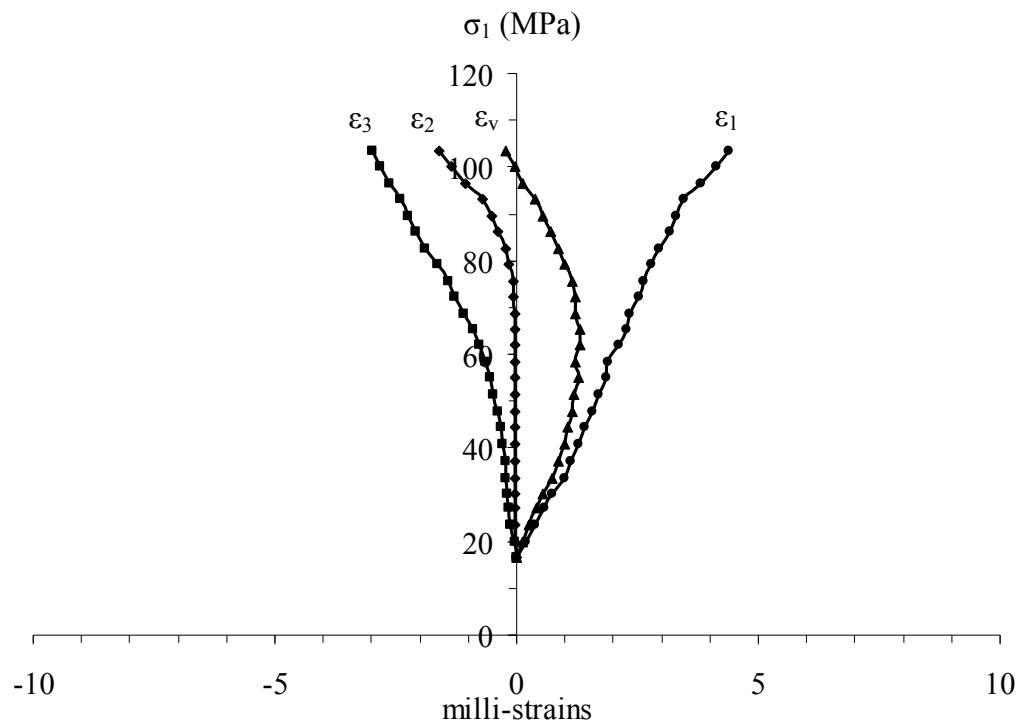


Figure 4.14 Stress-strain curves of Phra Wihan sandstone at condition $\sigma_2 = 6.6$ MPa and $\sigma_3 = 3$ MPa.

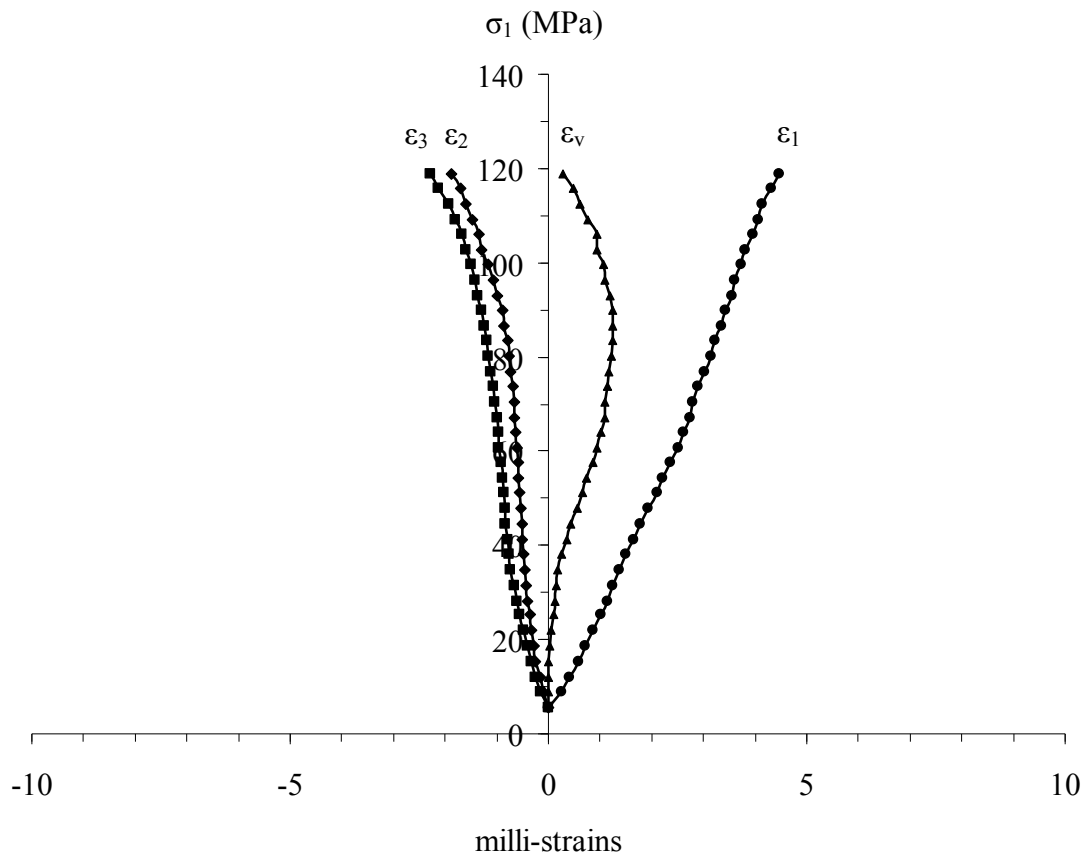


Figure 4.15 Stress-strain curves of Phu Phan sandstone at condition $\sigma_2 = 6.6$ MPa and $\sigma_3 = 3.0$ MPa.

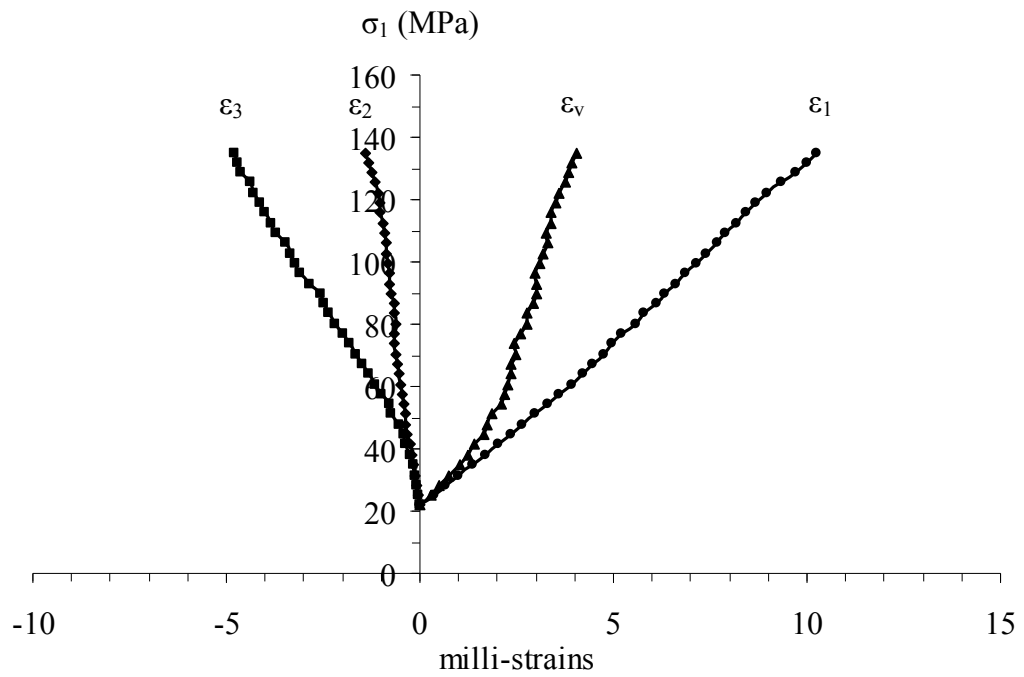


Figure 4.16 Stress-strain curves of Phu Phan sandstone at condition $\sigma_2 = 13.8$ MPa and $\sigma_3 = 6.6$ MPa.

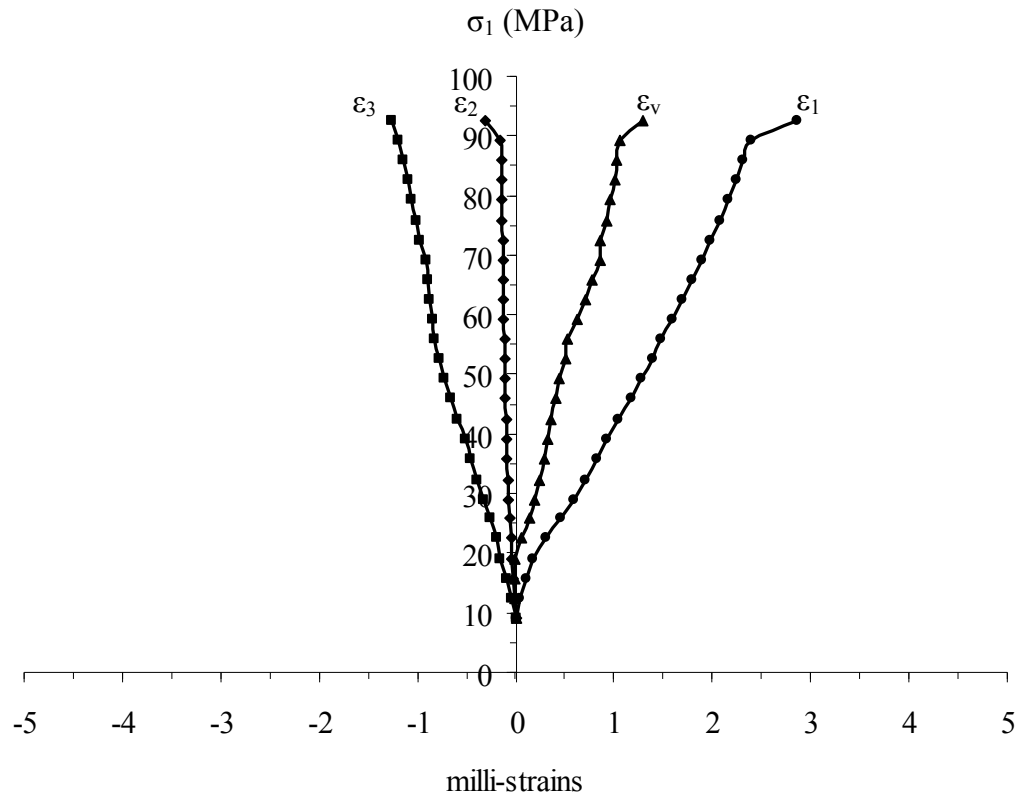


Figure 4.17 Stress-strain curves of Phu Phan sandstone at condition $\sigma_2 = 10.1$ MPa and $\sigma_3 = 0$ MPa.

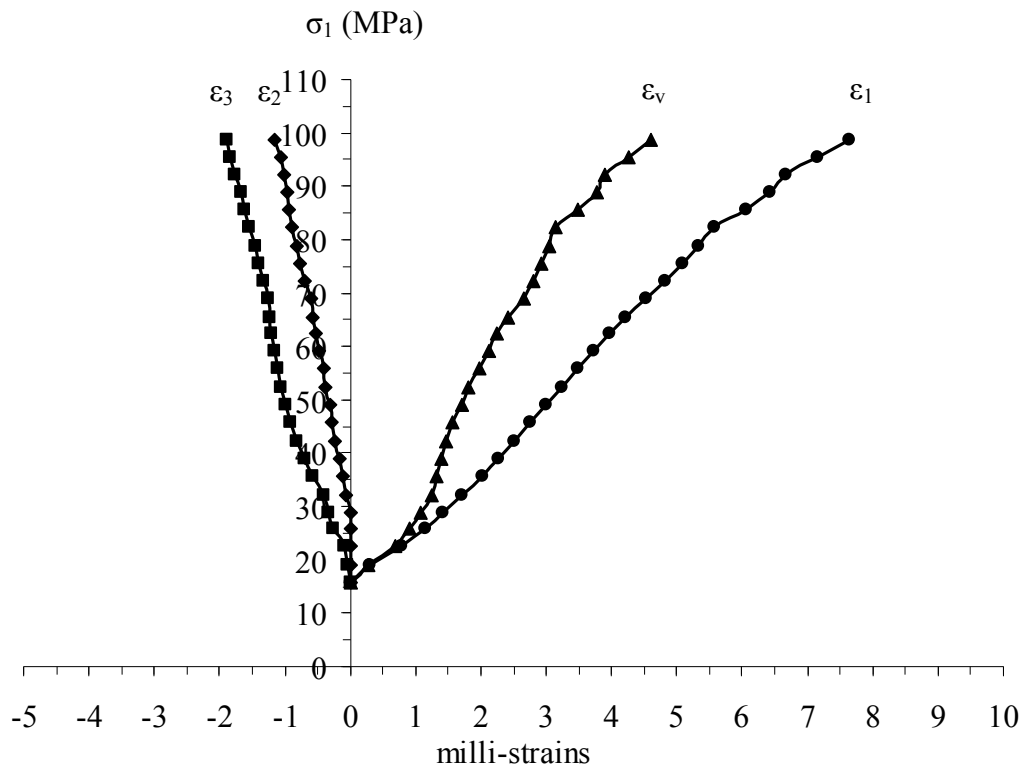


Figure 4.18 Stress-strain curves of Phu Phan sandstone at condition $\sigma_2 = 13.8$ MPa and $\sigma_3 = 0$ MPa.

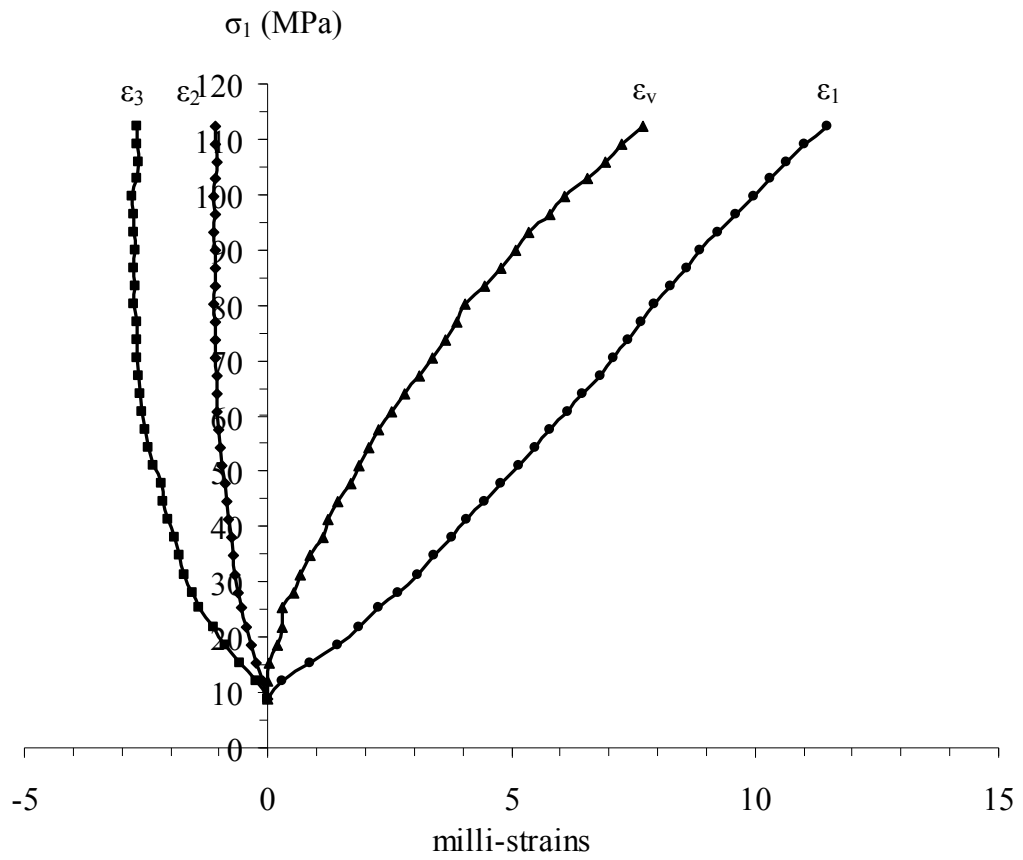


Figure 4.19 Stress-strain curves of Phu Phan sandstone at condition $\sigma_2 = 10.1$ MPa and $\sigma_3 = 3$ MPa.

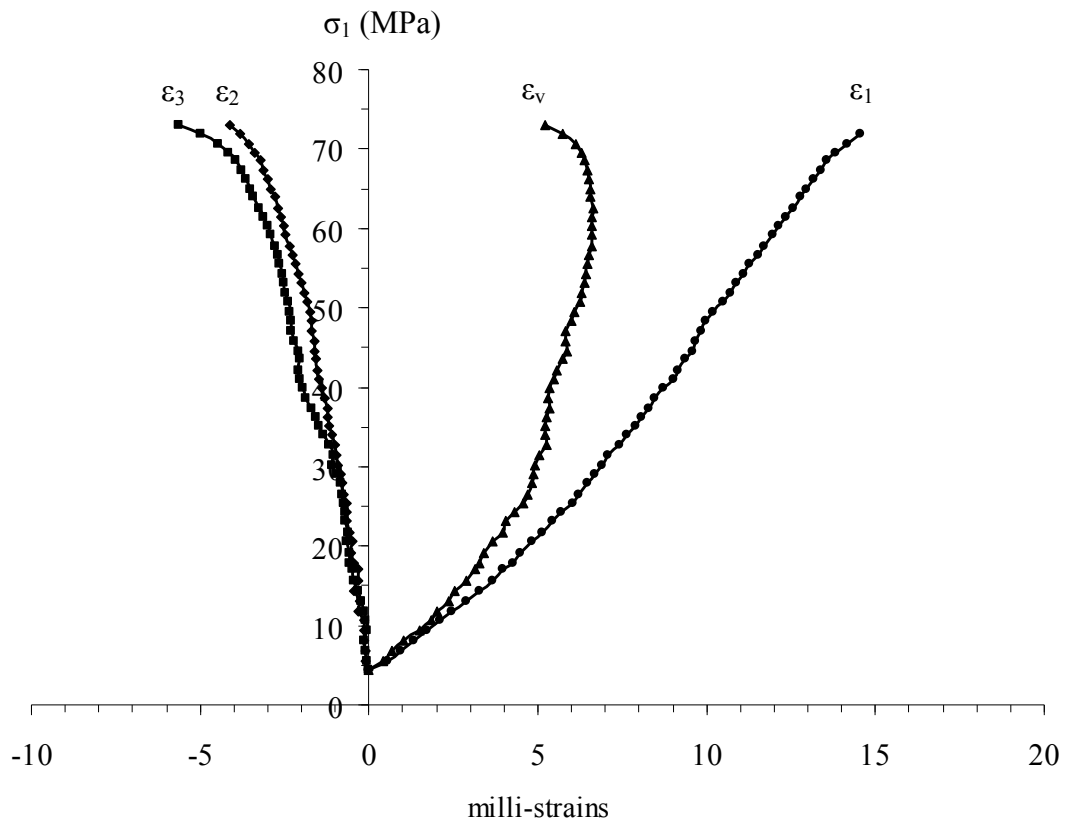


Figure 4.20 Stress-strain curves of Phu Kradung sandstone at condition $\sigma_2 = 6.6$ MPa and $\sigma_3 = 6.6$ MPa.

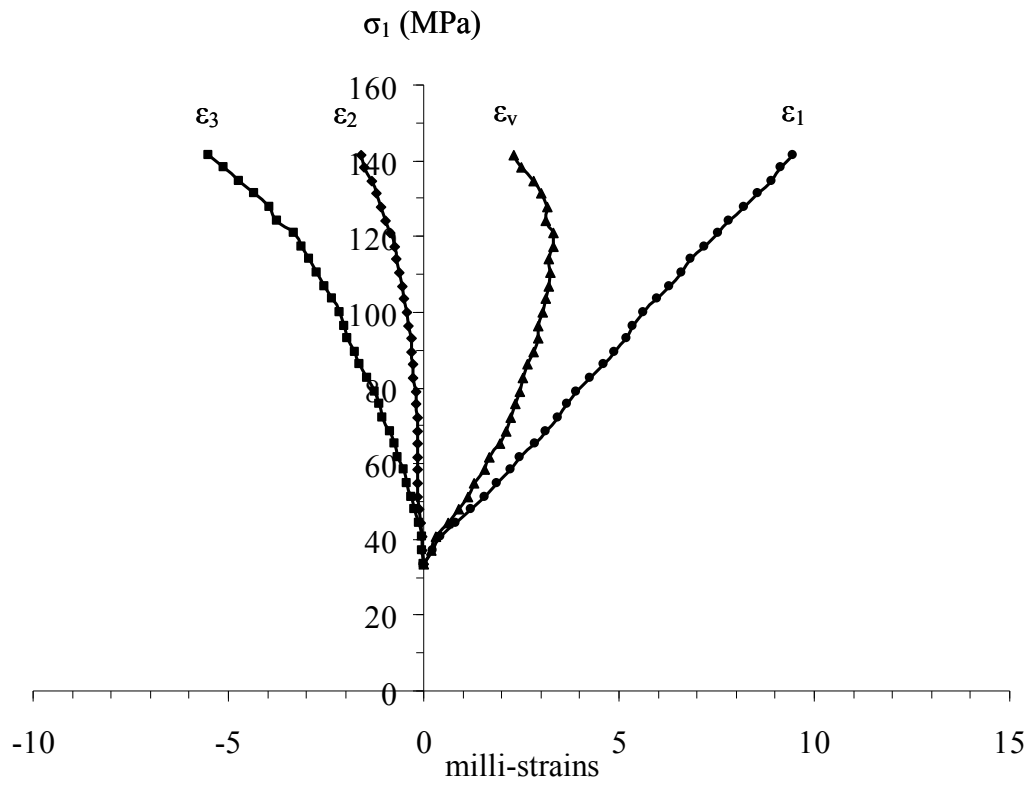


Figure 4.21 Stress-strain curves of Phu Kradung sandstone at condition $\sigma_2 = 13.8$ MPa and $\sigma_3 = 6.6$ MPa.

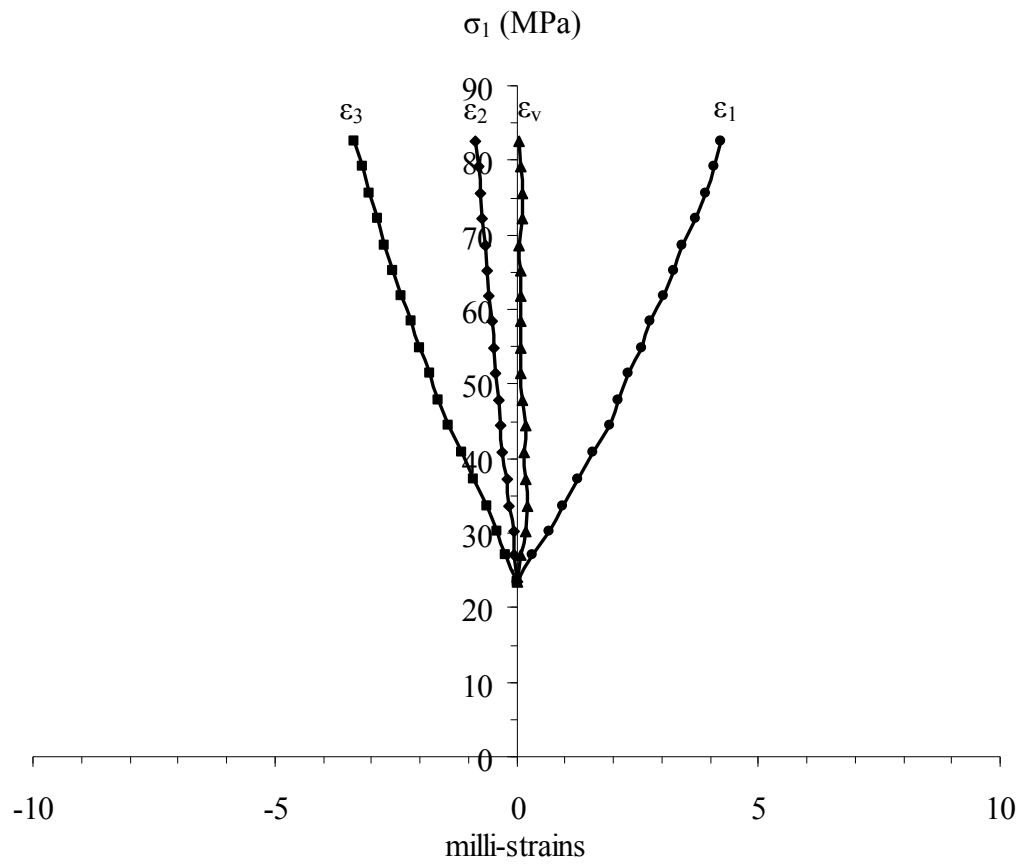


Figure 4.22 Stress-strain curves of Phu Kradung sandstone at condition $\sigma_2 = 10.1$ MPa and $\sigma_3 = 3$ MPa.

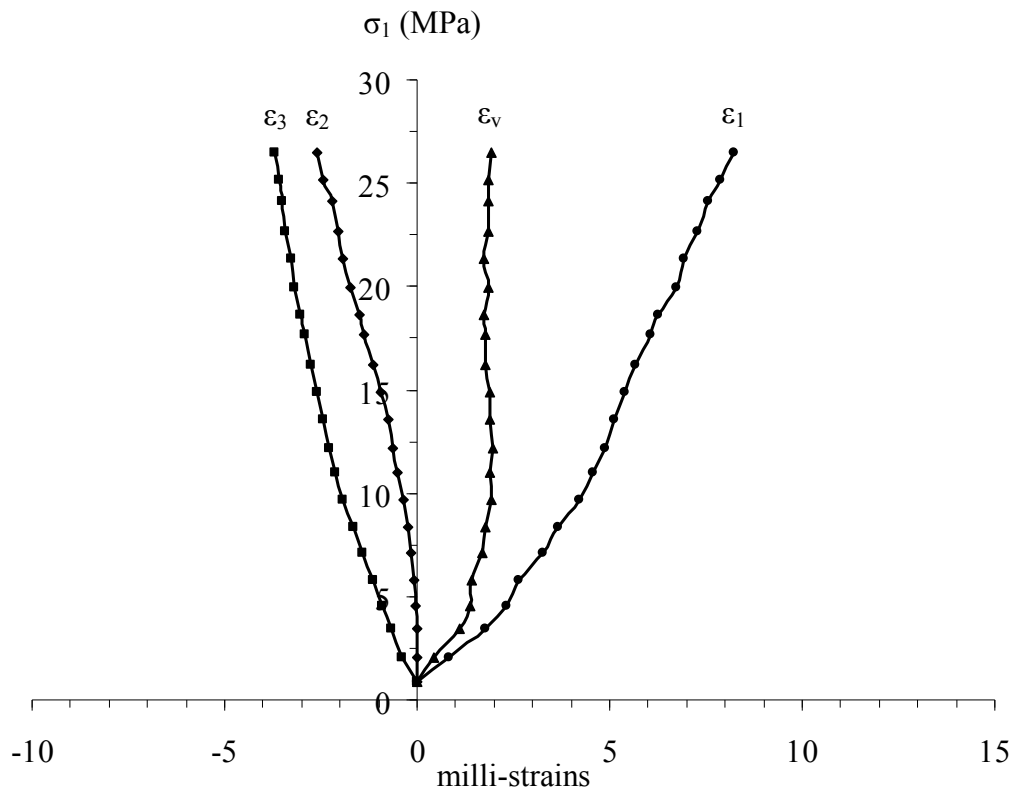


Figure 4.23 Stress-strain curves of Phu Kradung sandstone at condition $\sigma_2 = 3$ MPa and $\sigma_3 = 1.2$ MPa.

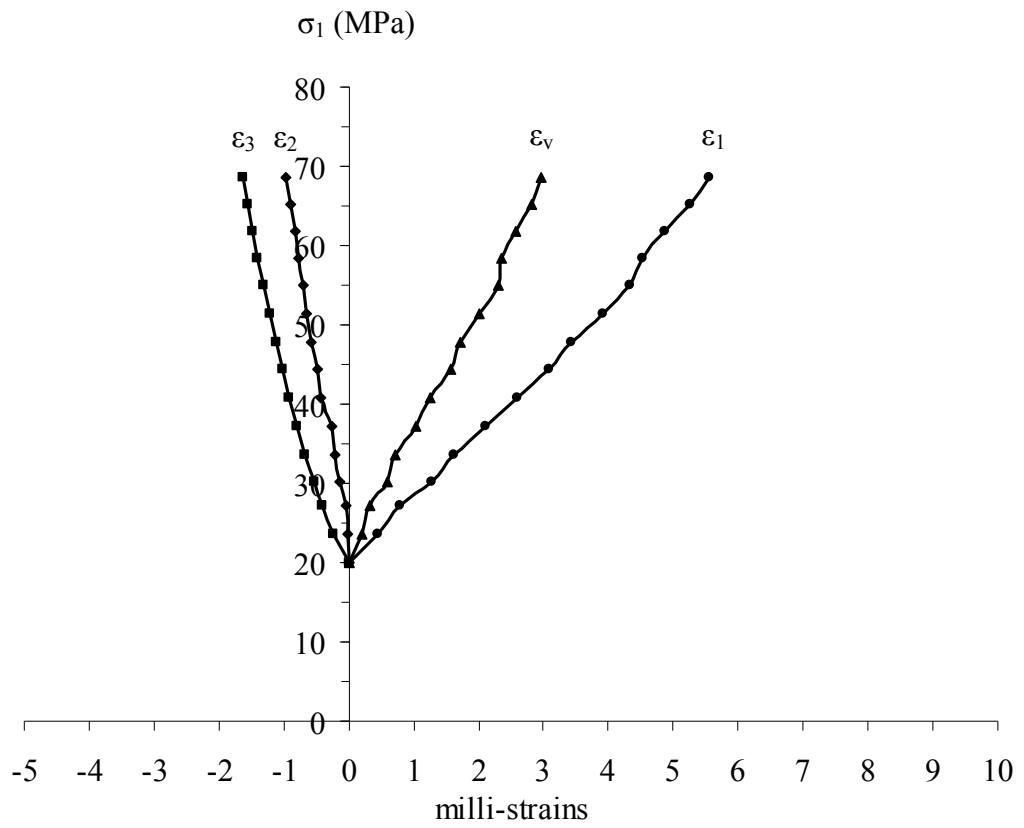


Figure 4.24 Stress-strain curves of Phu Kradung sandstone at condition $\sigma_2 = 10.1$ MPa and $\sigma_3 = 0$ MPa.

Table 4.4 Elastic properties from characterization test and true triaxial compression test.

Test method		Rock Types		
		PW	PP	PK
Uniaxial compression test	E (GPa)	11.5 ± 1.2	11.9 ± 1.2	8.6 ± 0.5
	Triaxial compression test	E (GPa)	9.7±1.5	9.6±0.4
	v	0.28±0.04	0.19±0.06	0.25±0.02
True triaxial compression test	E _p (GPa)	11.2±0.7	11.0±0.4	10.9±0.4
	v _p	0.35±0.04	0.28±0.12	0.29±0.07
	E _n (GPa)	9.3±0.51	9.5±0.6	9.4±0.7
	v _n	0.23±0.05	0.17±0.05	0.22±0.03

CHAPTER V

DISCUSSIONS, CONCLUSIONS, AND RECOMMENDATIONS FOR FUTURE STUDIES

5.1 Discussions and Conclusions

The test results indicate that the invented polyaxial load frame perform well for the assessment of the effects of σ_2 on the deformation characteristics of the sandstones. Measuring the specimen deformations by monitoring the movement of the cantilever beams is sufficiently accurate and sensitive to detect the transversely isotropic behavior of the PK, PW and PP sandstones. An advantage of the polyaxial frame is that it can test rock specimens with a wider range of sizes and shapes as compared to most true triaxial cells previously developed. A disadvantage of the polyaxial load frame equipped with cantilever beam system is the limitation of the applied lateral loads to induce σ_2 and σ_3 . As a result the strength of strong rocks under very high σ_2 and σ_3 can not be measured. The performance of the load frame is demonstrated here by assessing the effects of σ_2 on the elasticity and poisson's ratio of PP, PW and PK sandstones. PP, PW and PK sandstones show transversely isotropic properties where the elastic modulus in the direction parallel to the bedding planes is greater than that normal to the bedding. The Poisson's ratio on the plane parallel to the bedding is lower than those on the plane normal to the bedding. The discrepancies of the results of the conventional triaxial tests and true triaxial tests are probably become the difference in specimen shapes and the transversely anisotropic of the sandstone.

5.2 Recommendations for future studies

A more testing is required to assess the effect of the intermediate principal stress on various rock types, especially those rock with low strengths and exhibiting anisotropic behavior. The load configurations for the poly axial load frame is flexible and allows us to perform a variety of test configurations, for example polyaxial creep testing, four-point beam bending tests with lateral confinement, Brazilian and ring tension tests with axial compression, effect of loading rate on strength of rock in true triaxial stress state, modified point load testing under confinement and borehole stability testing under biaxial and polyaxial stresses.

REFERENCES

- Alexeeva, A. D., Revvaa, V. N., Alyshev, N. A., and Zhitlyonok, D. M. (2004). True triaxial loading apparatus and its application to coal outburst prediction. **International Journal of Coal Geology**. 58 : 245–250.
- ASTM D7012-04. Standard Test Method for Compressive Strength and Elastic Moduli of Intact Rock Core Specimens under Varying States of Stress and Temperatures. **Annual Book of ASTM Standards (Vol. 04.09)**. Philadelphia: American Society for Testing and Materials.
- Brown, E., T. (1981). Rock Characterization Testing and Monitoring : ISRM Suggested Methods. The Commission on Rock Testing Method. **International Society for Rock Mechanics**, Pergamon Press.
- Chang, C., and Haimson, B. (2005). Non-dilatant deformation and failure mechanism in two Long Valley Caldera rocks under true triaxial compression. **International Journal of Rock Mechanics & Mining Sciences**. 42 : 402–414.
- Haimson, B. (2006). True Triaxial Stresses and the Brittle Fracture of Rock. **Pure and Applied Geophysics**. 163 : 1101–1113.
- Haimson, B., and Chang, C. (1999). A new true triaxial cell for testing mechanical properties of rock, and its use to determine rock strength and deformability of Westerly granite. **International Journal of Rock Mechanics and Mining Sciences**. 37 : 285-296.
- Hibbeler, R. C. (2003). **Mechanics of Materials**. Singapore: Prentice-Hall, Inc. pp 255-704.

- Jaeger, J. C. and Cook, N. W. (1979). **Fundamentals of Rock Mechanics**. London : Chapman and Hall. pp 169-173.
- Kwaśniewski, M., Takahashi, M. and Li, X. (2003). Volume changes in sandstone under true triaxial compression conditions. **ISRM 2003–Technology roadmap for rock mechanics**, South African Institute of Mining and Metallurgy. pp 683-688.
- Norton, R. L. (2006). **Machine Design An Integrated Approach**. New Jersey: Pearson Education, Inc. pp 811-816.
- Oku, H., Haimson, B., and Song S. R. (2007). True triaxial strength and deformability of the siltstone overlying the Chelungpu fault (Chi-Chi earthquake), Taiwan. **Geophysical Research Letters**. Vol. 34. L09306.
- Singh, B., Goel, R. K., Mehrotra, V. K., Garg, S. K., and Allu, M. R. (1998). Effect of Intermediate Principal Stress on Strength of Anisotropic Rock Mass. **Tunnelling and Underground Space Technology**. Vol. 13, No. 1, pp 71-79.
- Smart, B. G. D., Somerville, J.M., and Crawford, B. R. (1999). A rock test cell with true triaxial capability. **Geotechnical and Geological Engineering**. **17**: 157–176.
- Tiwari, R. P., and Rao, K.S. (2004). Physical modeling of a rock mass under a true triaxial stress state. **International Journal of Rock Mechanics and Mining Sciences**. Vol. 41, No. 3. pp 1-6
- Tiwari, R. P., and Rao, K.S. (2006). Post failure behaviour of a rock mass under the influence of triaxial and true triaxial confinement. **Engineering Geology**. **84**: pp 112–129.

- Walsri, C., Poonprakon, P., Thosuwan, R., and Fuenkajorn, K. (2009). Compressive and tensile strengths of sandstones under true triaxial stresses. **Proceedings of The second Thailand Symposium on Rock Mechanics**, Thailand, pp 199-218.
- Wawersik, W. R., Carlson, L.W., Holcombl, D. J., and Williams, R. J. (1997). New Method For True-Triaxial Rock Testing. **International Journal of Rock Mechanics and Mining Sciences**. Vol. 34, No. 3-4.
- Yang, X. L., Zou, J. F., and Sui, Z. R. (2007). Effects of intermediate principal stress on rock cavity stability. **J. Cent. South Univ. Technol.** s1-0165-05.

APPENDIX A

LIST OF PUBLICATIONS

LIST OF PUBLICATIONS

Walsri, C., Poonprakon, P., Thosuwan R. and Fuenkajorn, K., 2009. **Compressive and tensile strengths of sandstones under true triaxial stresses.** In Proceedings 2nd Thailand Symposium on Rock Mechanics. Chonburi, Thailand. 12 - 13 March 2009.

Thosuwan R., Walsri, C., Poonprakon, P. and Fuenkajorn, K., 2009. **Effects of intermediate principal on compressive and tensile strengths of sandstones.** In International Symposium on Rock Mechanics “Rock Characterization, Modelling, and Engineering Design Methods. University of Hong Kong, Hong Kong. 19-22 May 2009.

Compressive and tensile strengths of sandstones under true triaxial stresses

C. Walsri, P. Poonprakon, R. Thosuwat & K. Fuenkajorn
Geomechanics Research Unit, Suranaree University of Technology, Thailand

Keywords: True triaxial, polyaxial, intermediate principal stress, sandstone, anisotropic

ABSTRACT: A polyaxial load frame has been developed to determine the compressive and tensile strengths of three types of sandstone under true triaxial stresses. Results from the polyaxial compression tests on rectangular specimens of sandstones suggest that the rocks are transversely isotropic. The measured elastic modulus in the direction parallel to the bedding planes is slightly greater than that normal to the bedding. Poisson's ratio on the plane normal to the bedding planes is lower than those on the parallel ones. Under the same σ_3 , σ_1 at failure increases with σ_2 . Results from the Brazilian tension tests under axial compression reveal the effects of the intermediate principal stress on the rock tensile strength. The Coulomb and modified Wiebols and Cook failure criteria derived from the characterization test results predict the sandstone strengths in term of $J_2^{1/2}$ as a function of J_1 under true triaxial stresses. The modified Wiebols and Cook criterion describes the failure stresses better than does the Coulomb criterion when all principal stresses are in compressions. When the minimum principal stresses are in tension, the Coulomb criterion over-estimate the second order of the stress invariant at failure by about 20% while the modified Wiebols and Cook criterion fails to describe the rock tensile strengths.

1 INTRODUCTION

The effects of confining pressures at great depths on the mechanical properties of rocks are commonly simulated in a laboratory by performing triaxial compression testing of cylindrical rock core specimens. A significant limitation of these conventional methods is that the intermediate and minimum principal stresses are equal during the test while the actual in-situ rock is normally subjected to an anisotropic stress state where the maximum, intermediate and minimum principal stresses are different ($\sigma_1 \neq \sigma_2 \neq \sigma_3$). It has been commonly found that compressive strengths obtained from conventional triaxial testing can not represent the actual in-situ strength where the rock is subjected to an anisotropic stress state (Yang et al., 2007; Haimson, 2006; Tiwari & Rao, 2004, 2006; Haimson & Chang, 1999). A variety of devices have been developed for rock testing under true triaxial stresses. Some recent ones include those proposed by Reddy et al. (1992), Smart (1995), Wawersik et al. (1997), Haimson & Chang (2000), and Alexeev et al. (2004). These devices are mostly designed for testing rock specimens under compression.

From the experimental results on brittle rocks obtained by the researchers above (e.g., Colmenares & Zoback, 2002; Haimson, 2006) it can be generally concluded that in a $\sigma_1 - \sigma_2$ diagram, for a given σ_3 , σ_1 at failure initially increases with σ_2 to a certain magnitude, and then it gradually decreases as σ_2 increases. The effect of σ_2 is more pronounced under higher σ_3 . Cai (2008) offers an explanation of how the intermediate principal stress affects the rock strength based on the results from numerical simulations on fracture initiation and propagation. He states that the intermediate principal stress confines the rock in such a way that fractures can only be initiated and propagated in the direction parallel to σ_1 and σ_2 . The effect of σ_2 is related to the stress-induced anisotropic properties and behavior of the rock and to the end effect at the interface between the rock surface and loading platen in the direction of σ_2 application. The effect should be smaller in homogeneous and fine-grained rocks than in coarse-grained rocks where pre-existing micro-cracks are not uniformly distributed.

Several failure criteria have been developed to describe the rock strength under true triaxial stress states. Comprehensive reviews of these criteria have been given recently by Colmenares & Zoback (2002), Al-Ajmi & Zimmerman (2005), Haimson (2006), Benz & Schwab (2008), Cai (2008), Haimson & Hudson (2008) and You (2008). Among several other criteria, the Mogi and modified Wiebols and Cook criteria are perhaps the most widely used to describe the rock compressive strengths under true triaxial stresses. These strength criteria however have rarely been verified when one or two of the principal stresses are in tension. Obtaining rock strengths under an anisotropic stress state is not only difficult but expensive. A special loading device (e.g., polyaxial loading machine or true triaxial load cell) is required. As a result test data under true triaxial stress conditions have been relatively limited. Most researchers above have used the same sets of test data (some obtained over a decade ago) to compare with their new numerical simulations, field observations (notably on breakout of deep boreholes) or to verify their new strength criteria and concepts. Due to the cost and equipment availability for obtaining true triaxial strengths, in common engineering practices application of a failure criterion that can incorporate the three-dimensional stresses has been very rare.

This research involves the development of a simple and low-cost polyaxial load frame to test rock specimens under true triaxial stress states. The frame performance is assessed by conducting polyaxial compression tests and Brazilian tension tests under axial compression to study the deformation and failure characteristics of sandstone specimens. The Coulomb and modified Wiebols and Cook failure criteria derived from the results of conventional tests are used to describe the compressive and tensile strengths of the rocks under true triaxial stress states.

2 ROCK SAMPLES

The tested sandstones are from three sources: Phu Phan, Phra Wihan and Phu Kradung formations (hereafter designated as PP, PW and PK sandstones). These fine-grained quartz sandstones are selected primarily because of their highly uniform texture, density and strength. Their average grain size is 0.1-1.0 mm. They are commonly found in the north and northeast of Thailand. Their mechanical properties and responses play a significant role in the stability of tunnels, slope embankments and dam foundations in the region. For the polyaxial compression testing rectangular block specimens are cut and ground to have a nominal dimension of 5×5×10 cm. The perpendicularity and parallelism of the specimens follow the ASTM (D 4543) specifications. The longest axis is parallel to the bedding planes and to the direction of the major principal stress. Though having different shape the

specimens used here have volume and length-to-diameter ratio comparable to those used in the conventional uniaxial and triaxial compression test methods. The Brazilian tension test uses disk specimens with a nominal diameter of 50 mm with a thickness-to-diameter ratio of 0.5 to comply with ASTM D 3967-95. The core axis is normal to the bedding planes. All specimens are oven-dried before testing.

3 POLYAXIAL LOAD FRAME

The development of the polyaxial load frame is based on three key design requirements: (1) capable of maintaining constant lateral stresses (σ_2 and σ_3) during the test, (2) capable of testing specimen with volume equal to or larger than those used in the conventional triaxial testing, and (3) allowing monitoring of specimen deformation along the principal axes. Figure 1 shows the polyaxial load frame developed in this research. To meet the load requirement above, two pairs of cantilever beams are used to apply the lateral stresses in mutually perpendicular directions to the rock specimen. The outer end of each opposite beam is pulled down by dead weight placed in the middle of a steel bar linking the two opposite beams underneath (Figure 2). The inner end is hinged by a pin mounted on vertical bars on each side of the frame. During testing all beams are arranged perfectly horizontally, and hence a lateral compressive load results on the specimen placed at the center of the frame. Due to the different distances from the pin to the outer weighting point and from the pin to the inner loading point, a load magnification of 17 to 1 is obtained from load calibration with an electronic load cell. This loading ratio is also used to determine the lateral deformation of the specimen by monitoring the vertical movement of the two steel bars below. The maximum lateral load is designed for 100 kN. The axial load is applied by a 1000-kN hydraulic load cell. The load frame can accommodate specimen sizes from 2.5×2.5×2.5 cm to 10×10×20 cm. The different specimen sizes and shapes can be tested by adjusting the distances between the opposite loading platens. Note that virtually all true triaxial and polyaxial cells previously developed elsewhere can test rock samples with the maximum size not larger than 5×5×10 cm.

4 POLYAXIAL COMPRESSION TESTS

The polyaxial compression tests are performed to determine the compressive strengths and deformations of the PK, PP and PW sandstones under true triaxial stresses. The intermediate (σ_2) and minimum (σ_3) principal stresses are maintained constant while σ_1 is increased until failure. Here the constant σ_2 is varied from 0 to 17 MPa, and σ_3 from 0 to 6 MPa. Neoprene sheets are used to minimize the friction at all interfaces between the loading platen and the rock surface. Figure 3 shows the applied principal stress directions with respect to the bedding planes for all specimens. The measured sample deformations are used to determine the strains along the principal axes during loading. The failure stresses are recorded and mode of failure examined.

4.1 Test Results

Figure 4 plots the stress-strain curves from the start of loading to failure for some sandstone specimens. The elastic modulus and Poisson's ratio are calculated for the directions normal and parallel to the bedding planes. Under the stress orientation used here where σ_1 and σ_2 are parallel to the bedding planes, the three-dimensional principal stress-strain relations given by Jaeger & Cook (1979) can be simplified to obtain a set of governing equations for a transversely isotropic material as:

Compressive and tensile strengths of sandstones under true triaxial stresses

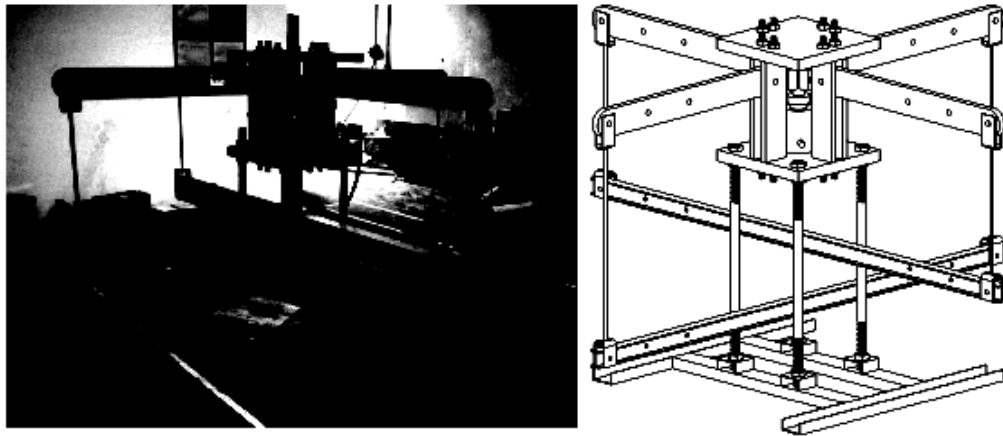


Figure 1. Polyaxial load frame developed for compressive and tensile strength testing under true triaxial stress.

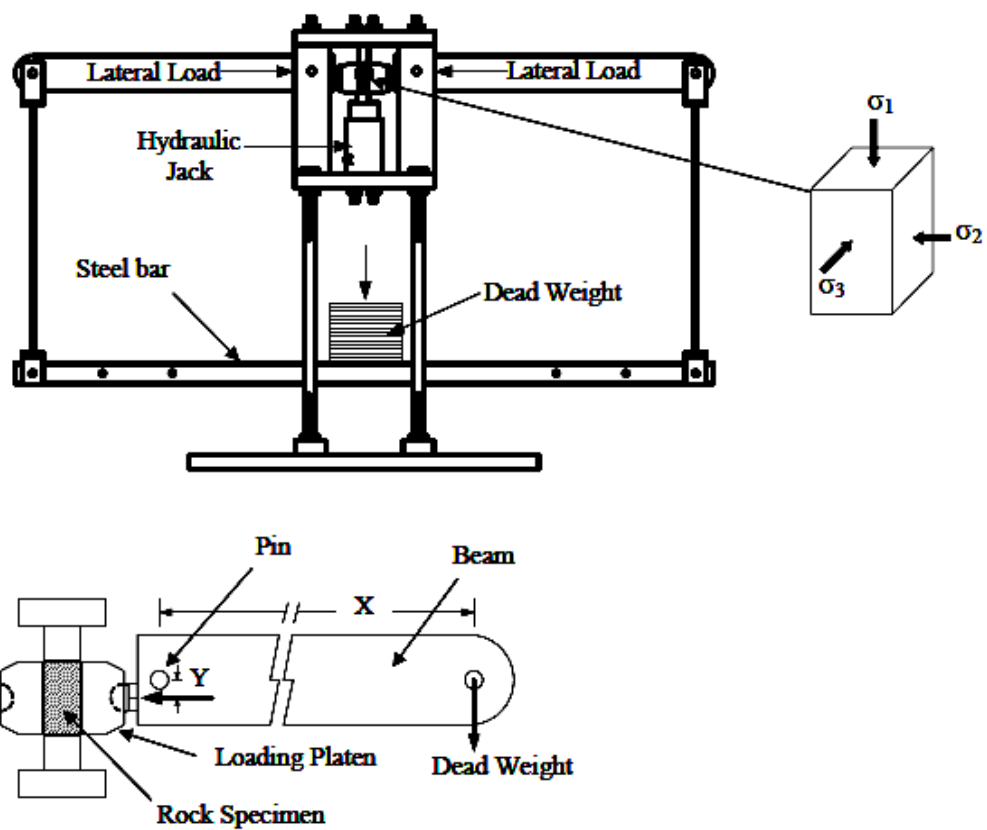
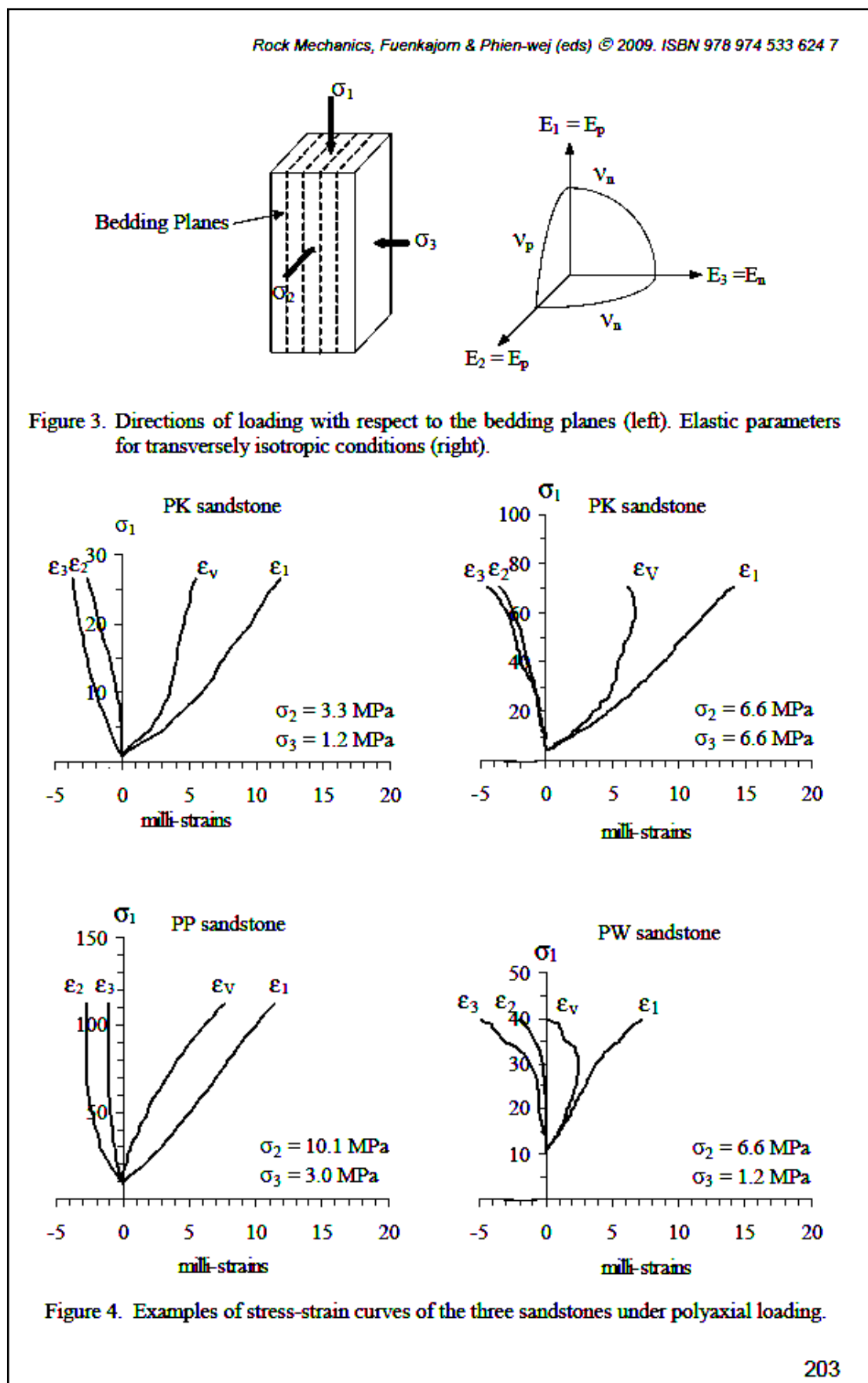


Figure 2. Cantilever beam weighed at outer end applies lateral stress to the rock specimen.



Compressive and tensile strengths of sandstones under true triaxial stresses

$$\varepsilon_1 = \frac{\sigma_1}{E_p} - \frac{\sigma_2 \nu_p}{E_p} - \frac{\sigma_3 \nu_n}{E_n} \quad (1)$$

$$\varepsilon_2 = -\frac{\sigma_1 \nu_p}{E_p} + \frac{\sigma_2}{E_p} - \frac{\sigma_3 \nu_n}{E_n} \quad (2)$$

$$\varepsilon_3 = -\frac{\sigma_1 \nu_n}{E_p} - \frac{\sigma_2 \nu_n}{E_p} + \frac{\sigma_3}{E_n} \quad (3)$$

where: σ_1 , σ_2 and σ_3 are principal stresses, ε_1 , ε_2 and ε_3 are principal strains, E_n and E_p are elastic moduli normal and parallel to the bedding planes, and ν_n and ν_p are Poisson's ratio's on the planes normal and parallel to the bedding.

The calculations of the Poisson's ratios and tangent elastic moduli are made at 50% of the maximum principal stress. The PW and PP sandstones exhibit a small transversely isotropic behavior. The elastic modulus in the direction normal to the bedding planes is slightly lower than that parallel to the bedding planes. The Poisson's ratio on the plane parallel to the beds is less than that across the beds. Table 1 summarizes the elastic parameters with respect to the bedding plane orientation.

Figure 5 plots σ_1 at failure as a function of σ_2 tested under various σ_3 's for the PW and PP sandstones. The results show the effects of the intermediate principal stress, σ_2 , on the maximum stresses at failure by the failure envelopes being offset from the condition where $\sigma_2 = \sigma_3$. For all minimum principal stress levels, σ_1 at failure increases with σ_2 . The effect of σ_2 tends to be more pronounced under a greater σ_3 . These observations agree with those obtained elsewhere (e.g. Haimson & Chang, 2000; Colmenares & Zoback, 2002; Haimson, 2006). Post-failure observations suggest that compressive shear failures are predominant in the specimens tested under low σ_2 while splitting tensile fractures parallel to σ_1 and σ_2 directions dominate under higher σ_2 (Figure 6). The observed splitting tensile fractures under relatively high σ_2 suggest that the fracture initiation has no influence from the friction at the loading interface in the σ_2 direction. As a result the increase of σ_1 with σ_2 should not be due to the interface friction. This does not agree with a conclusion drawn by Cai (2008) that friction at the interface in the σ_2 direction contributes to the increase of σ_1 at failure. Under the conditions when $\sigma_2 = \sigma_3$, the magnitudes of σ_1 at failure agree well with the triaxial compressive strength test results obtained by Kenkhunthod and Fuenkajorn (2009).

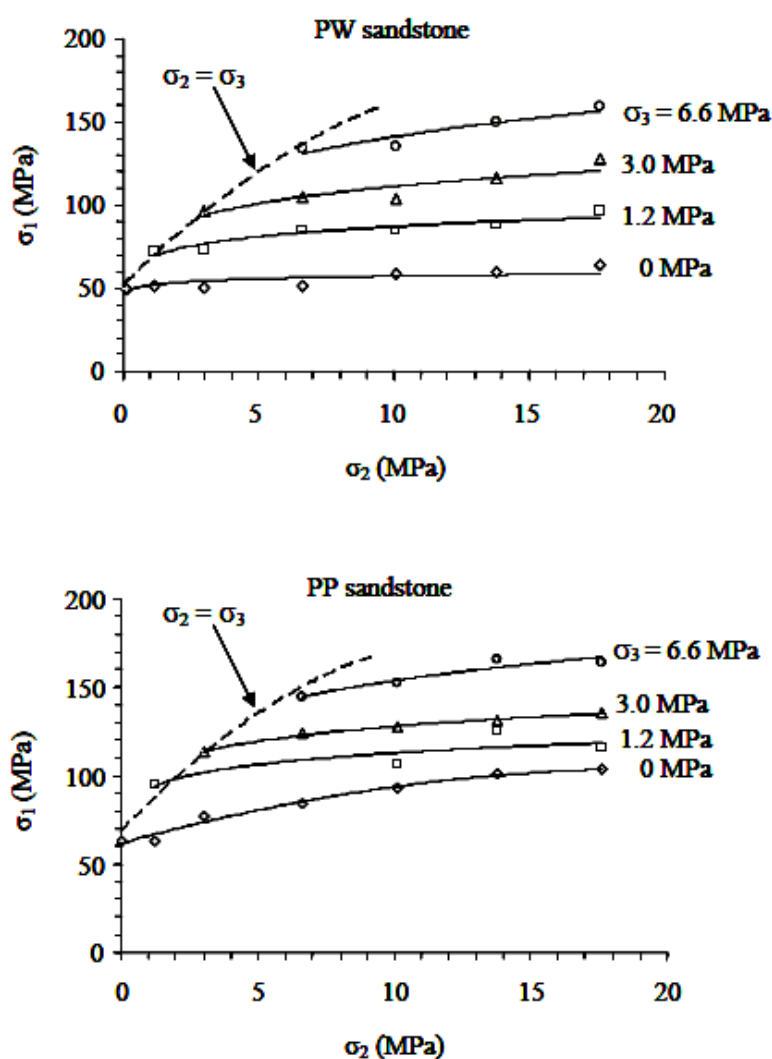
4.2 Strength Criteria

The Coulomb and modified Wiebols and Cook failure criteria are used to describe the polyaxial strengths of the PW and PP sandstones. They are selected because the Coulomb criterion has been widely used in actual field applications while the modified Wiebols and Cook criterion has been claimed by many researchers to be one of the best representations of rock strengths under polyaxial compression. To represent the rock strengths under true triaxial stresses the second order stress invariant ($J_2^{1/2}$) and the first order stress invariant or the mean stress (J_1) are calculated from the test results by the following relations (Jaeger & Cook, 1979):

$$J_2^{1/2} = \sqrt{(1/6)\{(\sigma_1 - \sigma_2)^2 + (\sigma_1 - \sigma_3)^2 + (\sigma_2 - \sigma_3)^2\}} \quad (4)$$

Table 1. Elastic properties in the direction normal and parallel to bedding planes.

	Rock Types	E_p (GPa)	E_n (GPa)	ν_p	ν_n
Polyaxial Compression Test	PW	10.0	8.6	0.38	0.28
	PP	11.1	10.3	0.36	0.33
Brazilian Tension Test	PW	9.2	N/A	0.21	N/A
	PP	14.8	N/A	0.19	N/A
	PK	5.9	N/A	0.11	N/A

Figure 5. Maximum principal stress (σ_1) at failure as a function of σ_2 for various σ_3 values.

Compressive and tensile strengths of sandstones under true triaxial stresses

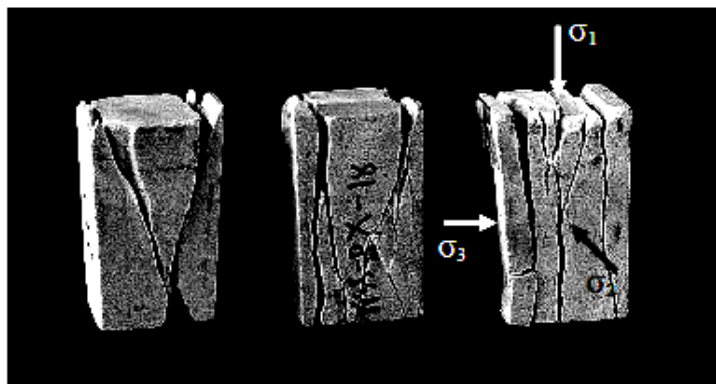


Figure 6. Post-tested specimens of PW sandstone. Left: $\sigma_1 = 51$, $\sigma_2 = 1.2$, $\sigma_3 = 0$ MPa. Middle: $\sigma_1 = 50$, $\sigma_2 = 3.0$, $\sigma_3 = 0$ MPa. Right: $\sigma_1 = 58.8$, $\sigma_2 = 10.0$, $\sigma_3 = 0$ MPa.

$$J_1 = (\sigma_1 + \sigma_2 + \sigma_3) / 3 \quad (5)$$

Here the Coulomb criterion is derived from the uniaxial and triaxial compressive strengths of the rocks where σ_2 and σ_3 are equal. Figures 7 and 8 compare the polyaxial test results with those predicted by the Coulomb criterion for PW and PP sandstones. The predictions are made for $\sigma_3 = 0, 1.2, 3.0$ and 6.6 MPa (as used in the tests) and under stress conditions from $\sigma_2 = \sigma_3$ to $\sigma_1 = \sigma_2$. In the $J_2^{1/2} - J_1$ diagram, $J_2^{1/2}$ increases with σ_3 but it is independent of J_1 because the Coulomb criterion ignores σ_2 in the strength calculation. Under a low σ_2 and σ_3 the Coulomb prediction tends to agree with the test results obtained from the PW sandstone. Except for this case, no correlation between the Coulomb predictions and the polyaxial strengths can be found. The inadequacy of the predictability of Coulomb criterion under polyaxial stress states obtained here agrees with a conclusion drawn by Colmenares & Zoback (2002).

The modified Wiebols and Cook criterion given by Colmenares & Zoback (2002) defines $J_2^{1/2}$ at failure in terms of J_1 as:

$$J_2^{1/2} = A + BJ_1 + CJ_1^2 \quad (6)$$

The constants A, B and C depend on rock materials and the minimum principal stresses (σ_3). They can be determined under the conditions where $\sigma_2 = \sigma_3$, as follows (Colmenares & Zoback, 2002):

$$C = \frac{\sqrt{27}}{2C_1 + (q-1)\sigma_3 - C_0} \times \left(\frac{C_1 + (q-1)\sigma_3 - C_0}{2C_1 + (2q+1)\sigma_3 - C_0} - \frac{q-1}{q+2} \right) \quad (7)$$

$$\text{where: } C_1 = (1 + 0.6\mu_1)C_0 \quad (8)$$

$C_0 =$ uniaxial compressive strength of the rock.

$$\mu_1 = \tan\phi \quad (9)$$

$$q = \{(\mu_1^2 + 1)^{1/2} + \mu_1\}^2 = \tan^2(\pi/4 + \phi/2) \quad (10)$$

$$B = \frac{\sqrt{3}(q-1)}{q+2} - \frac{C}{3}(2C_0 + (q+2)\sigma_3) \quad (11)$$

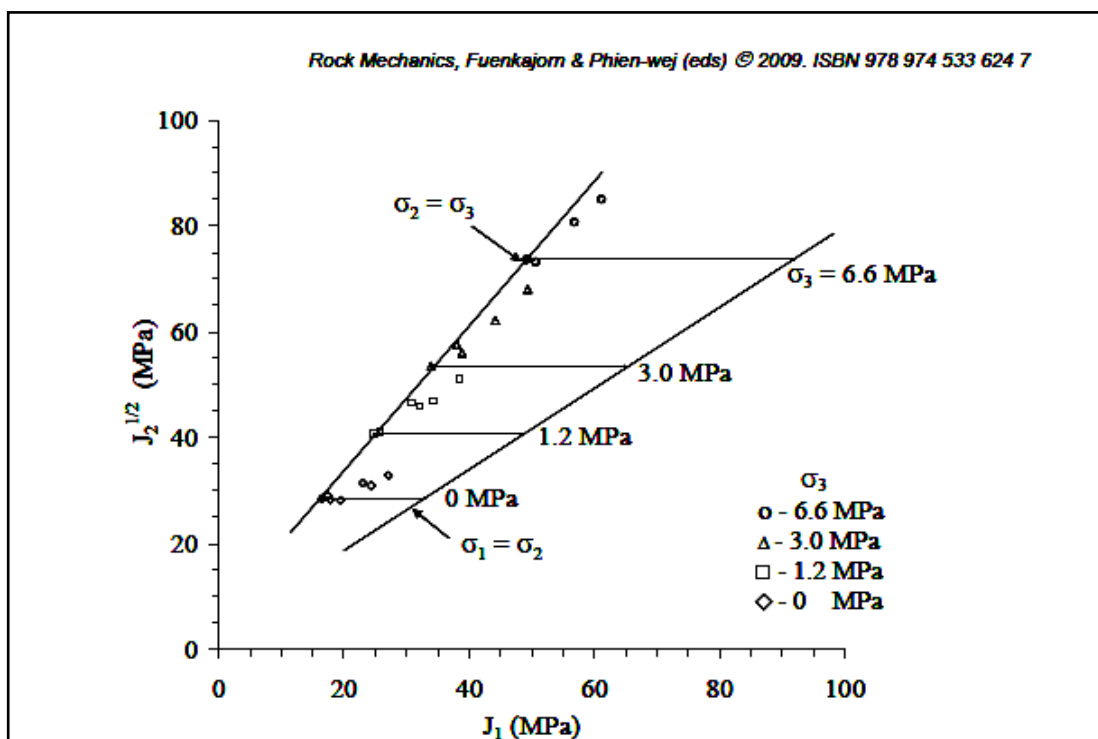


Figure 7. $J_2^{1/2}$ as a function of J_1 from testing PW sandstone compared with the Coulomb criterion predictions (lines).

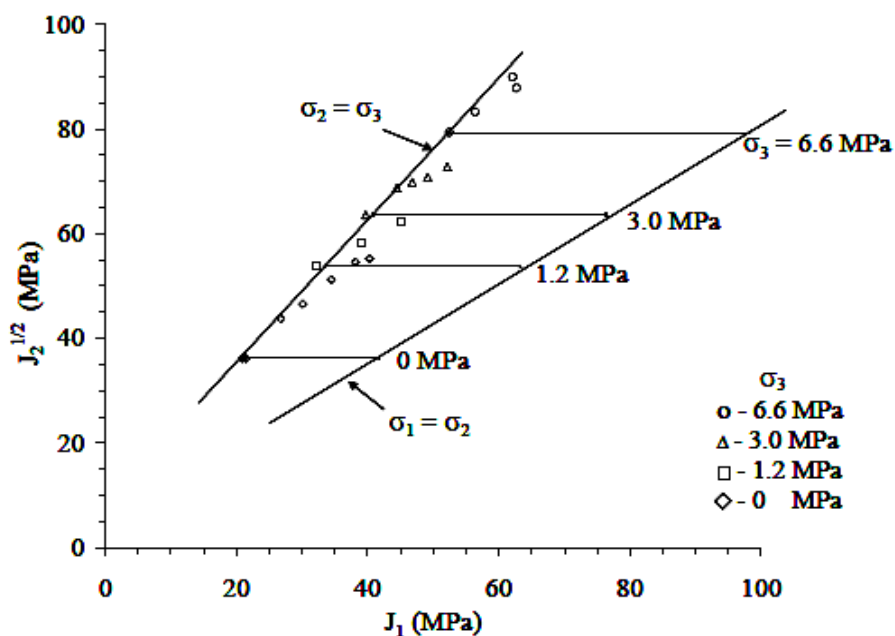


Figure 8. $J_2^{1/2}$ as a function of J_1 from testing PP sandstone compared with the Coulomb criterion predictions (lines).

$$A = \frac{C_0}{\sqrt{3}} - \frac{C_0}{3} B - \frac{C_0^2}{9} C \quad (12)$$

The numerical values for A, B and C for PW and PP sandstones are given in Table 2 for each σ_3 tested here. Substituting these constants into equation (6), the upper and lower limits of $J_2^{1/2}$ for each rock type can be defined under conditions of $\sigma_2 = \sigma_3$ and $\sigma_1 = \sigma_2$. The predictions are made for $\sigma_3 = 0, 1.2, 3.0$ and 6.6 MPa. Figures 9 and 10 compare the test results with those predicted by the modified Wiebols and Cook criterion. The predictions tend to be higher than the sandstone strengths under low σ_3 . Under a higher σ_3 the criterion well represents the polyaxial strengths of the rocks. This conforms to the results obtained by Colmenares & Zoback (2002) that predictive capability of the modified Wiebols and Cook criterion improves as the minimum principal stress increases.

5 BRAZILIAN TENSION TESTS UNDER AXIAL COMPRESSION

The Brazilian tension tests with axial compression have been performed on PP, PW and PK sandstone disks to determine the effects of the intermediate principal stress on the rock tensile strength. The polyaxial load frame is used to apply a constant axial stress on the disk specimen while the diametral line load is increased until failure (Figure 11). The constant axial stress is varied from zero (Brazilian test) to as high as the rock compressive strength. Neoprene sheets are used to minimize the friction between the rock surface and loading platen in the axial direction.

5.1 Brazilian Tension Test Results

Figure 12 plots the line load at failure (P_f) as a function of the axial stress (σ_z) for the three sandstones. The failure load linearly decreases with increasing axial stress. At $P_f = 0$ the axial stress becomes the uniaxial compressive strength of the rock. The tensile stresses (σ_x) and compressive stresses (σ_y) induced at the crack initiation point in the middle of the specimen also decrease with increasing axial stress (Figure 13). These stresses are calculated from the solutions given by Jaeger & Cook (1979). The test results reveal a linear transition from the Brazilian tensile strength to the uniaxial compressive strength, which can be best demonstrated by using Mohr's circles, as shown in Figure 14.

Post-failure observations show that under low σ_z a single splitting extension crack along the loading diameter is normally induced in the disk specimen. Multiple extension cracks are developed as σ_z increase. When σ_z reaches the uniaxial compressive strength of the rocks, the specimens fail without applying the diametral line load. At this point the specimens are crushed, resulting in multiple shear fractures and extension cracks (Figure 15). It is postulated that the axial stress produces tensile strains perpendicular to its direction due to the effect of the Poisson's ratio. At the crack initiation point this tensile strain is combined with

Table 2. Parameters A, B and C for PW and PP sandstones.

Rock types	PW Sandstone				PP Sandstone			
σ_3 (MPa)	0	1.2	3.0	6.6	0	1.2	3.0	6.6
A (MPa)	1.37	0.54	-0.41	-1.7	1.97	1.16	0.17	-1.2
B	1.92	1.94	1.96	1.99	1.91	1.92	1.94	1.96
C (MPa ⁻¹)	-0.016	-0.014	-0.012	-0.009	-0.013	-0.013	-0.01	-0.008

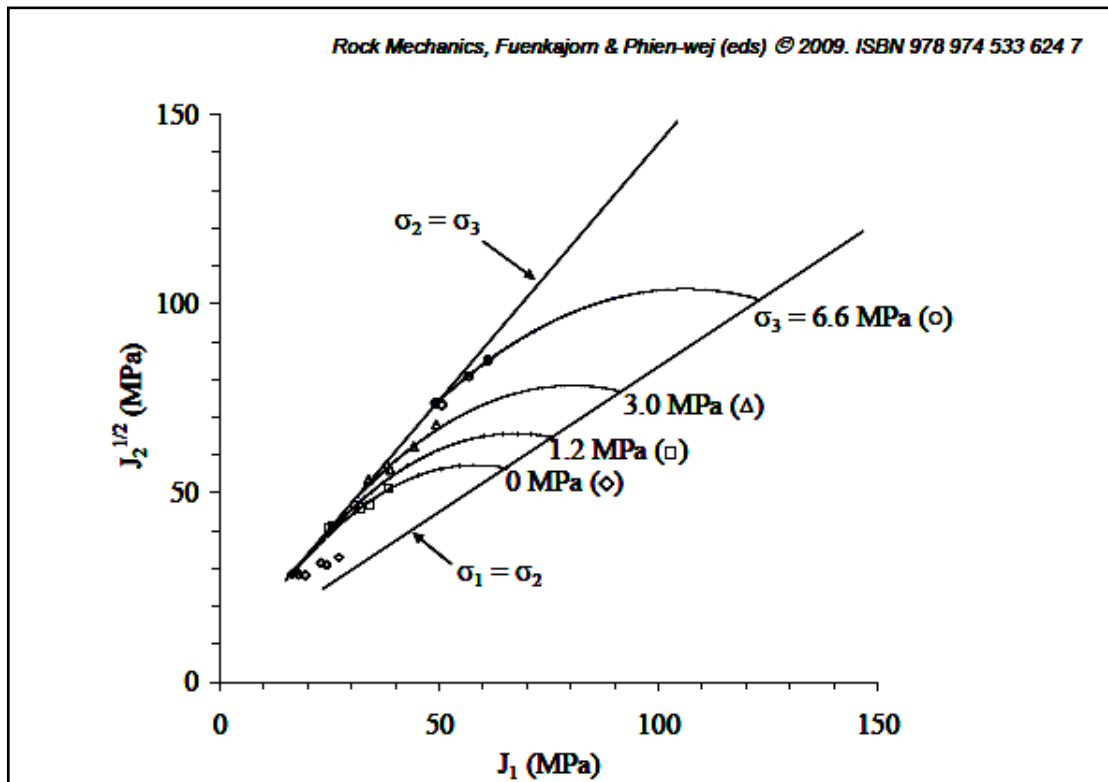


Figure 9. $J_2^{1/2}$ as a function of J_1 from testing PW sandstone compared with the modified Wiebols and Cook criterion predictions (lines).

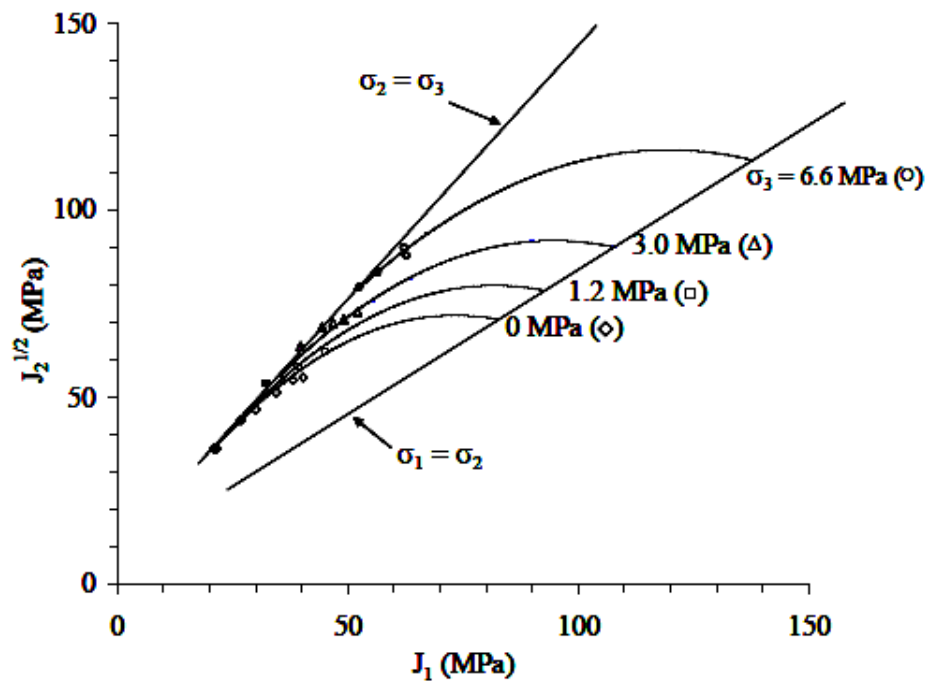


Figure 10. $J_2^{1/2}$ as a function of J_1 from testing PP sandstone compared with the modified Wiebols and Cook criterion predictions (lines).

Compressive and tensile strengths of sandstones under true triaxial stresses

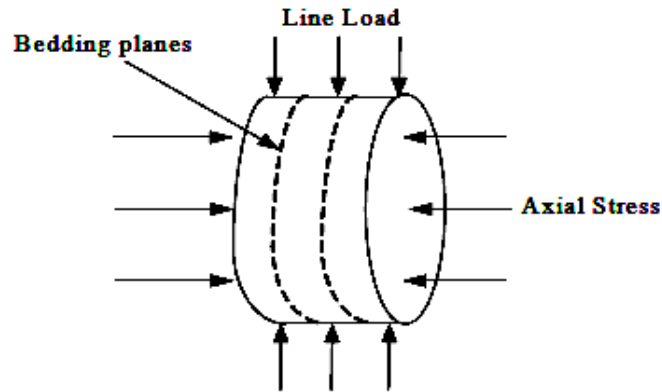


Figure 11. Brazilian tension test specimen under axial compression.

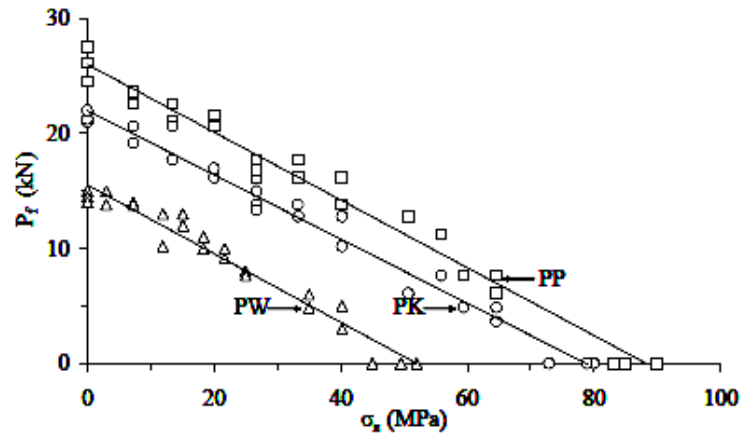


Figure 12. Line load at failure (P_f) as a function of applied axial stress (σ_x).

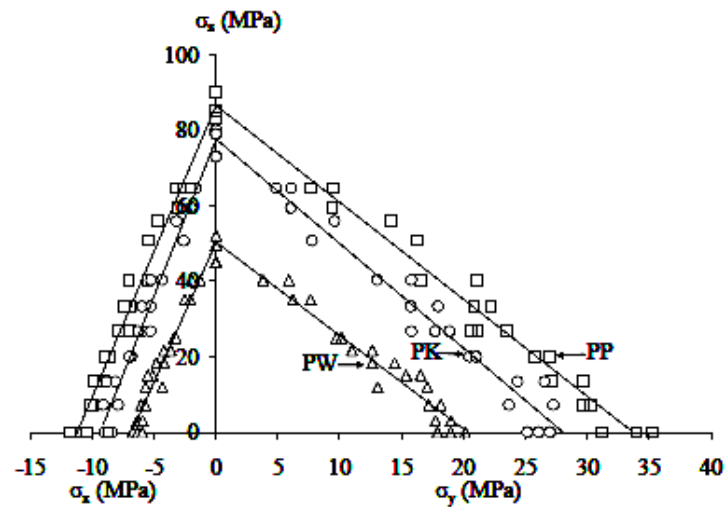


Figure 13. Induced compressive (σ_y) and tensile stresses (σ_z) at failure as a function of applied σ_z .

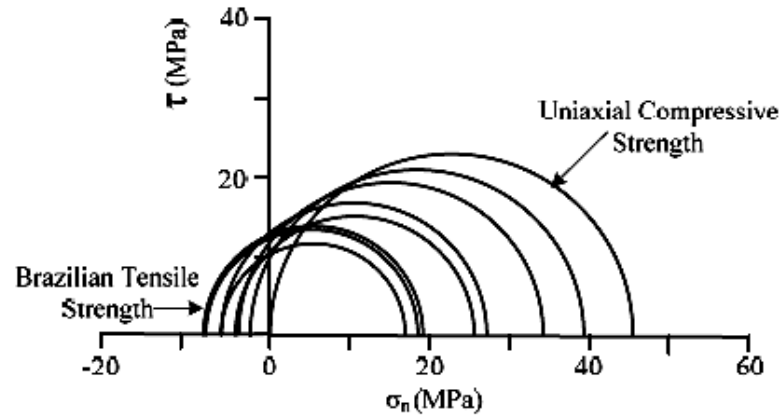


Figure 14. Mohr's circles from testing of PW sandstone showing transition from Brazilian tensile strength to uniaxial compressive strength.

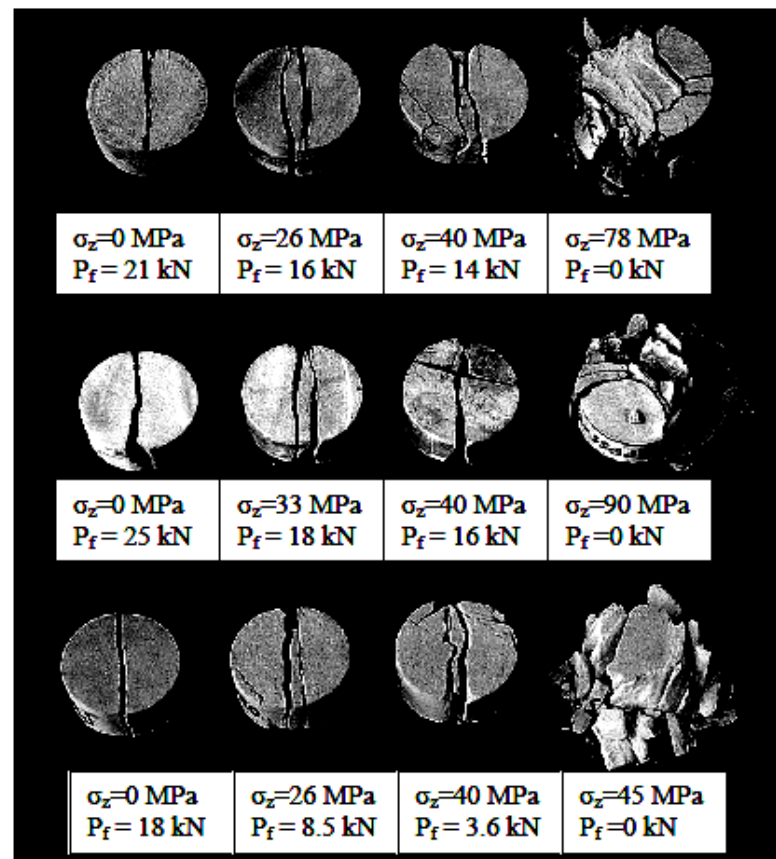


Figure 15. Some post- test specimens of PK sandstone (top), PP sandstone (middle) and PW sandstone (bottom).

the horizontal tensile stress that is induced by the line load. The line load at failure therefore decreases with increasing σ_z . Calculation of the σ_z -induced tensile strain for the entire specimen is however not that simple because the rock is under both tension and compression and the elastic properties under tension and compression may be different (Jaeger & Cook, 1979; Chen et al., 1998). More discussion on this issue is given in the next section.

Under no axial stress the elastic modulus and Poisson's ratio of the sandstones are measured by installing strain gages at the center of the sandstone specimen. The gages measure the vertical compressive strain, ε_y , (along the loading diameter) and horizontal tensile strain, ε_x , induced during line loading. Three samples have been tested for each rock type. Figure 16 plots the measured strains as a function of the applied load, P. The elastic modulus and Poisson's ratio can be calculated using the following equations (Hondros, 1959):

$$\nu = -\frac{3\varepsilon_x + \varepsilon_y}{3\varepsilon_y + \varepsilon_x} \quad (13)$$

$$E = \frac{2P(1-\nu)^2}{\pi Dt(\varepsilon_x + \nu\varepsilon_y)} \quad (14)$$

These equations assume that the rock is linearly elastic and isotropic and that the elastic modulus in tension is equal to that in compression. The E and ν above are compared with those obtained from the polyaxial compression testing in Table 1. Since all Brazilian disks are prepared to have bedding planes normal to the disk axis, only elastic modulus and Poisson's ratio parallel to the bedding can be measured. The discrepancy of the elastic parameters obtained from the two test types may be because the rock elastic modulus under tension is lower than that under compression and there is intrinsic variability among the tested specimens.

5.2 Strength Criteria under Tension

The Coulomb and modified Wiebols and Cook failure criteria are used to describe the rock strengths when the minimum principal stress is in tension. First the results of the Brazilian tests under axial compression are calculated in terms of $J_2^{1/2}$ as a function of J_1 . The induced horizontal tensile stress (σ_x) always represents the minimum principal stress (σ_3) in this test. Under low axial stress, the vertical compressive stress (σ_y) at the crack initiation point represents the maximum principal stress (σ_1), and the axial stress represents the intermediate principal stress (σ_2). When the axial stress is increased beyond a certain magnitude, σ_z becomes σ_1 , and σ_y becomes σ_2 .

From the test results the stress invariant $J_2^{1/2}$ as a function of mean stress J_1 is compared with the predictions by the Coulomb criterion in Figure 17 for PP, PW and PK sandstones. Since the Coulomb criterion ignores σ_2 at failure, the predicted $J_2^{1/2}$ is independent of J_1 for each σ_3 . The predicted $J_2^{1/2}$ decreases with σ_3 when the applied axial stress (σ_z) represents σ_1 , and increases with σ_3 when the induced vertical stress (σ_y) represents σ_1 . These stress variations conform well to the actual test results. The Coulomb criterion over-estimates the actual strengths for all levels of σ_3 . On average the discrepancies are about 15-20%.

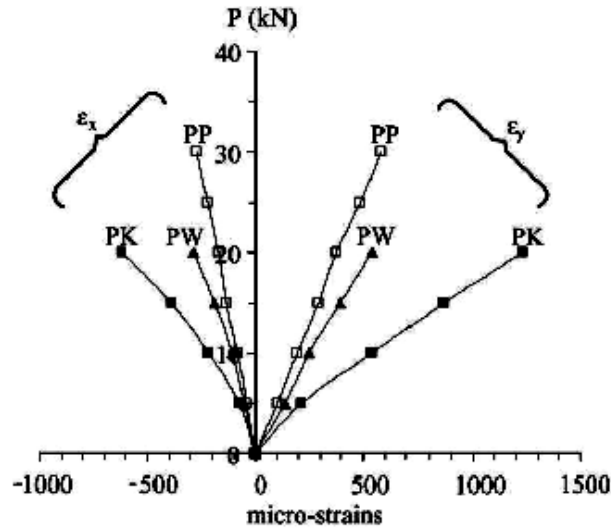


Figure 16. Strain measurements from Brazilian testing on PP, PW and PK sandstones.

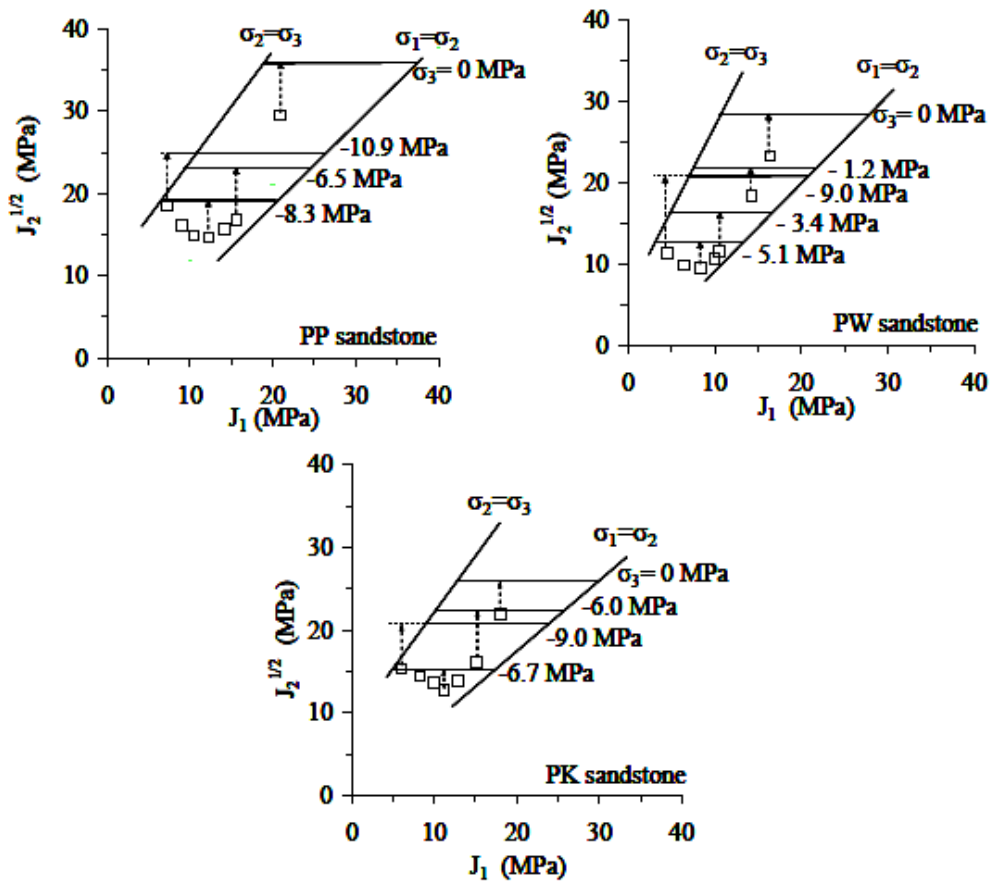


Figure 17. $J_2^{1/2}$ as a function of J_1 for Brazilian testing on PP, PW and PK sandstones compared with the Coulomb criterion predictions.

Compressive and tensile strengths of sandstones under true triaxial stresses

Figure 18 compares the measured strengths with the predictions by the modified Wiebols and Cook criterion for the three sandstones. The criterion is not sensitive to the observed variations of the rock strengths in the $J_2^{1/2} - J_1$ diagram. The predicted $J_2^{1/2}$ curves continue to decrease as the minimum stress decreases. This does not strictly reflect the actual observations where $J_2^{1/2}$ increases after the induced vertical stress becomes the maximum principal stress. It appears that the modified Wiebols and Cook criterion can not describe the rock strengths when the minimum principal stress is in tension.

7 DISCUSSIONS AND CONCLUSIONS

The invented polyaxial load frame performs well for the assessment of the effects of σ_2 on the compressive and tensile strengths of the sandstones. Measuring the specimen deformations by monitoring the movement of the cantilever beams is sufficiently accurate and sensitive to detect the transversely isotropic behavior of the PW and PP sandstones. An advantage of the polyaxial frame is that it can test rock specimens with a wider range of sizes and shapes as compared to most true triaxial cells previously developed. Such flexibility allows us to perform a variety of test configurations, for example polyaxial creep testing, four-point beam bending tests with lateral confinement, Brazilian and ring tension tests with axial compression, and borehole stability testing under biaxial and polyaxial stresses.

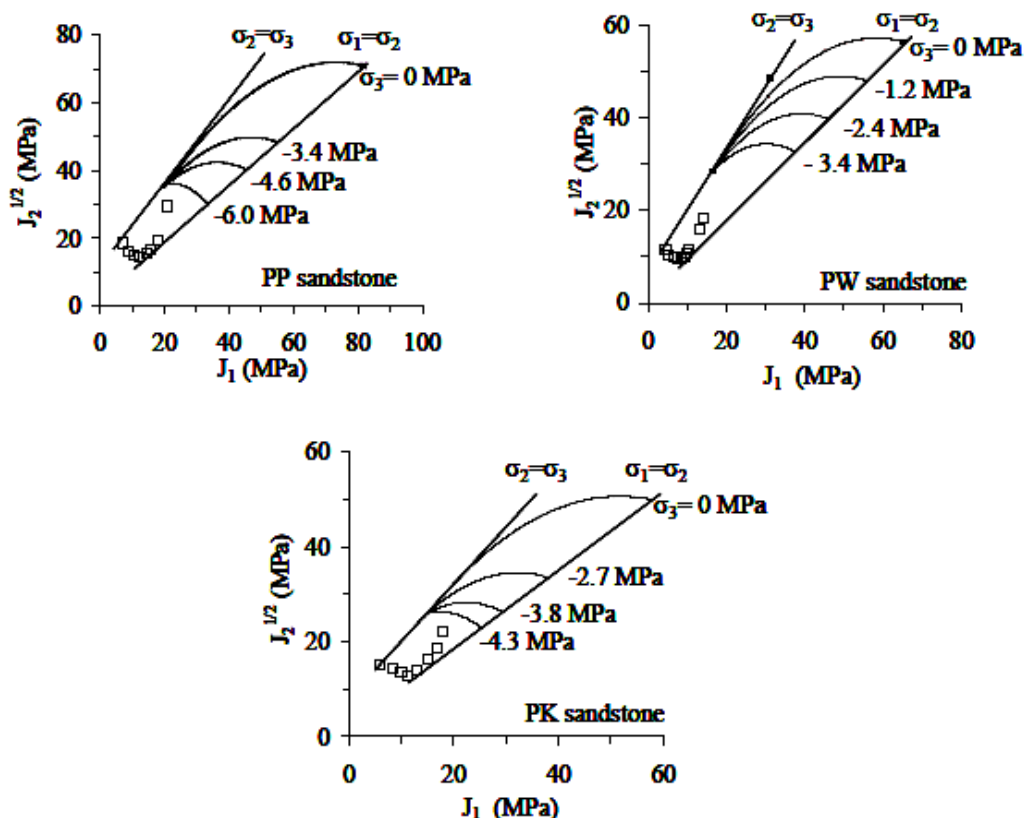


Figure 18. $J_2^{1/2}$ as a function of J_1 for Brazilian testing on PP, PW and PK sandstones compared with the modified Wiebols and Cook criterion.

Neoprene sheets used here can effectively reduce the friction between the rock surface and loading platen, as evidenced by the fact that σ_1 at failure measured under $\sigma_2 = \sigma_3$ for these sandstones is comparable to the corresponding triaxial compressive strengths of the rocks obtained by the conventional method (Kenkhunthod & Fuenkajorn, 2009). It can be concluded that the interface friction did not contribute to the increase of σ_1 at failure under true triaxial testing as suggested by Cai (2008).

Under true triaxial compressive stresses the modified Wiebols and Cook criterion can predict the compressive strengths of the tested sandstones reasonably well. Due to the effect of σ_2 the Coulomb criterion can not represent the rock strengths under true triaxial compressions, particularly under high σ_2 to σ_3 ratios. The Coulomb criterion however performs better when the minimum principal stress is in tension. It can describe the decrease and increase of $J_2^{1/2}$ at failure due to the variation of the minimum principal tensile stresses with the discrepancy of about 15-20%. It is clear that the modified Wiebols and Cook criterion can not be correlated with the rock strengths when the minimum principal stress is in tension

It is postulated that the effects of the intermediate principal stress are caused by two mechanisms working simultaneously but having opposite effects on the rock polyaxial strengths; (1) mechanism that strengthens the rock matrix in the direction normal to $\sigma_1 - \sigma_3$ plane, and (2) mechanism that induces tensile strains in the directions of σ_1 and σ_3 .

The intermediate principal stress can strengthen the rock matrix on the plane normal to its direction, and hence a higher differential stress is required to induce failure. This is simply the same effect obtained when applying a confining pressure to a cylindrical specimen in the conventional triaxial compression testing. Considering this effect alone, the higher the magnitude of σ_2 applied, the higher σ_1 (or $J_2^{1/2}$) is required to fail the specimen. Nevertheless it is believed that the relationship between σ_2 magnitudes and the degrees of strengthening can be non-linear, particularly under high σ_2 . Such relation depends on rock types and their texture (e.g., distribution of grain sizes, pore spaces, fissures and micro-cracks, and types of rock-forming minerals).

At the same time due to effect of the Poisson's ratio σ_2 can produce tensile strains in the directions normal to its axis (or on the plane parallel to σ_1 and σ_3). These tensile strains increase from the minimum on the mid-section plane to the maximum on the specimen surfaces where the rock can freely dilate. These tensile strains cause splitting tensile fractures of the rock specimen. This is supported by the results of the Brazilian testing under axial compression. The applied σ_2 produces σ_2 tensile strains adding to the line load-induced tensile stress at the specimen center. As a result a smaller magnitude of the line load is required to split the Brazilian specimen when it is under an axial compression. Based on this mechanism alone the higher the σ_2 that is applied, the lower σ_1 or $J_2^{1/2}$ is required to fail the specimen. Since the induced tensile strains by σ_2 in the polyaxial specimen is not uniformly distributed on the $\sigma_1 - \sigma_3$ plane, quantitative determination of the effect of σ_2 under this mechanism is not easy. The elastic properties under tension may differ from those in compression. The calculation is also complicated by the same mechanism induced by σ_1 and σ_3 . Nevertheless it is suggested that the rock polyaxial strength is governed not only by the magnitudes of the three principal stresses, but also by its deformation properties.

The two mechanisms work simultaneously during polyaxial loading but with different degrees of influence depending on the magnitudes of the principal stresses at failure and of the rock elastic properties. When σ_2 is close to σ_3 (i.e. low $\sigma_2:\sigma_3$ ratio or high $\sigma_1:\sigma_2$ ratio) the

rock is strengthened by the increase of σ_2 . Under this condition, the strengthening mechanism dominates, and σ_1 at failure increases with σ_2 . Here the rock fails under compressive shear mode because the tensile strain induced by σ_2 is small. The rate of rock strengthening however decreases as σ_2 increases. When σ_2 approaches σ_1 (i.e. high $\sigma_2:\sigma_3$ ratio or low $\sigma_1:\sigma_2$ ratio) the tensile strain induced by σ_2 becomes more pronounced and overcomes the strengthening rate. Under this condition, σ_1 at failure decreases with increasing σ_2 , and the rock is failed by splitting tensile fractures. The different modes of failure obtained under different stress conditions have been observed from the test results here. Between the two extreme conditions above the combined effects from the two mechanisms will determine the rock polyaxial strengths and its failure characteristics. For the polyaxial strength results obtained here and elsewhere (e.g. Colmenares & Zoback, 2002; Haimson, 2006; and You, 2008) the proposed mechanisms can explain why at a given σ_3 , σ_1 at failure initially increases with σ_2 when σ_2 is low, and decreases with increasing σ_2 when σ_2 becomes larger. This phenomenon is particularly obvious when σ_3 is very low. It is recommended that rock deformation properties be incorporated into a failure criterion to fully describe the rock strengths under true triaxial stresses. Deserving special attention is the derivation of a strain energy-based criterion which can take both the principal stresses and principal strains (or elastic properties) at failure into consideration.

ACKNOWLEDGMENT

This research is funded by Suranaree University of Technology. Permission to publish this paper is gratefully acknowledged.

REFERENCES

- Al-Ajmi, A.M. & Zimmerman, R.W., 2005. Relation between the Mogi and the Coulomb failure criteria. *International Journal of Rock Mechanics & Mining Sciences*. 42:431-439.
- Al-Ajmi, A.M. & Zimmerman, R.W., 2005. Relation between the Mogi and the Coulomb failure criteria. *International Journal of Rock Mechanics & Mining Sciences*. 42: 431-439.
- Alexeev, A.D., Revva, V.N., Alyshev, N.A. & Zhitlyonok, D.M., 2004. True triaxial loading apparatus and its application to coal outburst prediction. *International Journal of Coal Geology*. 58: 245-250.
- Alexeev, A.D., Revva, V.N., Alyshev, N.A. & Zhitlyonok, D.M., 2004. True triaxial loading apparatus and its application to coal outburst prediction. *International Journal of Coal Geology*. 58: 245-250.
- ASTM D3967-95. Standard Test Method for Splitting Tensile Strength of Intact Rock Core Specimens. *Annual Book of ASTM Standards*. 04.08. American Society for Testing and Materials: Philadelphia.
- ASTM D3967-95. Standard Test Method for Splitting Tensile Strength of Intact Rock Core Specimens. *Annual Book of ASTM Standards*. 04.08. American Society for Testing and Materials, Philadelphia.
- ASTM D4543-85. Standard Practice for Preparing Rock Core Specimens and Determining Dimensional and Shape Tolerances. *Annual Book of ASTM Standards*. 04.08. American Society for Testing and Materials: Philadelphia.
- ASTM D4543-85. Standard Practice for Preparing Rock Core Specimens and Determining Dimensional and Shape Tolerances. *Annual Book of ASTM Standards*. 04.08. American Society for Testing and Materials, Philadelphia.
- Benz, T. & Schwab, R., 2008. A quantitative comparison of six rock failure criteria. *International Journal of Rock Mechanics and Mining Sciences*. 45: 1176-1186.

- Cai, M., 2007. Influence of intermediate principal stress on rock fracturing and strength near excavation boundaries—Insight from numerical modeling, *International Journal of Rock Mechanics & Mining Sciences*. 45:269-772.
- Cai, M., 2008. Influence of intermediate principal stress on rock fracturing and strength near excavation boundaries—Insight from numerical modeling, *International Journal of Rock Mechanics & Mining Sciences*. 45: 763-772.
- Chang, C. & Haimson, B., 2005. Non-dilatant deformation and failure mechanism in two Long Valley Caldera rocks under true triaxial compression. *International Journal of Rock Mechanics & Mining Sciences*. 42: 402-414.
- Chang, C. & Haimson, B., 2005. Non-dilatant deformation and failure mechanism in two Long Valley Caldera rocks under true triaxial compression. *International Journal of Rock Mechanics & Mining Sciences*. 42: 402-414.
- Chen, C. H., Pan, E. & Amadei B., 1998. Determination of the deformability and tensile strength of anisotropic rocks using Brazilian tests. *International Journal of Rock Mechanics & Mining Sciences*. 35: 43-61.
- Chen, C. H., Pan, E. & Amadei B., 1998. Determination of the Deformability and Tensile Strength of Anisotropic Rocks Using Brazilian tests. *International Journal of Rock Mechanics & Mining Sciences*. 35: 43-61.
- Claesson, J. & Bohloli, B., 2002. Brazilian test: stress field and tensile strength of anisotropic rocks using an analytical solution. *International Journal of Rock Mechanics & Mining Sciences*.
- Colmenares, L.B. & Zoback, M.D., 2002. A statistical evaluation of intact rock failure criteria constrained by polyaxial test data for five different rocks. *International Journal of Rock Mechanics & Mining Sciences*. 39: 695-729.
- Colmenares, L.B. & Zoback, M.D., 2002. A statistical evaluation of intact rock failure criteria constrained by polyaxial test data for five different rocks. *International Journal of Rock Mechanics & Mining Sciences*. 39: 695-729.
- Haimson, B. & Chang, C., 1999. A new true triaxial cell for testing mechanical properties of rock, and its use to determine rock strength and deformability of Westerly granite. *International Journal of Rock Mechanics and Mining Sciences*. 37: 285-296.
- Haimson, B. & Chang, C., 2000. A new true triaxial cell for testing mechanical properties of rock, and its use to determine rock strength and deformability of Westerly granite. *International Journal of Rock Mechanics and Mining Sciences*. 37: 285-296.
- Haimson, B., 2006. True triaxial stresses and the brittle fracture of rock. *Pure and Applied Geophysics*. 163: 1101-1113.
- Haimson, B., 2006. True Triaxial Stresses and the Brittle Fracture of Rock. *Pure and Applied Geophysics*. 163: 1101-1113.
- Hondros, G., 1959. The evaluation of Poisson's ratio and the modulus of materials of low tensile resistance by the Brazilian (indirect tensile) tests with particular reference to concrete. *Australian Journal of Applied Sciences*. 10: 243-268.
- Hondros, G., 1959. The Evaluation of Poisson's Ratio and the Modulus of Materials of low Tensile Resistance by the Brazilian (Indirect Tensile) Tests with Particular Reference to Concrete. *Australian Journal of Applied Sciences*. 10: 243-268.
- Jaeger, J.C. & Cook, N.G.W., 1979. *Fundamentals of Rock Mechanics*. London: Chapman and Hall.
- Jaeger, J.C. & Cook, N.G.W., 1979. *Fundamentals of Rock Mechanics*. London: Chapman and Hall.
- Jianhong, Y., Wu, F. Q. & Sun J.Z., 2008. Estimation of Tensile Elastic Modulus using Brazilian disc by applying diametrically opposed concentrated loads. *International Journal of Rock Mechanics & Mining Sciences*.

Compressive and tensile strengths of sandstones under true triaxial stresses

- Kenkhunthod, N. & Fuenkajorn, K., 2009. Effects of loading rate on compressive strength of sandstones under confinement. *Proceedings of the Second Thailand Rock Mechanics Symposium*, Nakhon Ratchasima: Suranaree University of Technology.
- Kwaśniewski, M., Takahashi, M. & Li, X., 2003. Volume changes in sandstone under true triaxial compression conditions. *ISRM 2003–Technology Roadmap for Rock Mechanics*, South African Institute of Mining and Metallurgy.
- Liao, J. J., Yang, M. T. & Hsieh, H. Y. 1997. Direct tensile behavior of a transversely isotropic rock. *International Journal of Rock Mechanics & Mining Sciences*. 34(5): 831-849.
- Ohokal, M., Funatol, A. & Takahashi, Y., 1997. Tensile test using hollow cylindrical specimen. *International Journal of Rock Mechanics & Mining Sciences*. Vol. 34, No. 3-4, 1997 ISSN 0148-9062.
- Oku, H., Haimson, B. & Song, S.R., 2007. True triaxial strength and deformability of the siltstone overlying the Chelungpu fault (Chi-Chi earthquake), Taiwan. *Geophysical Research Letters*. 34(9).
- Reddy, K.R., Saxena, S.K. & Budiman, J.S., 1992. Development of a true triaxial testing apparatus. *Geotechnical Testing Journal*. 35(2): 89-105.
- Reddy, K.R., Saxena, S.K. & Budiman, J.S., 1992. Development of a True Triaxial Testing Apparatus. *Geotechnical Testing Journal*. 15(2): 89-105.
- Schwab, R. & Benz, T., 2008. a quantitative comparison of six rock failure criteria. *International Journal of Rock Mechanics and Mining Sciences*. 45: 1176-1186.
- Singh, B., Goel, R.K., Mehrotra, V.K., Garg, S.K. & Allu, M.R., 1998. Effect of intermediate principal stress on strength of anisotropic rock mass. *Tunneling and Underground Space Technology*. 13: 71-79.
- Smart, B. G. D., 1995. A true triaxial cell for testing cylindrical rock specimens. *International Journal of Rock Mechanics and Mining Sciences*. 32(3): 269-275.
- Tepnarong, P. 2001. Theoretical and Experimental Studies to Determine Compressive and Tensile Strength of Rock, Using Modified Point Load Testing. *M.S. Thesis*, Suranaree University of Technology, Thailand.
- Tiwari, R.P. & Rao, K.S., 2004. Physical modeling of a rock mass under a true triaxial stress state. *International Journal of Rock Mechanics and Mining Sciences*. 41(30):2A 141-6.
- Tiwari, R.P. & Rao, K.S., 2004. Physical modeling of a rock mass under a true triaxial stress state. *International Journal of Rock Mechanics and Mining Sciences*. 41(30).
- Tiwari, R.P. & Rao, K.S., 2006. Post failure behaviour of a rock mass under the influence of triaxial and true triaxial confinement. *Engineering Geology*. 84: 112-129.
- Wawersik, W.R., Carlson, L.W., Holcomb, D.J. & Williams, R.J., 1997. New method for true-triaxial rock testing. *International Journal of Rock Mechanics and Mining Sciences*. 34(3-4): 365-385.
- Wawersik, W.R., Carlson, L.W., Holcomb, D.J. & Williams, R.J., 1997. New method for true-triaxial rock testing. *International Journal of Rock Mechanics and Mining Sciences*. 34(330): 3-4.
- Wijk, G., 1978. Some new theoretical aspects of indirect measurements of tensile strength of rock. *International Journal of Rock Mechanics & Mining Sciences*. 15: 149-160.
- Yang, X. L., Zou, J. F. & SUI, Z. R., 2007. Effect of intermediate principal stress on rock cavity stability. *Journal Central South University Technology*. s1-0165-05
- You, M., 2008. True-triaxial strength criteria for rock. *International Journal of Rock Mechanics and Mining Sciences*. 46: 115-127.
- You, M., 2008. True-triaxial strength criteria for rock. *International Journal of Rock Mechanics and Mining Sciences*. 46: 115-127.

Effects of Intermediate Principal Stress on Compressive and Tensile Strengths of Sandstones

Paper No.298

R. Thosuwat C. Walsri
Suranaree University of technology
Nakorn Ratchasima

P. Poonprakon

K. Fuenkajorn

ABSTRACT

A series of true triaxial compression tests and indirect tension tests with axial confinements are performed to assess the effects of the intermediate principal stresses on the elasticity and strengths of three types of sandstones. These sandstones are commonly found in the north and northeast of Thailand. Their mechanical properties and responses play a significant role on the stability of the tunnels, slope embankments and dam foundations in the region. A true understanding of the failure behavior of these rocks is highly desirable. In particular, knowledge of the rock tensile strength as affected by the intermediate principal stress is rare.

Over 50 rectangular shaped specimens (50x50x100 mm) are tested using a polyaxial load frame. Lateral stresses are applied with different magnitudes between two mutually perpendicular directions ($\sigma_2 \neq \sigma_3$), and varying from 0 up to 20 MPa. The axial stress (σ_1 - along the longest axis) is increased until failure. Neoprene caps are inserted at the interfaces between loading platens and specimen surfaces to minimize the friction. The failure stresses are presented in form of octahedral shear strength (τ_{oct}) vs. mean stress (σ_m) diagram. Comparisons of the results with those obtained from the uniaxial and triaxial strength testing indicate that under the same σ_m , σ_2 can notably decrease the τ_{oct} at failure. The failure envelope is lower for the greater σ_2/σ_3 ratio. The results also indicate that the sandstones are transversely anisotropic. The elastic modulus in the direction normal to the bedding planes is about 2-4 times greater than that parallel to the bedding planes. The Poisson's ratio on the plane parallel to the beds is about three times smaller than that across the beds. These hold true for all sandstones tested here.

The effect of σ_2 on the tensile strengths is assessed by conducting the indirect tension test under confinement. The constant σ_2 with magnitudes varying from 0 to 40 MPa is applied along the axial direction of 50 mm-diameter disk samples using the polyaxial load frame. Then the line load is diametrically applied until failure occurs. The intermediate principal stress (σ_2 - axial stress in this case) significantly decreases the magnitude of the line load required to fail the disk samples. Using linear elastic theory the stress states are derived for the sample center (where the tensile crack is initiated) which is under uniaxial strain condition. A more complete failure criterion (taken σ_2 into consideration) is developed using $\tau_{oct} - \sigma_m$ diagram by combining the results of tension test under confinements with those of the true triaxial compression tests. The octahedral shear strengths of the rocks under the mean stresses that are lower than that obtained from the uniaxial compressive strength can be obtained.

Key Words: sandstone, true triaxial, polyaxial, intermediate principal stress, Brazilian test

BIOGRAPHY

Mr. Roengchai Thosuwan was born on February 2, 1984 in Kamphaengphet province, Thailand. He received his Bachelor's Degree in Engineering (Geotechnology) from Suranaree University of Technology in 2006. For his post-graduate, he continued to study with a Master's degree in the Geological Engineering Program, Institute of Engineering, Suranaree university of Technology. During graduation, 2006-2009, he was a part time worker in position of research assistant at the Geomechanics Research Unit, Institute of Engineering, Suranaree University of Technology. He has published two technical papers related to rock mechanics, titled **“Compressive and Tensile Strengths of Sandstones under True Triaxial Stresses”** published in the Proceeding of the Second Thailand symposium on rock mechanics, Chonburi, Thailand; and **“Effects of Intermediate Principal on Compressive and Tensile Strengths of Sandstones”** in the Proceeding of International Symposium on Rock Mechanics, University of Hong Kong, Hong Kong. For his work, he is a good knowledge in geomechanics theory and practice.